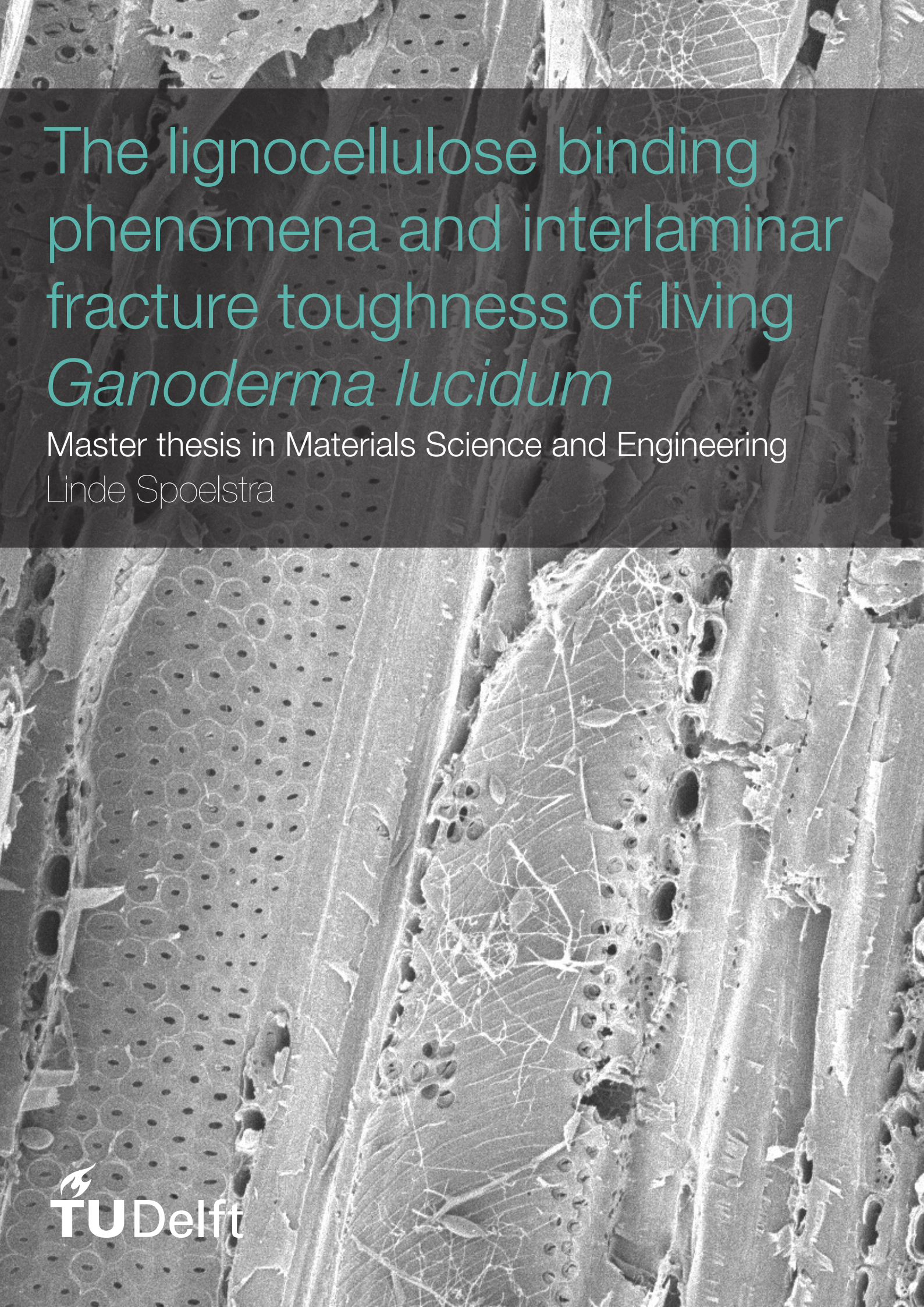

The lignocellulose binding phenomena and interlaminar fracture toughness of living *Ganoderma lucidum*

Master thesis in Materials Science and Engineering

Linde Spoelstra

TU Delft

The lignocellulose binding phenomena and interlaminar fracture toughness of living *Ganoderma lucidum*

by

Linde Spoelstra

to obtain the degree of Master of Science and Engineering
at the Delft University of Technology
to be defended publicly on Tuesday the 11th of July 2023, at 14:00 PM.

Student number: 4493702

Thesis committee:	Dr. K. Masania	TU Delft, supervisor
	Dr. M.A. Bessa	TU Delft and Brown University, supervisor
	Dr. Y. Gonzalez Garcia	TU Delft, chair
	Dr. G.A. Filonenko	TU Delft

An electronic version of this thesis is available at http://repository.tudelft.nl/.

Cover: *Ganoderma lucidum* growing inside hornbeam veneer.

TU Delft

Acknowledgements

This master thesis marks the end of a seven-year-long university journey. Starting with a degree in Liberal Arts and Sciences, I am proud to have finished a thesis in Materials Science and Engineering in Delft. I would like to extend my gratitude to all those who helped me along its way.

First and foremost, I would like to express my sincere thanks to my supervisor, Kunal Masania, for taking me to the absolute forefront of materials science. I now know what type two - or three - fun looks like in research. Your expertise and excitement in bio-inspired materials and drive to connect people have been a true inspiration. Furthermore, a big long distance thank you to my supervisor Miguel Bessa in the US, for providing me guidance and uplifting insights into research journeys whenever needed. I would also like to express my gratitude to Yaiza Gonzalez Garcia and Georgy Filonenko for taking their time to assess my work in its final state.

Where my close and appreciated buddy *Ganoderma lucidum* could cause moments of desperation over the course of this work, I could always rely on the support and fun provided by the people of the Shaping Matter Lab. You truly have made me smile a lot during my time here at the Aerospace faculty, and I am forever intrigued by the amazing work you put together. A special bless to Mu and Satya, thanks for putting all my efforts into perspective. Also Ran, thank you for all the fruitful discussions we had.

Then, I cannot leave the lab without stating my appreciation to all DASML technicians. Johan, Victor, Alexander, Chantal, Roy, and especially Dave and Pietro, thank you for your kindness, patience, and enthousiasm. Also thank you Michele, at the Civil Faculty. You all made me feel comfortable with the hands-on work that comes with a degree in materials engineering.

Lastly, moving across three different cities and five different universities has surrounded me with many dear friends, whom I'd all like to thank for making my life in and around academia so much fun. Especially to those also pursueing their MSc in materials - both Zoom and Delft would have not been as charming without you. And finally, the biggest dankjulliewel to my dearest parents and brother, whose endless love and support have always facilitated my growth.

Linde Spoelstra
The Hague, July 2023

Abstract

Mycelium based composites (MBC) have revolutionised the field of material production, where a living fungus is employed to overgrow and bind lignocellulosic substrate materials together. Their bio-based nature, low embodied energy, and biodegradability, mark their great potential to reduce the increasing pressure conventional materials put on the environment. Unfortunately, the material's applications are limited due to its low mechanical properties, that are equivalent to those of foams or natural fibre boards. Furthermore, where the material is primarily used and studied in its heat-treated non-living form, harnessing the biological power of the fungus shows to give the material self-healing and sensing capabilities. The required hydrolysed state is however shown to further decrease its mechanical properties, and yet hardly evaluated in literature. Especially the mechanics of the mycelium-lignocellulose interface are inadequately studied, and important to evaluate for a broadening of the living composite material's applications.

In this study we present the development of a double cantilever beam (DCB) test according to ASTM D5528, setup to quantify the interlaminar fracture toughness (G_I) of *Ganoderma lucidum* (*G. lucidum*) grown in between wood veneers. The data was evaluated using an analytical approach based on a decrease in the beams' compliance. The specimens were fabricated with the use of additive manufacturing, allowing precise control over the placement of the fungus and its provided nutrients. Its growth behaviour into the substrate was qualitatively assessed through optical microscopy and scanning electron microscopy (SEM), and its digestive ability on the surface by fourier-transform infrared spectroscopy (FTIR).

A mycelium-laden ink presented by Gantenbein et al. (2023) was reproduced with a 75% lower agar content to serve a stable source of mycelium on the DCB specimens [1]. A growth period between 3 and 4 weeks from the printed hydrogel was required for substantial mycelium-substrate binding, which stabilised after 4 weeks of growth. Furthermore, the provision of malt extract (ME) was required, but not needed to be higher than 5% of the ink's weight. The G_I was in these conditions reported to be 1.83 J/m^2 on hornbeam veneers, where a maximum value of 3.46 J/m^2 was reached. Variable growth generated substantially different mechanical properties, which resulted in the lower G_I of mycelium grown on beech and spruce samples, caused by the use of an older fungal inoculum of a different reference plate. A stronger binding on beech than spruce did suggest a more important role of the substrate chemistry than its density. The mycelium always showed cohesive failure, showing the low G_I to not result from poor substrate adhesion, but rather from the mechanics of the hyphae network developed. Microscopy and FTIR evaluations showed the ability of *G. lucidum* to digest the hornbeam's lignin. The full depths of hornbeam and beech veneer substrates with 5 and 3 mm thickness were colonised, where vessel elements served as the main pathway for the hyphae.

This study was, to the best of our knowledge, the first to isolate the binding behaviour of a living mycelium in a mode-I loading condition. It thereby provides valuable new insights in the field of living MBC, and contributes to the further development of this advanced, eco-friendly, and living material. The setup can now be utilised to study the binding behaviour of different fungi on substrates of varying chemistry and porosity. Furthermore, aiming to elucidate the use of additive manufacturing in the composite production, this study opened up pathways into controlling the composite's properties in the future.

Contents

Nomenclature

Abbreviations

Abbreviation	Definition
3PB	three-point bending
ASTM	American Society for Testing and Materials
DCB	double cantilever beam
DIW	direct ink writing
ELM	engineered living material
FTIR	fourier-transform infrared spectroscopy
IB	internal bond strength
ISO	International Organization for Standardization
MBC	mycelium based composites
MBM	mycelium based materials
ME	malt extract
MEA	malt extract agar
ML	machine learning
NEN-EN	Nederlands Normalisatie-Instituut, Europese normen
SEM	scanning electron microscope/microscopy

Symbols

Symbol	Definition	Unit
a	crack length	[mm]
a_0	initial crack length	[mm]
b	DCB arm width	[mm]
δ	displacement	[mm]
d	DCB arm thickness	[mm]
E	elastic modulus	[GPa]
η	viscosity	[Pas]
$\dot{\gamma}$	shear rate	[1/s]
G_I	interlaminar fracture toughness	[J/m^2]
I	beam moment of inertia	[mm^4]
L	3PB span width	[mm]
N	3PB loading speed	[mm/min]
P	load	[N]
τ	shear stress	[Pa]
t	time	[s]

List of Figures

List of Tables

1 Introduction

1.1. Background motivation

Conventional methods of material manufacturing, usage, and disposal, put an increasing pressure on the environment that needs to be diminished [2]. The non-natural waste-streams that they generate cause pollution and disturb ecosystems, where the large energy consumption and carbon footprints of material production processes accelerate climate change. Over 20% of the energy used worldwide is used for materials production, where UNEP, the United Nations environment programme, has reported the global greenhouse gas emissions from material production to have increased from 5 gigatonnes of CO2 equivalent ($GtCO_2e$) in 1995 to 11.5 $GtCO_2e$ in 2015 worldwide [2, 3]. This extreme elevation in emissions comes from sectors requiring large material volumes such as the packaging and building industry, which grow to serve the demands of an increasing world population and its consumption.

Where both the world population and its desires are predicted to only increase further in the upcoming decades, governmental bodies such as the European Commission needed to set goals for the development of materials with a lower carbon footprint by 2050 [4]. Material manufacturers are forced to make production processes more efficient, and are motivated to rely less on finite resources such as petroleum and minerals. Here, bio-based materials can aid the transition towards a more sustainable and circular economy [5].

Bio-based materials become more prominent in commercial applications, and inspire researchers in material development. The inherent variability of bio-based materials still limits their use in high-performance applications that seek excellent mechanical properties and reliability, such as in the Aerospace industry. However, nature's ability to grow molecular assemblies that generate materials with a microstructure optimised for the purpose they serve, has inspired researchers to develop more bottom-up material manufacturing approaches [6, 7]. Furthermore, the ability of living materials to regenerate upon damage and reshape upon external stimuli, as for example recognised in skin, has inspired the production of self-healing materials [8]. One class of materials that gained researchers' and the public's attention in the last 10-15 years for its fully bio-based nature, its ability to manufacture its own microstructure, and its capability to regenerate, is mycelium based materials (MBM) [9].

1.2. Mycelium based composites

The fungus' growth characteristics are utilised in MBM, where it develops large mycelium networks of interconnected strands called hyphae [10]. These hyphae can overgrow, degrade, and penetrate many lignocellulosic substrate materials [11]. They can thus be used to bind such fibrous materials together, creating foam-like materials called mycelium based composites (MBC). In a suitable growth environment the fungus will hereby upgrade waste-stream natural fibres into functional materials [11]. From a sustainability perspective, this upcycling makes MBC ideal materials, given the carbon-capturing fibres, low-energy manufacturing process, and material's biodegradability. They already serve commercial applications as packaging and insulation materials as produced by for example Mogu and Ecovative, as displayed in Figure 1A [12, 13]. Designers furthermore show their potential as a structural component, like in Figure 1B. Their applications are however still limited by their weak mechanical properties.

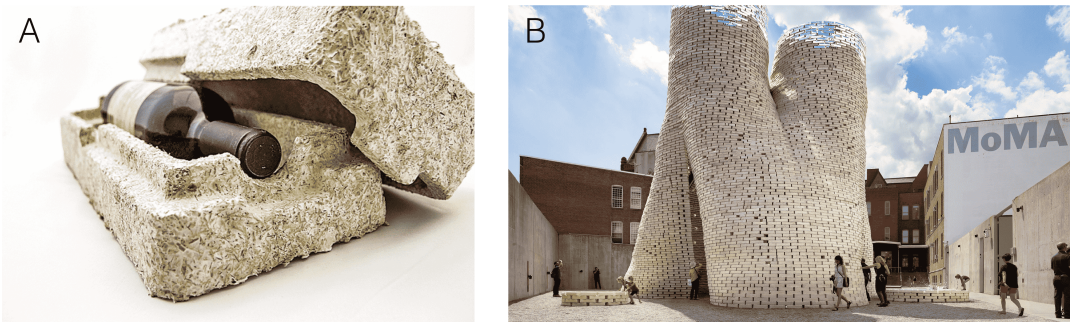

Figure 1: The application of a MBC as packaging material produced by Ecovative (A) [14], and an explorative project for its potential as a structural component (B) [15].

The composite's mechanical properties are furthermore mutually exclusive with its ability to exhibit living behaviour. Literature demonstrates that by subjecting the material to heat-pressing, its foam-like densities and mechanical properties can be enhanced towards those of natural fibre-boards [16]. In both cases the material is usually heat-treated to kill the fungus. This ceases all of its biological activity, whereas more recent studies have highlighted the remarkable potential of the living material to regenerate when damaged, and respond to the external environment by electrochemical signaling [17, 1, 18]. It is revolutionising that a biological component can add advanced properties to materials without the need of synthetic additives or electronics. Nevertheless, harnessing the full responsive power of the fungus' biology is likely to compromise the material's mechanical properties, as it requires a hydrolysed state of the composite. Hardly any research is yet performed on these innovative living materials, presenting challenges due to their fragility and sensitivity to their environment [9]. Consequently, there is a research gap concerning the extend of this mechanical properties loss, and how the materials can be optimised while keeping the fungus alive.

Literature on MBC highlights one component of the material in specific to be not well understood and hard to study, which is the mycelium matrix and lignocellulosic fibre interface [19]. Its microstructure depends on various factors, including the growth behaviour of the mycelium, the chemistries and microstructure of both components, and their interactions [20, 16]. It is however known from conventional composite materials that the fibre-matrix interface plays a crucial role in enabling the composite's fibres to respond to external loads [21]. Without an effective load transfer from the matrix to the fibres, they will not be able to improve the material's stiffness and strength. While theories exist on the interaction mechanisms between the two materials in MBC, no work has yet been presented that accurately quantifies the micromechanics of this interface while studying its microstructure [22, 23, 24, 25]. Hence to optimise the mechanical properties of living MBC, and further explore the potential reinforcements in their structure, it is imperative to develop a more thorough understanding of this interface.

1.3. Thesis work and layout

The current work aims to systematically evaluate the mechanics of the mycelium-substrate interface, where the mycelium is in its undried, hence living state. This will better the understanding of the living composite mechanics, which is essential for the optimisation of its properties in future composite designs. Thereby it will contribute to broadening the material's applications, that furthermore can utilise its powerful biological characteristics. It will require the development of a mechanical testing setup that allows the quantification of the materials' interface. Wood veneers can here serve as a substrate of well defined geometry and well-understood lignocellulosic chemistry. It is furthermore of interest to control systematic specimen production with the use of additive manufacturing, to simultaneously explore this technique's promising ability to automate MBC manufacturing in the future. Additionally, appropriate interface analysis methods should be provided, to give insight into the microstructure of the mycelium and substrate interaction, which in MBC literature has not yet been evaluated throughout a substrate's depth.

First, Chapter 2 will give a review of the relevant literature on the proposed topic, to create a good understanding of the microstructure, manufacturing, and properties of MBC. It will generate the knowledge gap that is intended to be filled by the current work. Chapter 3 sets the exact research definition, and will lay out the research questions with an overarching hypothesis. It presents the order of the deliverable tasks required to answer the research questions. Chapter 4 is focused on the all materials and methods used to: replicate and optimise a required printable mycelium-laden ink, setup the proposed mechanical testing method, and systematically evaluate the mycelium-lignocellulose interface. Chapter 5 will present, discuss, and summarise the results found during the hydrogel development, mechanical testing, and interface evaluation. Then, Chapter 6 will discuss all observations of Chapter 5 together, after which the research questions will be answered and a conclusion will be drawn in Chapter 7. Finally, recommendations and suggestions for future work are set out in the last chapter, Chapter 8.

2

Literature review

Given that this thesis finds itself at the interface of fungal microbiology, or mycology, fungal wood decay, and material science, it is essential to develop a basic understanding of the underlying biology and living characteristics. This will facilitate a critical evaluation of the literature on MBC, and understanding of the bottlenecks that limit the applications and evaluation of the living material.

2.1. Mycelium based composite components

2.1.1. Fungi and mycelium

Of the 3.5 to 5.1 million species of fungi estimated to exist on earth, only those fungi growing a mycelium, a large interconnected network of filamentous hyphae strands, can be used in MBC [26]. A filamentous fungus' typical life cycle is presented in Figure 2, where it is hence not the mushroom or basidiocarp structure that is of interest, but the nutrient seeking hyphae that typically grow into the ground or organic matter. 79 species of such fungi were identified by Brandhof and Wösten (2022) to be used in literature on MBM [27].

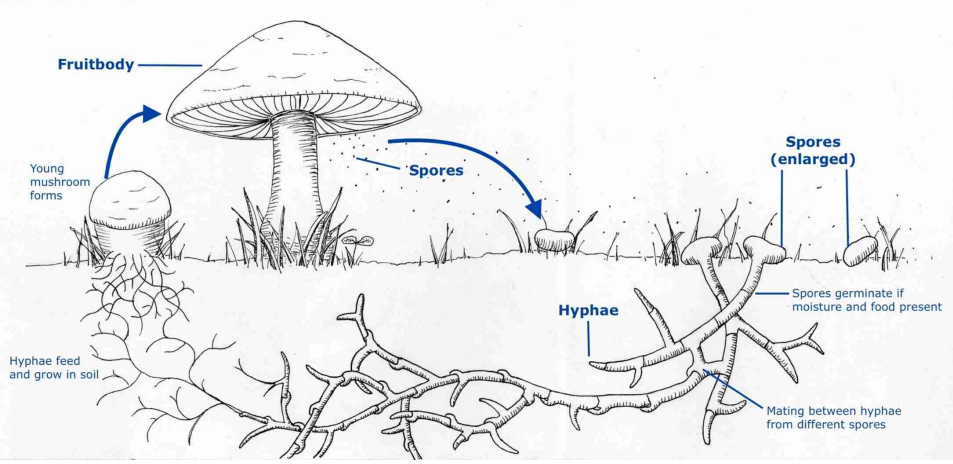

Figure 2: The life cycle of a filamentous fungus [28].

The use of these species is based on their digestive bahaviour, methods of reproduction, and morphology, or mycelium microstructure. Most belong to the phylum of Basidiomycetes and are saprothropic fungi, hence living on dead lignocellulosic matter. Solely white-rot fungi can digest the lignin in organic matter, which are therefore most commonly used [29]. The most represented genera are *Trametes*, *Ganoderma*, and *Pleurotus*. Their limited pathogenecity increases their applicability and acceptability by people [27]. They release haploid basidiospores that produce primary mycelia that merge and fuse their nuclei by a process called karyogamy, showing sexual reproduction [30]. The emerging hyphae are generally 1-30 μm thick, with lengths ranging from a few μm to several meters [10]. They can fuse by anastomosis to form larger mycelium networks. Hyphae morphologies vary in degree of

branching and cell wall thickness, where those species showing the most variation are suggested to provide the strongest composite materials [31, 29]. Hyphae are furthermore classified based on their location within the mycelium, as leading at the periphery, trunk at the interior, fusion at neighbouring connecting hyphae, and aerial when growing into the air. Both vegetative and arial hyphae are recognised in MBC materials, growing either on the surface or across substrate particles [32].

Hyphae grow at their tips by extension of their cell wall, also referred to as apical growth, that allows them to reach over many hectares. It is generally understood that turgor pressure exerted by the plasma membrane on the cell wall causes cell wall thinning and Ca^{2+} fluxes that initiate the transport of enzyme-carrying vesicles towards the hyphae's tip, as shown in Figure 3A [33, 34]. The vesicles are carried at high speed by motor proteins across microtubules and filamentous actin, allowing filamentous fungi to reach growth speeds of about 20 μm per minute [34]. The vesicles form an agglomerate called the "Spitzenkörper", who's location orientates the hyphae in response to external stimuli such as pressure or nutrient availability [35]. Once arrived at the hyphae tip, the vesicles carrying lipids and cell wall generating enzymes allow new cell wall generation.

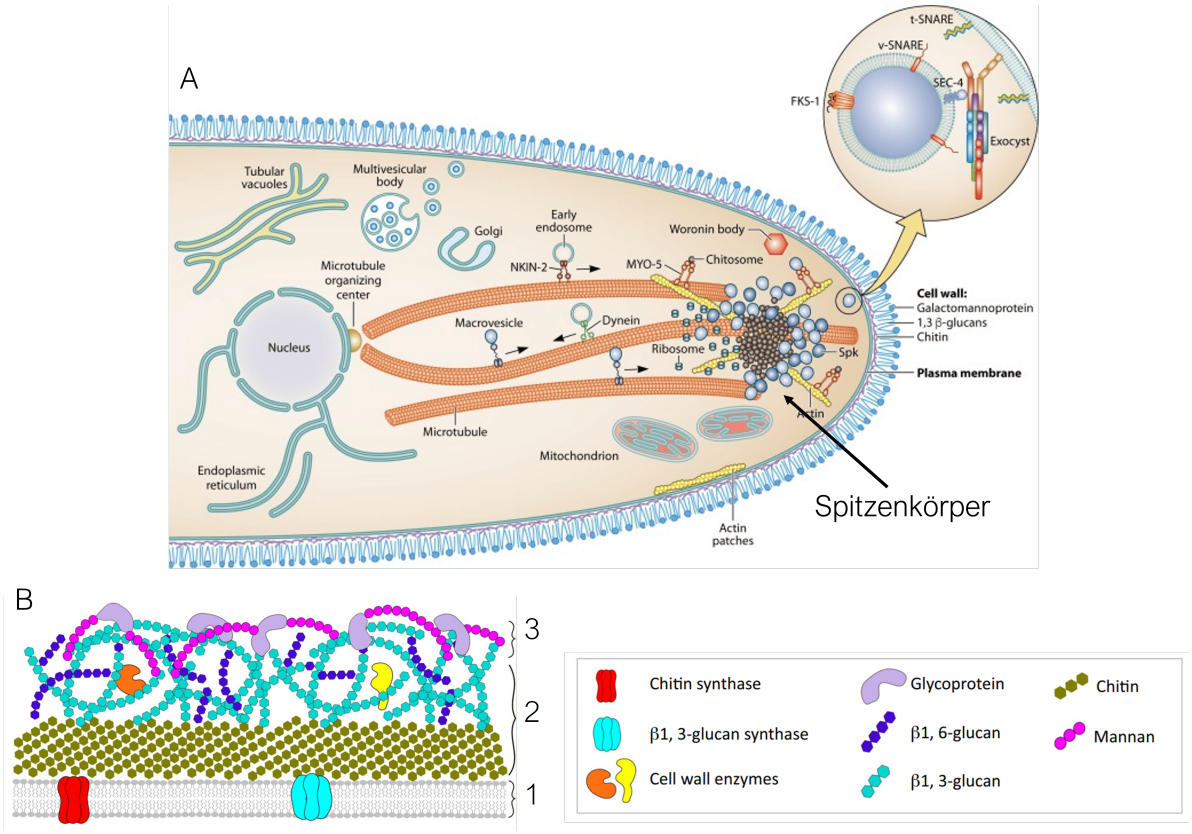

Figure 3: The enzymatic machinery involved in apical tip growth in filamentous fungi, showing the appearance of the Spitzenkörper (A) [36], and an illustration of the main constituents of their plasma membrane (1), inner cell wall (2), and outer cell wall (3)(B) [37]. Note that the scales of individual components do not match for illustrative purposes. Hyphae are typically between 1-30 μm in diameter, and the cell walls between 0.1 and 10 μm.

The mycelium's stiffness and strength result from this cell wall's structure as shown in Figure 3B, and the hyphae's ability to form networks and tissues [37]. An inner layer of β1,4-linked N-acetylglucosamines, called chitin, forms interchain hydrogen bonds and creates a highly crystalline structure, generating microfibrils that give hyphae their stiffness. Elastic moduli of fungal cell walls are reported to be on the order of 100 MPa [38]. The chitin is crosslinked to β1,3-glucan chains and an outer more protein-rich layer. The amorphous interconnected network of these polysaccharides generates strength. When the cell walls of hyphae fuse by anastomosis, the agglomerated structures grow even faster than individual hyphae [30]. An example is pseudo-laminar sheets, that have also been observed in MBC [39].

2.1.2. Natural fibres' microstructure

All particulate and fibrous matter used to build MBC originate from plants and wood, and are hence build up of lignocellulose [40]. The most common substrates being explored in MBC research are rice or millet husk/hulls [20, 41], (beechwood) sawdust [20, 41, 42, 9, 43], cotton powder or ginning waste [42, 44, 45, 46], but also hemp hurds or pits, and (wheat) straw [9, 43, 46, 16]. Hence primarily waste-based sources, that all have the same basic hierarchical structure, as shown in Figure 4A and B. Longitudinal cells contain a lumen surrounded by cell walls of different layers, each in which cellulose microfibrils and hemicelluloses are bonded to lignin by hydrogen and covalent bonds, respectively. The cellulose microfibrillar angle differs in every layer, where they are most prominent in the thick S2 layer, that therefore mainly constitutes the cell wall's strength. Lignin, solely digestible by white-rot fungi, is a highly complex macromolecule, as shown in Figure 4A. Next to giving structural support it decreases the plant fibres' permeability [47]. Taking a more macroscopic view, various plant cell types can be recognised. Especially in wood materials, the substrate to be used in the current study.

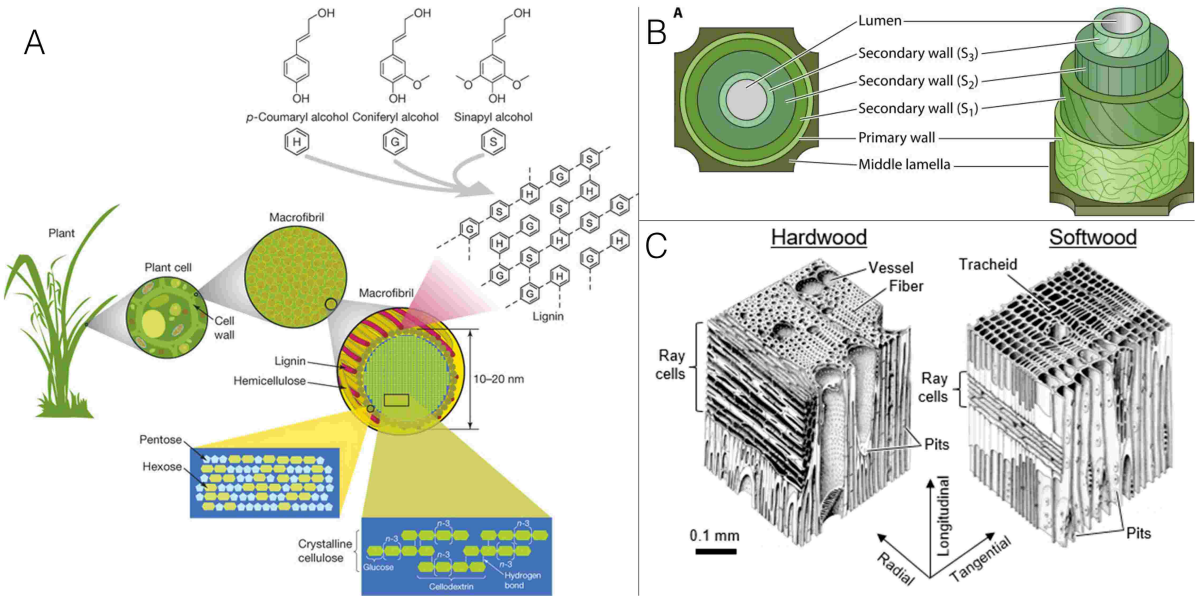

Figure 4: A: Hierarchical structure of plant cells [48]. B: Build-up of cell wall layers [49]. C: General cell structures found in hardwoods and softwoods [50].

The main cell types in woods are tracheids, vessels, parenchyma/rays, and fibres, as pictured in Figure 4C [51]. The first three cell types have larger lumina and more cell wall pits, in order to serve primarily nutrient and water transport purposes either along the longitudinal or radial direction of the tree. In softwoods, tracheids provide both nutrient transport and structural rigidity, where fibres in hardwoods have a smaller lumina and solely serve the structural function [52]. Generally, hardwoods have a higher strength and stiffness, due to their slower growth and their corresponding higher density. Furthermore, hardwoods contain generally less lignin, of which the syringil to guaiacyl ratio is higher than for softwoods [53]. Experimental work informs that woods with such a higher syringil content are easier for white-rot fungi to be degraded, and for some *Ganoderma* species syringil units are then also degraded before the guiacyl ones [54].

2.1.3. Fungal degradation and penetration

Fungi perform both intracellular and extracellular degradation of provided sugars and lignocellulose to use their subunits for cell wall generation. Simple sugars can directly be absorbed through the porous hyphal cell wall, its proteinaceous pores, or via endocytosis. The digestion of lignocellulose first requires enzymatic machinery that depolymerises and metabolises the complex molecules outside of the cell wall.

The pathways of substrate degradation rely on the lignocellulose structure and chemistry, and the fungal species being evaluated. Literature shows the species in this study, *G. lucidum*, to perform selective rot on wood. Hence lignin is degraded before cellulose and hemicellulose, especially during its mycelium growth phase in the first three months after growth initiation [55, 56, 54]. The lignin is degraded by oxidative enzymes such as laccases and peroxidases, which often require smaller non-enzymatic mediators. These penetrate the cell walls and solubilise substrate compounds, where enzymes erode the substrate's surface but cannot penetrate further than the nm scale [57]. Hemicellulose degradation requires the synergy of multiple hydrolitic enzymes, due to the more complex molecular structure and molecule's adhesion to both lignin and cellulose. Cellulose, finally, is the most difficult to degrade due to its coverage and crystallinity. It requires a synergy between both hydrolitic and oxidative enzymes [47]. All enzymes are overviewed and classified in the Carbohydrate-Active enZymes (CAZy) database, and act in the close proximity of the hyphae.

The fungus' growth strategy preceeds, facilitates, but is also guided by the digestion of nutrients. Mycelium growth on wood starts on the surface where the fungus uptakes simple sugars and starches available, after which the deconstruction of the wood cell walls will be initiated. Great sources to understand their ways are presented by Schwarze and Baum (2000), Schwarze et al. (2000), Schwarze et al. (2007), Keerik (2012), and Goodell (2020).[58, 59, 54, 60, 57]. Growth strategies vary widely for different fungal species, but for white-rot fungi are typically characterised by:

- Pit degradation and penetration, creation of bore holes
- Hyphal growth through the hollow cell lumina
- Cell wall penetration
- Cell wall erosion

The first two represent the natural guidance of the hyphae towards the path of least resistance. Hyphae growth of white-rot fungi occurs primarily along the wood cell's lumina, rather than through the cell walls. In selective rot, the fungus degrades the secondary cell wall from the cell lumina outwards, where the degradation reaches towards the lignin-rich middle lamella. The dissolution of this structure causes wood cell separation. Only at later stages of decay the other cell wall components get digested, and the material loses its structural integrity as the cellulose gets degraded. A single fungus can exhibit both selective and simultaneous rot, where in the latter strategy all three lignocellulose components are digested at the same time [54]. Here the hyphae also grow inside the cell lumina, and sink into the cell wall by erosion. The cell wall is degraded progessively and thereby thinned from the cell lumina outwards, and at some point the hyphae are able to form bore-holes and penetrate towards the middle lamella. The final stage of fungal decay in MBC depends on the provided growth time.

In MBC production, several parameters can be adjusted to maximise the fungal degradation and growth, and thereby binding of the substrate fibres.

- **Temperature** - Each fungal species has their own optimal growth temperature with the highest enzyme activity, with usually lays between 25-35 °C [61, 62]. The optimal temperature for *G. lucidum* is for example reported to be 30 °C [63].
- **pH** - A lower pH of around 4 or 6 is optimal for mycelium growth, where contaminating bacteria prefer a neutral pH of 7 [62, 63, 1, 64, 44].
- **Humidity** - A preferred humidity between 60-65% is essential for the fungi's metabolism, which will also prevent the substrate from drying [62, 61, 65].
- **Water content** - Fungal degradation of wood requires a moisture content (MC) of at least 30%, where the optimum differs for fungal species between 50-100%. This facilitates diffusion of the fungus' enzymes and other degradative components through the wood's porous structure [57].
- **Aeration** - Most fungi are obligate aerobes, meaning they require oxygen to degrade nutrients, grow, and survive [66]. Their growth is generally reduced if the level drops below atmospheric levels [62].
- **Light** - Studies on the growth of *G. lucidum*'s mycelium show an increased growth rate in dark conditions [67]. Furthermore, growing the material in the dark circumvents the possible influence

of changing light influx on the growth of the material, and thereby introduction of structural heterogeneities [42, 1, 18].

- **CO_2** - Environmental CO_2 levels are not often controlled in MBC literature, but can be increased to prevent the formation of fruiting bodies.

2.2. Mycelium based composite production and properties

MBM exist in the form of pure mycelium as films or foams, or in combination with lignocellulosic fibres as composites [68]. Care should be taken with the nomenclature of foams, where some also refer to mycelium based foams for non-pressed MBC [16]. These non-reinforced foams are flexible, do not provide the stiffness obtained in MBC, and do not serve the pathway for upcycling of lignocellulosic waste materials [69]. Primarily for their higher mechanical properties, the rest of this review is focused on MBC, where informative insights in work on pure mycelium materials will not be ignored.

2.2.1. Production methods and resulting hierarchical structure

No standardised production methods yet exist for MBC, but one can recognise conventional production procedures. Current reviews on MBC describe manufacturing processes based on moulding and additive manufacturing, where the first is the dominating production strategy [16, 11]. A flow chart of the steps involved is shown in Figure 5.

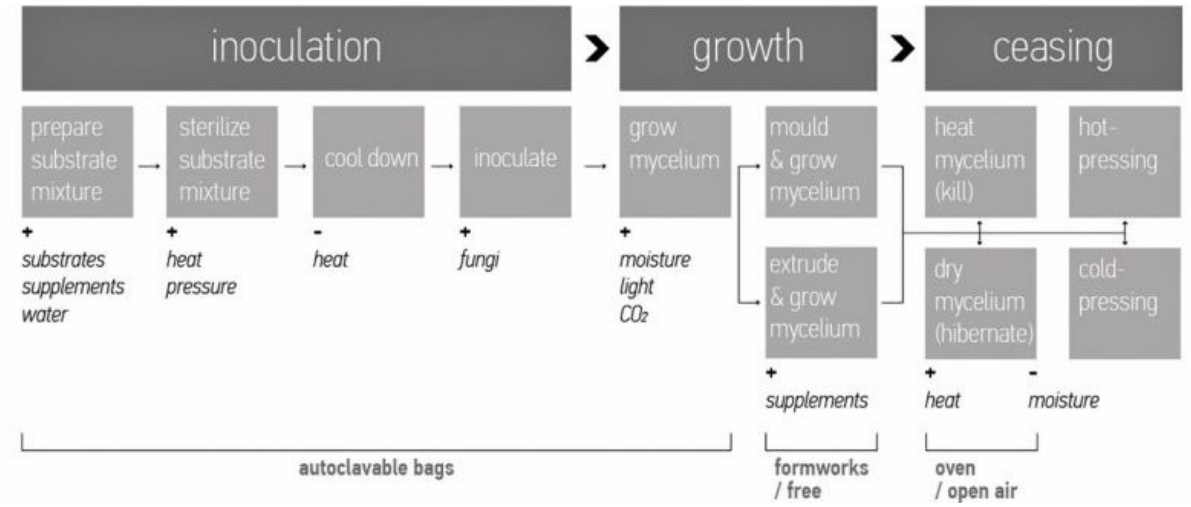

Figure 5: Typical production route of a MBC [70].

Exact procedures in literature are optimised to maximise the growth of a fungal species on the substrate of choice, generating a random fibre or particulate reinforced composite. The mycelium growth is initiated from a mature inoculum, and can originate from an overgrown agar plate, a liquid culture, but most often is introduced in the form of spawn [32, 71]. These inoculation methods introduce required additional nutrients, of often unreported composition, and amounts varying from 1 to 20 wt%. Occasionally, more supplementary nutrients like barley and malt extract are used, where its content influences the mycelium morphology [65]. The mycelium overgrows the substrate material for a period ranging from 1 to 4 weeks, either inside moulds or in 3D printed shapes as shown in Figure 6. Next to binding the randomly distributed fibres together by growth inside the structures, the mycelium develops a film on the outside [71, 72, 32]. This film and larger mould sizes can limit the required oxygen supply to the inside, which can be partially circumvented with additive manufacturing (AM) [73, 1, 74, 75, 76]. AM introduces an unforeseen structural design freedom to generate optimised structures as in Figure 6B, where also the provided nutrients can be locally controlled to adjust the mycelium microstructure, displayed in Figure 6C. Finally, the material is either dried to stop growth or ceased to kill the fungus, and commonly heat-pressed to increase the material's mechanical properties [55, 42, 77, 45].

Figure 6: A: The conventional manufacturing method of MBC using moulding of inoculated substrate material [78]. B: 3D printing of substrate containing pastes allows more design freedom in MBC structures [75]. C: 3D printing of mycelium-laden hydrogels allows the manufacturing of structures with controlled nutrient supply and mycelium microstructures [1].

Strategies known to increase composite mechanical properties such as fibre architecture and improved interface bonding have not yet been systematically evaluated. The latter is difficult to study and poorly understood, but generally written to originate from three factors. Firstly, hyphae are in theory mechanically interlocking the substrate as a result of hyphae penetration, as already described in section 2.1.3. Then, the hydrophobins are hydrophobic proteins on the outer surface of the mycelium cell wall, and play an important role in the substrate adhesion, especially to hydrophobic surfaces [23, 24, 25]. Lastly, theories are developed in MBC research where hydrogen bonds and esterification reactions occur between dead mycelium and substrate material after heat-pressing [22]. These results are solely based on fourier-transform infrared spectroscopy (FTIR) measurements and critically discussed by others, hence should be treated with care [19].

2.2.2. Mechanical properties

Due to the novelty of the material, no standardised testing methods have yet been established for MBC. Testing procedures in literature hence follow or are inspired by standards for natural fibreboards or plastic materials. Although this limits a direct comparison of MBC properties across studies, the reported results can be summarised to generate a basic understanding of the material's mechanics.

In compression, the most commonly tested property for MBC, the material reaches strengths ranging from 0.001 to 1 MPa [55, 17, 11]. Both stiffness and strength increase with robuster mycelium growth and increasing substrate density, for example achieved by chopping fibres [78, 16, 79]. Furthermore, residual water affects the compressive strength of the MBC, although this was never systematically evaluated [16]. Overall, the area under the compressive stress-strain curves has been used to quantify the composite's toughness, giving values ranging between 8 and 18 J [45, 80].

Tensile strengths vary from the order of 0.01 to 10 MPa, for non-pressed to heat-pressed composites [11, 81, 82]. This wide range is partially attributed to the fungal species being used, where differences in cell wall composition change their elastic strength and behaviour. In terms of tensile moduli, non-pressed and cold-pressed MBC find similar properties to foam-like materials, as presented in Figure 7. Heat-pressed materials reach into the properties of natural materials.

For MBC tiwh foam-like density the flexural moduli and flexural strengths are reported between 1-192 MPa and 0.07-0.29 MPa, and can be increased to 680 MPa and 4.6 MPa by heat-pressing, respectively [42, 83, 81, 22]. In contrast, soaking MBC samples decreases the flexural strength by ten-fold [32]. It is commonly known that the planar structure of vegetative hyphae that forms around the composite is advantageous to its mechanical properties and the first to fail in flexure, thereby marking the composite's strength [17, 42].

A small tabulation of mechanical properties in Table 2.1 shows some of the higher mechanical properties for unpressed MBC appearing in literature, normalised to their density. The material reaches

towards EPS for compressive and flexural properties, but underperforms in tension. The same applies for heat-pressed samples compared to natural fibre-board. Clearly, densification is not the sole reason for the increased properties in MBC, but these could also originate from differences in fibre types, their orientation, and/or additional chemical reactions induced.

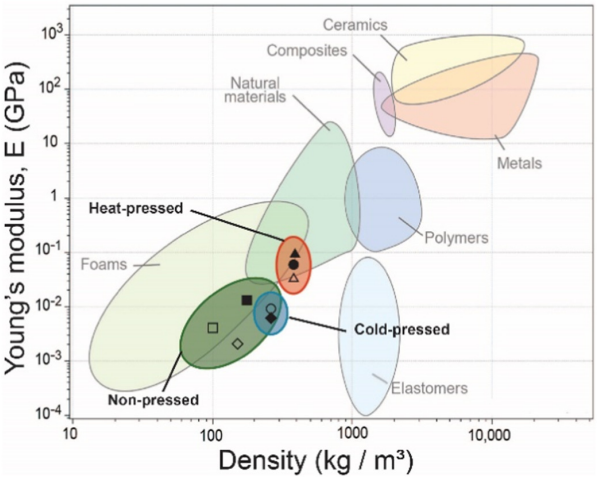

Figure 7: Ashby plot showing representative Young's moduli of MBC in its non-pressed, cold-pressed, and heat-pressed form as a function of density, presented by Appels et al. (2019) [42].

	Unpressed		**Heat-pressed**	
Density	<300 kgm^{-3}		300-1200 kgm^{-3}	
	Stiffness (kPa m^3 kg^{-1})	Strength (kPa m^3 kg^{-1})	Stiffness (kPa m^3 kg^{-1})	Strength (kPa m^3 kg^{-1})
Compression	28 [72]	8.2 [72]	-	-
	hemp hurds	*hemp hurds*	-	-
	998	18.9	-	-
Tensile	4.0 [84]	0.6 [84]	602 [85]	1.16 [85]
	sawdust	*sawdust*	*hemp*	*hemp*
	566	22.6	1600	9.3
Flexural	827 [83]	1.7[42]	2026 [72]	864 [72]
	sawdust	*sawdust*	*hemp hurds*	*hemp hurds*
	566	22.6	2700	10.7

Table 2.1: Comparison of some of the highest mechanical properties reported for MBC, normalised by their densities. Properties for EPS and natural fibreboard are shown in brown, and obtained from Granta EduPack for densities of 50 kgm^{-3} and 750 kgm^{-3}, respectively.

A review of Jones et al. (2020) showed that MBC strengths can differ 10-fold for different substrate types [86]. Furthermore, more flaky substrates could potentially improve the shear strength of a MBC by having an increased cohesion under stress due to particle locking, a mechanism reported to occur in granular materials [55, 87]. This effect however did not emerge in MBC modelling efforts of Islam et al. (2018), where varying particle sizes from 2 to 10 mm at constant volume fraction did not vary the materials compressive properties [88]. Also, Girometta et al. (2019) report in their review that the fibrous fabric substrates used by Jiang et al. (2016) and Ziegler et al. (2016) favor fungal colonization, in contrast to more incoherent and loose materials like hulls and straws that are often introduced in MBM [16, 89, 46]. It proves difficult to isolate the role played in material mechanics by the substrate mechanical properties, their size, their influence on mycelium growth, and the substrate-mycelium interface.

Only four studies present methods to quantify the mycelium-substrate interface. Three measure the internal bond strength (IB) by tension parallel to the surface of either heat-pressed or cold-pressed but heat-killed MBC. Elsacker et al. (2021) report 0.05 MPa and required the addition of bacterial cellulose, Liu et al. (2019) found a strength of 0.18 MPa if the composite was heat-pressed at 200 °C, and finally Sun et al. (2019) measured 0.06 MPa and required the addition of cellulose nanofibrils [85, 90, 91]. Ozdemir et al. (2022) performed pull-out tests of wood veneers embedded in a MBC material to evaluate their bond strength, and measured a bond strength of 0.34 MPa [72]. In all of these tests, the resulting fracture surface is poorly evaluated, and fungal penetration is not assessed.

Little studies report on the failure modes of their tested specimens, and evaluate the role of fungal adhesion and/or penetration on the mechanical properties. In compression, collapsing of the mycelium foam is followed by densification of the substrate material, where no clear point of failure can be identified [88]. Both bulging and shear failure can be observed, where the latter is prevented by the fibres [79, 92] Some studies report on crack appearance, but do not discuss crack initiation or development [70, 79]. In tension, the role of the mycelium-lignocellulose interface or mycelium network strength on the failure mechanism is not discussed, even though the strength and stiffness of lignocellulose is much higher than that of mycelium. Initial results do show pressing of MBC to increase the tensile strength and stiffness but to decrease the rupture strain from 4.7 to 0.7%, where the role of densified mycelium or fibre alignment due to pressing cannot be distinguished [42]. Besides, images of fracture surfaces do not portray adhesive of cohesive failure of the mycelium. SEM images by Kuribayashi et al. (2022) did highlight the hyphae to have cleaved wood cell walls, covered their lumen, and to have grown into their tracheids, although they could not further assess the depth of fungal penetration [32].

2.2.3. Additional composite reinforcement

The current means to improve the mechanical properties of MBC go beyond the optimisation of fungal growth and the material's consolidation, where the potential of additional reinforcement on a larger scale has been explored. Rigobello and Ayres (2022) found significant changes in their compressive Young's moduli and ultimate strengths by insertion of reed fibres coaxial to load and hessian jacketing coaxial to load [55]. The insertion of 5 rattan fibres furthermore increased the flexural modulus and modulus of rupture by approximately 5- and 10-fold, respectively [83]. No such drastic increases in flexural properties were found when inserting inner hessian or hessian jacketing, as shown in Figure 8A. Hence, the addition of architected fibres can improve the mechanical properties, but is not straightforward for MBC. A third study by Özdemir et al. (2022) introduced reinforcing veneer structures [72], as shown in Figure 8B. Where the introduction of one layer of high-density wood veneer reinforcement did not significantly change the flexural strength of the MBC, the introduction of one low-density reinforcement layer increased the flexural strength more than twice compared to the unreinforced block. These results were related to the failure mode of the reinforced composite.

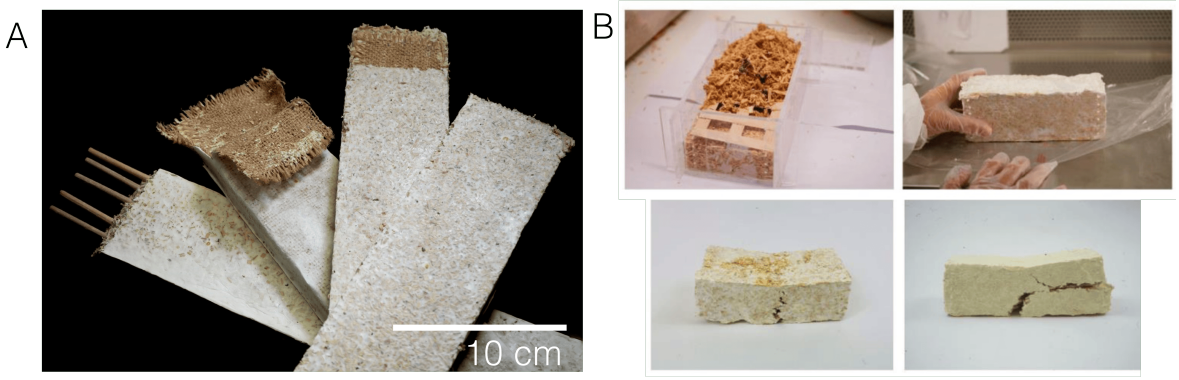

Figure 8: Additional reinforcement in MBC, by insertion of rattan fibres or jacketing (A) [83] or wood veneer (B) [72].

To increase MBC properties with reinforcement these should adequately bind to the MBC. For example, Rigobello et al. (2022) show that hessian jacketing around MBC did not debond at flexural failure, and a continuous interfacial bond between MBC and rattan fibres allowed them to increase the material's stiffness and strength with both reinforcements [83]. Contrastingly, wood veneer reinforced MBC showed increasing amounts of debonding and interlaminar shear failure between the mycelium and wood veneer with increasing reinforcement density, reflecting how the low interface strength fails to transfer loads to the stiffer and stronger reinforcement [72]. Similarly, Rigobello et al. (2022) reported on inherent reinforcement displacement during loading [83]. Also in mycelium sandwich materials, where a random fibre oriented MBC is laminated between lignocellulosic mats, one of the most common failure modes is interlaminar shear failure of the skins [16]. If this binding could be improved however, additional reinforcement could serve a natural way of strengthening the composites in their living state.

2.2.4. Living properties

MBM research in the last 5 years has progressed to utilise more of the living mycelium than solely its self-assembling capabilities, such as its regenerative growth. Mycelium portrays the ability to self-heal upon damage or bio-weld blocks of MBC together over distances up to 10 mm [93, 17, 1]. The latter provides another strategy for the upscaling of mycelium based structures. Next to its growth-related capabilities, the fungus is known to generate and transmit electrochemical signals across large distances for communication purposes.

Fungi use electrochemical signalling along their hyphae to respond to stressful situations, such as when it reaches nutrient depleted environments. Extensive biochemical cascades cause changes in the ionic balance along the hyphal cell wall. Ca-ion fluxes are understood to be the main contributor, passing mainly through channels and Ca^{2+} pumps [94, 95]. The importance of these ion fluxes was already recognised earlier in this this literature review, for the hyphae's growth at its tip. Material researchers are currently working to gather the microbiological processes behind this signal generation, to facilitate a subsequent interpretation of the signals that can be captured. Namely, recent work by Adamatzky et al. has shown that the electrochemical signalling of the fungus in response to the application of mechanical loads or light can be measured in the living materials [18, 96]. The authors even foresee the mycelium's use in fungal electronics [97]. Both functionalities of signalling and self-healing however set requirements to the state of the material.

For MBC to become truly engineered living materials (ELM), they need to be moisturised and provided sufficient nutrients to remain active. These living properties can also be regenerated within a few days from the material in its dormant state, given that the material has solely been air-dried and not given heat-treatments higher than 60°C [93, 17, 69]. Living composite materials are however reported to be more fragile, of which the mechanical properties have yet been poorly studied [9]. The study by Mcbee et al. (2022) reports a compressive strength of 0.12 MPa, compressive stiffness of 0.14 MPa, and flexural stiffness of 0.23 MPa for unpressed living MBC blocks [17]. Realising these are all a magnitude lower than those reported for the unpressed but dried MBC shown in Table 2.1 confirms the weaker properties of living MBC.

2.2.5. Microscopy of the mycelium substrate interface

The microstructure of MBC is typically assessed by means of either optical or scanning electron microscopy (SEM). This allows the observation of the mycelium morphology on substrates and the identification of hyphal penetration on the surface, as already shown in Figure 9A [91, 32]. It is not yet used used as a systematic means to understand the interaction between the mycelium and substrate material throughout the composite, and to assess the depth of fungal lignocellulose penetration and digestion. The latter is currently evaluated by means of mass loss or using FTIR [55, 78, 98]. The first requires careful drying procedures due to the hygroscopic nature of the substrate material. The latter can solely show trends in lignocellulose component amounts throughout the degradation period, but cannot easily quantify amounts of degradation in absolute terms. Literature in the field of wood decay show the potential of optical microscopy in combination with staining to assess hyphal growth on the substrate material and its digestion simultaneously.

The contrasting colours created by staining can identify molecular changes and help highlight structural differences [54]. The combination of safranin red and astra blue has been found to allow evaluation of white-rot decay in both hardwood and softwood specimens, as can for example be seen in the systematic studies of Srebotnik and Messner (1994) and Lehringer et al. (2010) [99, 100]. Their micrographs, as shown in Figure 9B and Figure 9C, display the degraded regions by white-rot fungi as blue, which increases in area with progressing degradation in Figure 9B. Safranin stains lignin red, where astra blue stains cellulose blue solely in case of lignin absence, allowing these dyes to be used as both indicative and quantitative tracers for lignin degradation [101]. It can hence be hypothesised that in future studies on MBC this approachable staining method can be used to identify delignification in the substrate, and thereby better the understanding of the mycelium-lignocellulose interface.

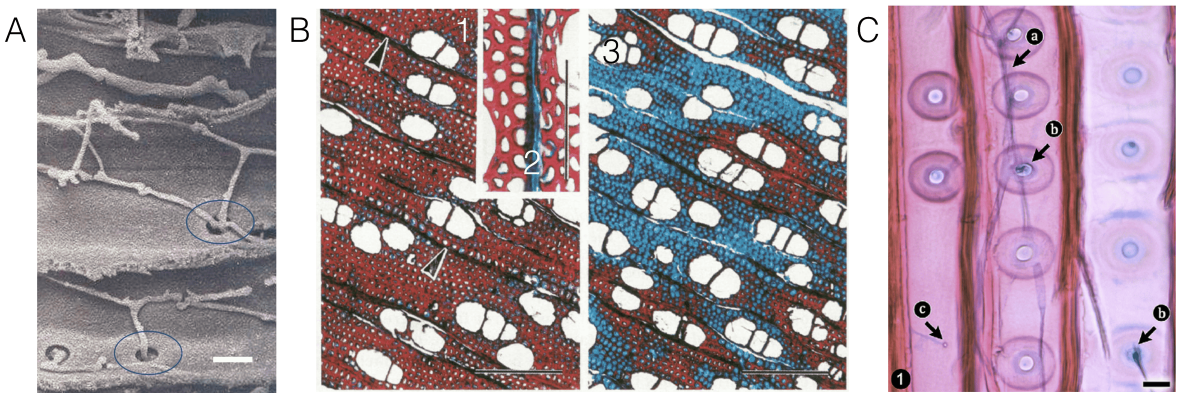

Figure 9: Microscopic evaluations of the mycelium-wood interaction. SEM image of hyphae penetrating bordered pits in softwood, marked with blue circles [57] (A). Scale bar is 10 μm. Transverse section showing the delignification by white-rot fungi in birch wood after 2 weeks (1,2) and 6 weeks (3) of decay (B) [99]. Scale bar is 250 μm. A radial section showing hyphae of *Physisporinus vitreus* growing through the lumen of Norway spruce wood after 3 weeks of incubation (C) [100]. Scale bar is 10μm.

2.3. Research gap

The current existing literature on MBC materials reflects their limited applications due to low mechanical properties, with a lack of understanding on the mechanics and microstructure of the mycelium-lignocellulose interface. This is complicated to study due to the biological variability, heterogeneity, and fragility of the material. The poor binding however limits the natural fibre's reinforcing ability, and potential to improve the material's properties in its living state. Given the basic understanding of mycelium growth, the varying factors in MBC production are hypothesised to vary this interfacial bonding. Hence it is of interest to systematically study the influence of provided nutrients, substrate material and porosity, and growth time on the fungus-substrate interface in its living state.

The most appropriate testing setup for this purpose should be chosen, which depends on its ability to test the weak, easily compressible mycelium adhesive. Furthermore, it should solely evaluate the mycelium's interfacial bonding, and not its substrate embracing growth. A list of commonly applied adhesive testing procedures and a conclusion on their applicability for this purpose is presented below.

- **Tape test** - The evaluation of the fracture surface will only be qualitative, given the similar colours of both the mycelium and substrate material. It will not result in a quantified understanding of the adhesion mechanics.
- **Peel test, 90°and 180°** - Use of a flexible lignocellulosic adherend will likely make it thin enough for the fungus to penetrate and form a film on the opposite side of inoculation, disturbing adhesion measurements.
- **Lap-shear test** - Would provide a stable testing method. Could be used to measure the mycelium's joint strength, but not accurately determine the adhesive's response upon progressive loads.
- **Interfacial shear test** - The shear loads are likely to condense the mycelium networks, and thereby complicate data interpretation.

- **Single lap three-point bending** - Would provide a stable testing method. Could be used to measure the mycelium's joint strength, but not accurately determine the adhesive's response upon progressive loads.
- **Tensile test** - Would provide a stable testing method. Allows evaluation of the adhering mycelium's stiffness and strength, but not a detailed understanding of damage propagation.
- **Single edge notch bend** - Would require testing of the bulk MBC. However, the inherent weakness of this material makes it prone to deformation at the loading points, and therefore a non-accurate testing method.
- **Compact tension** - The small adhesive volume in comparison to substrate material makes the samples vulnerable for testing the weak mycelium adhesive, and only allows a short crack length to be evaluated.
- **Double cantilever beam (DCB) test** - Would provide a stable testing method. Could be used to evaluate the mode I interlaminar fracture toughness (G_I) of the mycelium adhesive, improving the understanding of its reponse to mode I loading conditions.

Of the achievable testing methods, DCB would provide a means to fill the knowledge gap presented above. It could quantify the resistance of the mycelium matrix to crack propagation, which has not yet been reported in current literature. Additionally, the use of an applicable interface evaluation method will deepen the understanding of the mycelium-lignocellulose interface microstructure, and the degree to which this can be modified by changing the fungus' growth environment.

3

Research definition

3.1. Research objective

The research objective of this study is to evaluate and manipulate the ability of a living mycelium network to carry loads in a MBC material. It aims to do so by measuring the properties of an adhesive fungus in a mode I loading condition, which will be generated by a DCB testing setup. This study would be the first to quantify the G_I of a mycelium network in varying growth conditions.

The goal is to modulate the mycelium and mycelium-substrate microstructure by means of adjusting the fungus' growth time, substrate material, and supplied additional nutrients. The last will be facilitated by growing the mycelium network inside DCB specimens from a 3D-printed fungus-laden ink, that allows control on the exact location of the fungus and the sugar amount it is provided. This work will thereby furthermore set a basis for future work that aims to optimise living MBC mechanical properties by leveraging the great potential of automated 3D printing of the fungus.

3.2. Research questions and hypothesis

The research questions needed or aimed to be answered within the research objective can be subdivided into three sections. They cover the DCB test setup development and sample preparations, the evaluation of G_I of the living and hydrated fungus for varying sample configurations, and the evaluation of the fungus' growth and digestion of the substrate material.

Testing setup and sample configuration

1. What are the essential steps in the mycelium-laden ink production procedure of Gantenbein et al. (2023), to facilitate its use as a 3D printed inoculum in DCB samples [1]?
2. Can a DCB setup be developed and allow the quantification of the G_I of an adhesive mycelium network between lignocellulosic substrate materials?

G_I measurements

3. Can we measure an effect on the mycelium's G_I of:
   (a) a prolonged growth time?
   (b) an increased supply of easy digestible sugars in the inoculating ink?
   (c) a change in substrate material, providing a different substrate chemistry and porosity?

Interface evaluation

4. Does the mycelium's substrate penetration and digestion change as a function of the supplied amount of easy digestible nutrients, or with different substrate materials used?

The main hypothesis of this work is that a DCB setup can be used to evaluate the G_I of a mycelium adhesive network between lignocellulosic substrate materials. Here it is believed that the fungal growth can be well controlled and modulated by inoculating the test specimens by means of 3D printing with varying ME concentrations. Additionally, an optimal ME concentration and growth time can be found that correspond to the strongest substrate digestion and penetrating mycelium, which can be recognised by a low but relatively high G_I. It is hypothesised that both a better digestable and more porous substrate will facilitate deeper hyphae penetration, and thereby increase the measured G_I.

3.3. Project scope and outline

The presented research question are in chronological order with respect to the project scope and outline of this thesis work. For research question 1, the mycelium-laden ink of Gantenbein et al. (2023) will be replicated and tested for its rheological properties [1]. It will be optimised for the automated inoculation of DCB specimens by means of recipe modifications. Then, for research question 2, a DCB specimen will be designed with wooden veneers, and inoculated by means of 3D printing of the optimised hydrogel. A testing setup with the available equipment at the Aerospace faculty will be constructed. The DCB specimens will be prepared with:

- White-rot fungus *G. lucidum*
- Wooden veneers: 5 mm thick hornbeam, 3 mm thick beech, and 3 mm thick Norway spruce
- Printing ink: 0%, 5%, 10%, and 15% ME concentration
- Mycelium growth time: 3, 4, and 5 weeks

the last three materials or parameters are varied in order to allow answering of research questions 3a, 3b, and 3c. Hornbeam and beech are chosen for both being hardwoods of the same density, but with a reported better growth of *G. lucidum* on beech. Spruce is chosen for its lower density and therefore higher porosity. The ME concentrations are in line with the studies of Gantenbein et al. (2023) [1], where the mycelium growth time is varied around the typical 4 weeks for MBC materials.

Lastly, the interface of the mycelium and substrate will be evaluated by means of the following three methods:

- Optical microscopy, using safranin red and astra blue staining
- SEM
- FTIR

in order to answer research question 4.

The microbiological work, mechanical testing, and interface evaluation will be performed with the available methods and equipment at the Aerospace faculty of the TU Delft. Solely optical microscopy sample preparation and evaluation will be performed at the Civil Engineering faculty.

4

Materials and methods

4.1. Mycelium hydrogel development

The use of direct ink writing (DIW) as a method of automated fungi placement requires a mycelium-laden shear-thinning ink with a fast recovery, which Gantenbein et al. (2023) already succeeded to develop [1]. This ink was therefore initially replicated according to their standard recipe:

- Cellulose based thickener (Vivapur 811P, JRS, Rettenmaier Benelux C.V.) (30 g/L)
- Agar (15 g/L, 05040, Millipore)
- κ-carrageenan (15 g/L, 22048, Sigma Aldrich)
- Peptone (5 g/L, P6838, Millipore)
- ME (100 g/L, 70167, Millipore)

Of these substances, ME and peptone serve as the main nutrient supply for the fungus. The type and concentration of cellulose based thickener, agar and κ-carrageenan determine the viscoelastic properties of the ink by their gelling behaviour. The ink was produced following a procedure inspired by Gantenbein et al. (2023), of which the workflow is displayed in Figure 10 [1]. The individual steps are described in Appendix A, where it is important to note that the fungal inoculum was taken at a random location from earlier overgrown MEA plates inoculated with *G. lucidum* M9726 spawn of Mycelia. These plates were stored in the fridge for no longer than two months.

The yield stress and recovery time of produced non-inoculated inks were obtained by rheology experiments performed on a Thermo Scientific Haake MARS III Rheometer-FTIR. The yield stress is typically around 100 Pa and should be sufficiently high to control the printing process, where the recovery time marks the ink's transition from viscous to elastic, which should not exceed a few seconds to provide print stability. The testing procedures were as follows:

- **Yield point**
  Apply a step-wise increase of shear stress from 1 to 3000 Pa, increasing with 10 Pa per s.
  Record shear stress (τ) and shear-rate ($\dot{\gamma}$), until shear-rate exceeds the apparatus' range.
- **Recovery time**

  1. Apply an oscillatory τ of 1 Pa with a frequency of 1 Hz for 60 s.
  2. Apply a $\dot{\gamma}$ of 50 s^{-1} for 30 s.
  3. Apply an oscillatory τ of 1 Pa with a frequency of 1 Hz for 60 s.

  For stages 1 and 3, record the storage modulus, G', and loss modulus, G", as a function of time, t. For stage 2, measure the viscosity, η, as a function of t.

The yield point was determined by the cross-over of two linear fits on the yield point data set, fitting the data before and after the yield point. Where curve-fitting models are a more scientific approach to the yield point determination, the applied method is quick, easy, and common for retrieving a rough indication of the yield stress. The recovery time was taken as the time lag between the initiation of the third phase in the recovery test, and the moment at which the recorded storage modulus G' exceeds the loss modulus G", hence the elastic properties of the material are retrieved.

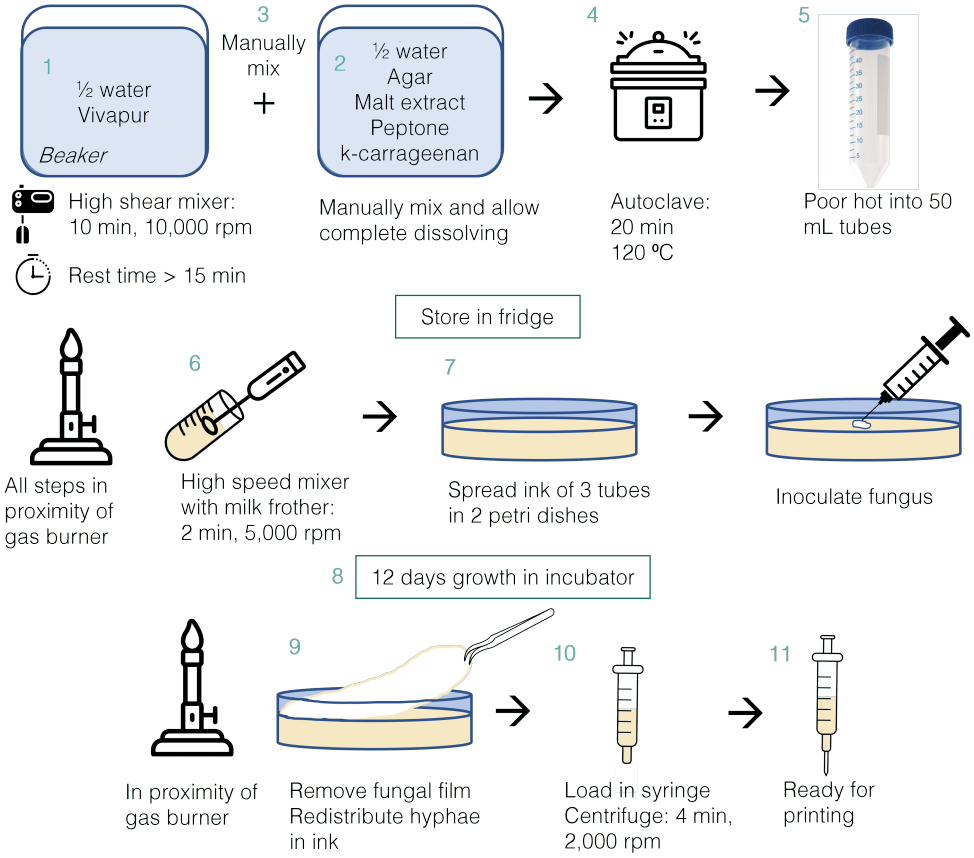

Figure 10: Workflow of mycelium-laden ink production, inspired by [1].

Printability was evaluated by 3D printing of hydrogel grids as presented by Gantenbein et al. (2023), and printing of single layers [1]. The first reflects the ink's ability to hold the weight of multiple print lines, and thereby form a stable structure in 3D. The second test allows the observation of single print line disturbances due to ink heterogeneity or clogging of the nozzle, and the widening of single print lines along the print. The latter could result from ink sagging upon its own weight, or due to build-up of pressure in the nozzle and corresponding larger extrusion volumes. Both discontinuous print lines and print line widening are undesired, where the first causes a discontinuous fungal inoculum and the latter decreases the amount of substrate area available for fungal growth and binding.

4.2. Double cantilever beam testing

The DCB testing setup, test specimens, and testing procedure were inspired by the ASTM standard D5528-21 for mode I interlaminar fracture toughness, G_I, for conventional unidirectional fiber-reinforced polymer matrix composites [102]. G_I is defined as the decrease in elastic strain energy U in the specimen, per increase in the adhesive crack area. With a constant crack width b this gives:

$$G_I = -\frac{1}{b}\frac{dU}{da} \tag{4.1}$$

with increasing crack length a. This definition will be used to quantify and discuss G_I for the living mycelium adhesive in specimens of the parameter sweeps earlier described in section 3.3.

4.2.1. Testing setup

A typical DCB specimen is depicted in Figure 11, where wood veneers were chosen as the lignocellulose substrate material, on which a tensile load F is introduced on the left specimen end. Their dimensions could be well defined in line with the ASTM standard, although specimens were thicker than the usual

3-5 mm. Namely, first 5 mm thick veneers were used with a stable mycelium thickness of 1 mm, after which 3 mm veneers were used to slow down crack propagation. Nevertheless, the veneer's stiffness and estimated mycelium G_I left the specimen thickness in the range advised by the standard. Similarly, an initial crack length a_0 of 39 mm created with a 60 mm insert was acceptable, and facilitated the evaluation of a crack development of 110 mm on average, with a specimen length of 180 mm and veneer holder of 10 mm at the end. The veneers' thickness was essential for handling of the specimens without damaging the mycelium. Furthermore, it facilitated the specimen insertion into the testing setup.

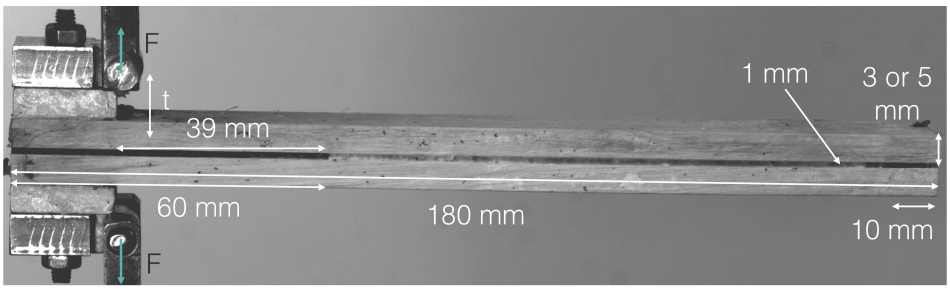

Figure 11: DCB specimens as designed for this study.

Intermediate aluminium blocks had to be screwed onto specimens, to create a stable load transfer from the testing bench to the specimen. This provides a cheap alternative in contrast to direct placement of either piano hinges or loading blocks as indicated by the ASTM standard [102]. Two M4 screws could fix the aluminium blocks to the veneer, where common glueing approaches were not compatible with the wooden substrates [1]. It is important to recognise that the pulling force will hereby be concentrated at the screw locations rather than evenly distributed across the entire specimen width. After specimen preparation the same screws could fixate loading blocks, that could position the specimen in the testing bench. A 10 kN bench equipped with a 100 N load cell could best capture the expected forces around 10 N, the upper load limit reached with preliminary experiments. Furthermore, load transfer plates were preferred over load transfer cylinders, as displayed in Figure 12. This allowed the testing of slightly misaligned specimens, without the introduction of shear forces that would cause the mycelium network to break and render specimens untestable.

4.2.2. Specimen preparation

Three different wood species' veneer was gathered for this study as listed in Table 4.1 [2], and prepared for inoculation. Bax Hout in Terheijden supplied untreated veneers, cut in dimensions of 180 x 25 x 3 or 5 mm from single wooden planks, taken mainly from the sapwood of trees. The species were selected based on their documented low durability against fungal infection, as confirmed by relevant literature on *G. lucidum* for the hardwoods hornbeam and beech, and other white-rot fungi for the softwood spruce [103, 104]. The latter was mainly selected for its lower density and thus larger porosity, hypothesised to induce more fungal penetration and thereby potentially better fungal adhesion. Before testing, the aluminium load block were attached to the veneers as described previously. Then, the arms were soaked in distilled water for 44 to 48 hours for hornbeam and beech, and 22 to 24 hours for spruce, and autoclaved for 20 minutes at 121 ℃ (Hirayama HG-50). After a few hours of cooling down, the specimens were inoculated by automated means [3].

[1] Adhesion experiments were performed with Loctite EA 3440 epoxy, Bison universal epoxy Kombi Metaal, Pattex Epoxy Super Mix Universal, and Bison PU Bruislijm. Aluminium load block surfaces were roughened by glass beads and glued to dry hornbeam veneer according to the glue's instructions. After further specimen treatment of soaking and autoclaving (to be described in subsection 4.2.2) all blocks could be manually removed, and glues showed both cohesive and adhesive failure.

[2] Wood durability is in literature commonly scaled from 1 to 5, with 5 indicating the highest susceptibility to infection.

[3] A maximum effort was put into working in a sterile environment to prevent contamination of the specimens. All working benches, equipment and materials used were autoclaved if possible, else cleaned with 70% ethanol. Ink and specimen production was performed in close proximity of a gas burner

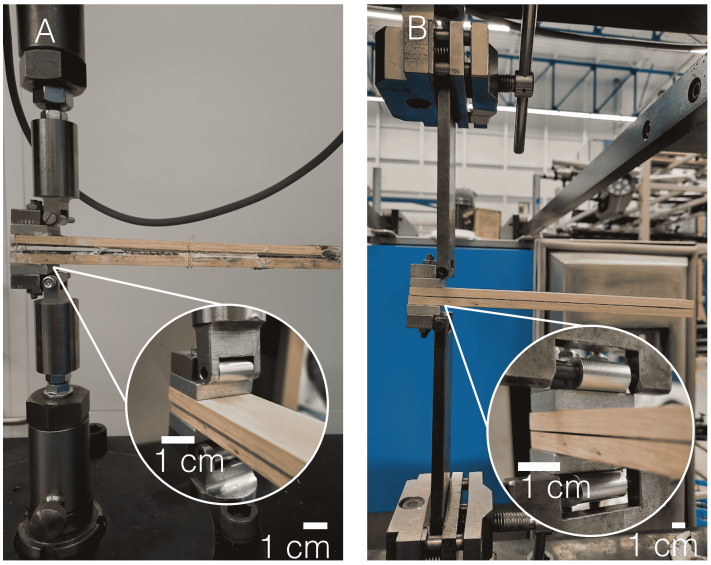

Figure 12: DCB specimens can be inserted into the testing back with the use of two load transfer methods. A shorter setup is achieved with loading cylinders, that provide only a tight space for load block insertion (A). A longer setup is created when using loading plates, that provide more freedom for load block insertion (B).

Name	**Species**	**Density (kgm^{-3})**	**Durability** [105]
Hornbeam	*Carpinus betulus*	750	5
Beech	*Fagus sylvatica*	710	5
Spruce	*Picea abies*	460	4

Table 4.1: Wood species used in this study.

The mycelium-laden ink described in section 4.1 was produced beforehand, and 3D printed with a 0.84 mm nozzle on the bottom veneer arm in a custom-build Ultimaker 2+, as shown in Figure 13A. The Grasshopper file developed by Gantenbein et al. (2023) was adjusted to generate a G-code for printing, designed to meet three criteria [1]. Firstly, a height of 2 layers ensured such that both stacked veneers were equally inoculated. Then, an in-between print line gap of 2.5 mm was set to be reached after veneer stacking, the maximum bridging distance of the fungus reported by Gantenbein et al. (2023) that allows the fungus to cross between adjacent print lines and form a continuous network [1]. Lastly, the dimensions of the print corresponded to the crack area to be evaluated, of approximately 110x25 mm. This resulted in a zigzag line pattern that covered the width and partially length dimensions of the veneers, as shown in Figure 13B.

After printing, the arms were stacked with a small, 10x25x1 mm, and a big, 60x25x1 mm, 3D printed polycarbonate growth stopper placed between them, see Figure 13B. This maintained a constant gap for mycelium growth and created an initial crack length. Similarly, polycarbonate corner blocks were printed to facilitate alignment of the veneers regardless of their dimensions, when held together with elastic bands. Finally, strips of stretched Parafilm were wrapped around the complete specimen to confine the fungi to grow on the surface areas between the specimen arms, see Figure 13C. This left the specimens ready for growth.

The mycelium growth was optimised by controlling the environment of the specimens after their production. Specimens were placed in groups of four in plastic containers containing sufficient oxygen, and a layer of distilled water to bring the humidity to 90%. This is higher than the recommended 60-65% in section 2.1.3, but showed more growth in preliminary experiments, and was the same as supplied by Gantenbein et al. (2023) [1]. Inside a growth chamber the mycelium grew in the dark at a stable temperature of 26°C. Unlike the humidity and temperature, the moisture content of the veneers could not be controlled, and was therefore shortly evaluated separately.

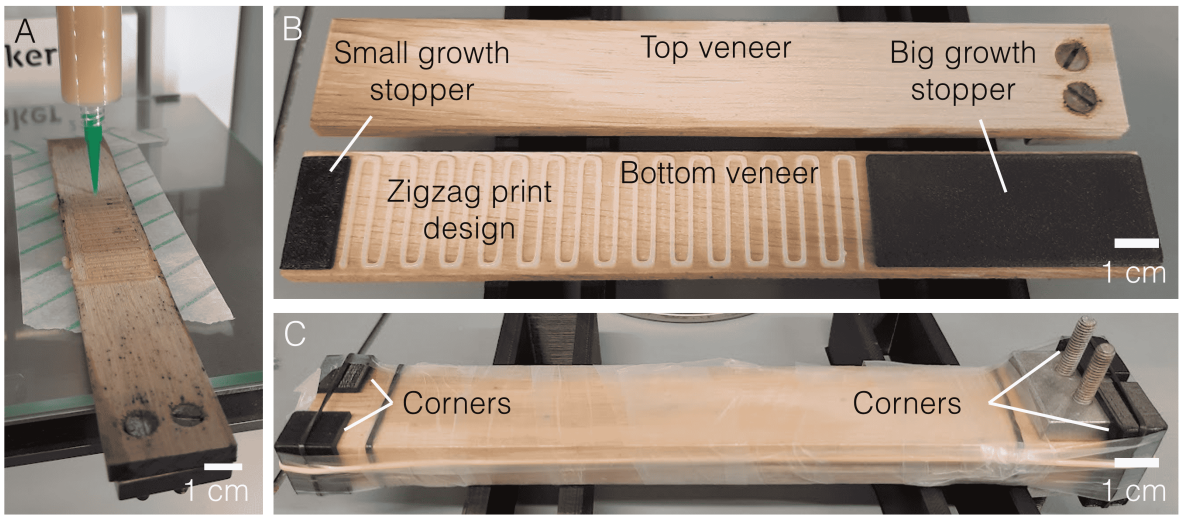

Figure 13: Printing of the mycelium-laden ink on the bottom veneer (A), placing of the growth stopper inserts (B), and stacking, aligning, and wrapping of the complete specimen (C).

The moisture content of non-inoculated veneers did not decrease below the critical value of 30% when subjected to the same conditions as inoculated specimens. Three pairs of veneers were soaked for 46 hours for hornbeam and beech, and 23 hours for spruce. All samples were autoclaved and wrapped in Parafilm, to be put in the same growth conditions as inoculated specimens. Their moisture content was calculated based on their weight:

$$M_f = \frac{W_f - W_i + 0.11 * W_i}{W_f} \tag{4.2}$$

Where M_f is the final moisture content, W_f is the final weight of the specimen, and W_i is the initial weight of the specimen. The initial moisture content was reported to be 10 to 12%, and therefore taken as 11% for all specimens. The moisture content of veneers should minimally be 30% to allow fungal growth during the planned experiments.

All samples were prepared according to the above presented procedure and systematically made ready for testing after growth. First, intermediate loading blocks were attached to the specimen's aluminium blocks before Parafilm removal, to limit damage to the specimens. Subsequently, mycelium growth around the large growth stopper was removed with a 0.03 mm metal sheet and 1 mm wire. After removing the Parafilm, any mycelium films on the sides of the specimen were carefully scraped of using a razor blade. The specimen was now ready for direct testing in its undried state. An overview of the tested specimens is shown in Figure 14, for which the choice was described previously in section 3.3.

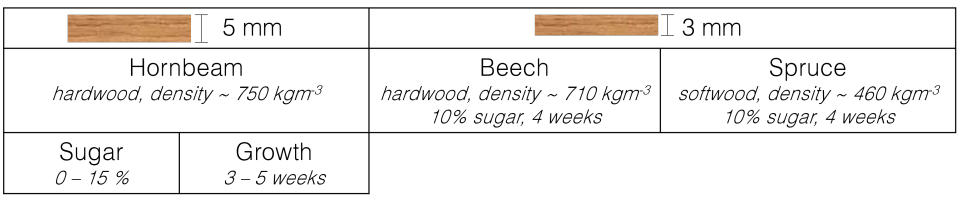

Figure 14: An overview of the specimens to be evaluated for their G_I in this study.

4.2.3. Testing and data processing procedure

The testing procedure adhered to the ASTM D5528-21 standard [102]. Any specimen, along with its attached loading blocks, could be placed in the loading clamps using two long bolts, as depicted in Figure 12B. First, a non-soaked dummy specimen arm was inserted in the test setup to zero the force, creating a small pre-compression in test specimens that could be corrected for during data analysis. The actual DCB tests were performed with a low controlled vertical crosshead movement of 1 mm/min, to avoid viscosity effects in the hypothesised weak mycelium interface. The test continued until the specimen fell apart, or the crosshead was displaced with 20 mm. The reported displacement had an error of only 0.5% compared to an extensometer, falling within the acceptable range of 2% specified by ASTM 5528-21. Together with the recorded load the Zwick data was used for subsequent data analysis.

The G_I was determined using an analytical approach, as standard methods of optical crack recording were not possible with the porous mycelium network. Therefore, data analysis relied on the methods presented by Ran Tao (TU Delft), of which graphical representation is presented in Figure 15 [106]. It obtains G_I at every point of the load, P, versus extension, δ curve after the peak load, P_{max} has been reached. This peak is assumed to occur at an extension, or displacement, that corresponds to a crack length equal to the intial delamination length a_0. Hereafter, G_I is calculated using the formula:

$$G = \left(\frac{9P^4\delta^2}{4E_{xx}Ib^3} \right)^{1/3} \tag{4.3}$$

with E_{xx} the arm's Young's modulus, I its moment of inertia, and b its width, where E_{xx} can be obtained from a linear fit to the initial part of the loading curve. I and b result from the veneer's dimensions. The formula determines G_I purely on a decrease in the arm's compliance. It relies strongly on the assumption of the simple beam theory with clamped boundary condition, a linear elastic arm, and a thin adhesive with no deformations. It then allows one to calculate a predicted crack length after testing.

A virtual crack length, a, at each point on the load deflection curve can be calculated using the modified beam theory (MBT) method. Again relying on the simple beam theory's assumptions, this gives:

$$a = \frac{3P\delta}{2bG_I} \tag{4.4}$$

Hence a is analytically determined and not measured optically. This allows one to only test and evaluate one loading cycle, in comparison to conventional fatigue DCB tests. Finally, the ASTM standard warns for two potential errors that could be introduced by large arm displacement and its stiffening due to the attached load blocks.

The large displacement correction factor, F, is required if the displacement to crack length ratio δ/a is bigger than 0.4 at any point during the test. F accounts for the shortening of the moment arm and the tilting of the load attachment blocks and is calculated as follows:

$$F = 1 - \frac{3}{10} * \left(\frac{\delta}{a} \right)^2 - \frac{3}{2} \left(\frac{\delta t}{a^2} \right) \tag{4.5}$$

where t is the height from the loading point to arm's mid-height, see Figure 11A. Additionally, a displacement correction factor N can account for stiffening of the arms due to the load blocks. This cannot be neglected as the end of the insert is 40 mm away from the load line in this study. N is given by:

$$N = 1 - \left(\frac{L'}{a} \right)^3 - \frac{9}{8} \left[1 - \left(\frac{L'}{a} \right)^2 \right] \left(\frac{\delta t}{a^2} \right) - \frac{9}{35} \left(\frac{\delta}{a} \right)^2 \tag{4.6}$$

where L' is the distance from the load line to the edge of the loading block right of this line, which is zero for this study. Both correction factors can only be calculated at the delamination onset corresponding to a crack length of a_0, as it is not further recorded. This however gives a good indication of the error introduced by shortening and stiffening of the specimen arms during testing. The correction factors would appear in the virtual crack length as follows:

$$a = \frac{3P\delta}{2bG_I} \frac{F}{N} \tag{4.7}$$

with thus F/N values deviating much from 1 influencing the data analysis.

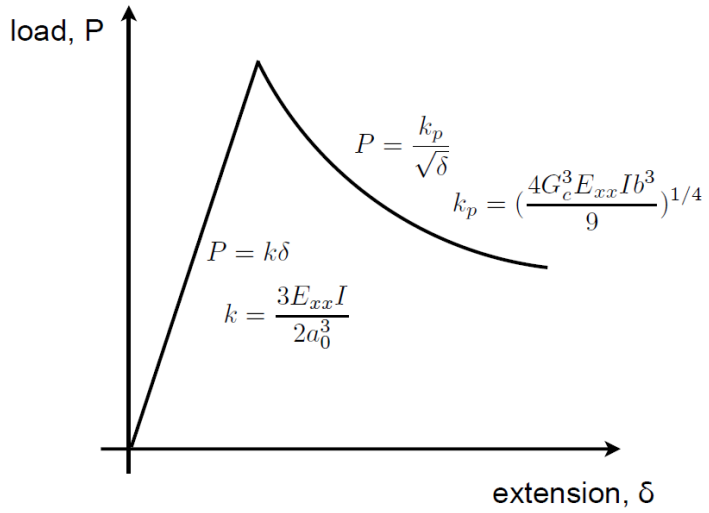

Figure 15: A typical load-extension curve of a DCB test, presented together with the analytical formulas that can be fitted to obtain G_I [106].

4.3. Flexural testing

Where the initial parts of mycelium DCB load displacement curves to be shown in section 5.2.2 are non-linear due to settling of the testing setup in this low force range, additional flexural testing on the specimen's arms was required to obtain the values for E_{xx}, to be used during data analysis. Therefore, three-point bending (3PB) tests were carried out on individual inoculated veneers.

Per wood species ten veneers were prepared for testing, which was assumed to cover the inherent variability of the entire veneer batch supplied. Samples were inoculated similarly to the DCB samples, with a 3D printed zigzag pattern that covered the entire length of the specimen. Then, small 1 mm diameter wires were placed to keep pairs of stacked veneers separated. Both the bottom and top veneer were tested, with the surface covered by mycelium oriented downwards. One supplementary batch of non-inoculated hornbeam veneers was tested to observe any differences in mechanical properties induced by mycelium growth.

Where no standard flexural testing methods exist for wooden beams of the thicknesses considered in this study, commonly used standards for wood or natural fibre based and/or composite materials were compared to find the most applicable procedure for the veneer size used in the DCB setup (25 x 180 x 3 or 5 mm). The methods considered were [4]:

- ASTM D1037 - Evaluating properties of wood-base fiber and particle panel materials [107]
- ASTM D143 - Standard test methods for small clear specimens of timber [108]
- ASTM D3043 - Standard methods for structural panels in flexure [109]
- ASTM D198 - Static tests of lumber in structural sizes [110]
- ASTM D4761 - Mechanical properties of lumber and wood-based structural materials [111]
- NEN-EN 310 [5] - Houtachtige plaatmaterialen. Bepaling van de elasticiteitsmodulus bij buiging en van de buigsterkte [112]

ASTM D198 and ASTM 4761 were not evaluated, as their setup sizes exceeded the specimen sizes of this study. The dimensions considered in the standards for panel-like materials were more appropriate, and therefore used as a basis for the final testing setup. 3PB was the best applicable final method.

[4] There was no general access to ISO standards, which were therefore not considered in this study
[5] NEN-EN standards are developed by the Netherlands Standardisation Institute and accepted in Europe.

Standard	Support type and radius	Span L : Thickness d	Loading speed N (mm/min)	Requirement of strain gauges
ASTM D1037	rounded supports radius 1.5*d	24	=0.005L^2/6d	dial gauge or linear voltage differential transducer
ASTM D143	knife edges with bearing plates	14	1.3	yoke-mounted displacement measurement device mid-plane
ASTM D3043	laterally turning bearing plates	48	=0.0015L^2/6d	dial gauge
NEN-EN 310	roller-bearing cylinders, 15 mm diameter	20	max load within 60$\pm$30 s	none

Table 4.2: Flexural standards for natural fibre materials, reviewed to determine the most the applicable procedure for this study.

Five test characteristics needed to be evaluated for 3PB tests on the wood veneers. These are: specimen dimensions, thickness to span ratio, support type and radius, loading speed, and requirement of strain gauges. As the specimen dimensions were kept equal to the arm dimensions of the DCB test, the description of the remaining four parameters by the standards is shown in Table 4.2. For support, the use of laterally rotating plates in standards ASTM D143 and ASTM D3034 is to permit slight twisting in the specimens. Since no such setup was accessible at the Aerospace faculty, neither roller-bearing cylinders with the right span distance, simple rounded supports as suggested by ASTM D1037 were being used. It should be noted that this could introduce inaccuracies in the data evaluation. Their radius was equal to the loading block, also according to the ASTM D1037 standard. The thickness to span ratio of 24 was chosen, well above the 14 generally recommended in wood testing standards. It should be kept constant to ensure failure only to occur due to the bending moment, and not due to shear deformations. Smaller ratios were not achievable for the 3 mm thick specimens with the used setup. Hence a span of 120 mm was set for 5 mm thick veneers, and 72 mm for the 3 mm veneers. The loading speed was subsequently calculated according to:

$$N = \frac{zL^2}{6d} \tag{4.8}$$

For z a value of 0.005 was taken as reported in ASTM D1037, giving a loading speed of 2.4 mm/min for 5 mm thick veneers, and 1.44 mm/min for 3 mm veneers. The ASTM D3043 standard applies a lower z value of 0.0015, but with a twice as L/d ratio fives a load speed that only differs with a factor of 0.1 for the samples of this study. Lastly, the use of a dial gauge was circumvented by using the crosshead displacement together with a compliance measurement of the testing apparatus.

The flexural modulus (E_{fl}) was obtained from the load-deflection curve according to the calculations presented in ASTM D1037 and NEN-EN 310, giving:

$$E_{\text{fl}} = \frac{L^3}{bd^3}\frac{\Delta P_{\text{fl}}}{\Delta y} \tag{4.9}$$

with L the span width, b the specimen width, d the specimen thickness, and ΔP/Δy, the load P versus deflection y curve. This slope could most accurately be determined between 10% and 40% of the maximum load P_{max} during testing, as indicated by both ASTM D1037 and NEN-EN310. The slope was taken between these two load points if the curve appears linear. This came from:

$$P_{\text{fl}} = \frac{4bd^3E_{\text{fl}}}{L^3}y \tag{4.10}$$

E_f could directly be put for E_{xx} in the analytical solution to the DCB results, as mechanically the same loading condition is induced on the specimen arm.

4.4. Interface evaluation

The mycelium and wood interface was studied by both microscopy and FTIR to evaluate the fungus' ability to grow into and degrade the substrate. The workflow of sample preparation for all three methods, to be described in the upcoming sections, is illustrated in Figure 16.

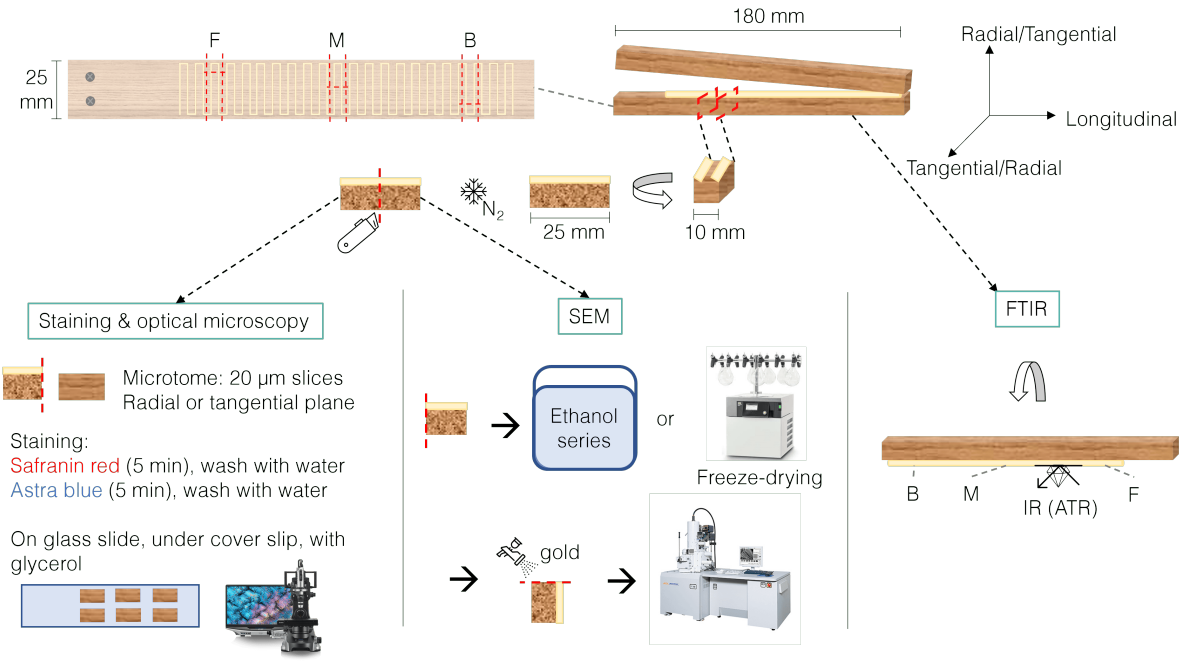

Figure 16: Sample preparation for the three interface evaluation methods, starting from a DCB sample. All methods were applied at the sample's front (F), middle (M), and back (B).

4.4.1. Microscopy: optical and SEM

Bottom arms of DCB samples of the ME series on hornbeam veneers were studied systematically, where at each ME concentration one representative sample was chosen. Of the 180x25x5 mm veneers, three pieces of 10 mm in width were cut by saw, at the front F, middle M, and back B of the specimen, as indicated in Figure 16. The pieces were not autoclaved to halt mycelium growth, as this did not allow cutting of thin slices by the microtome. Instead, the pieces of veneer were after DCB testing frozen by submersion in liquid nitrogen for 1 to 2 minutes, preserving the material's microstructure. Then, the specimens were directly cut with a sterilised craft knife at the right end for F, middle for M, and left end for B. These cut locations were chosen to account for the specimen's heterogeneous nature. All pieces were subsequently soaked overnight to be prepared for optical microscopy, where one half of the middle piece was made ready for SEM.

Optical microscopy: microtomy and staining

Veneers needed to be cut into thin slices using microtomy for observations with optical microscopy. The orientation of the specimen in the microtome was crucial for the success of the cut. The veneer was clamped in a Leica HistoCore Multicut T rotary microtome, equipped with MX35 Premier+ 34°/80mm blades, placed at an angle of approximately 4° towards a face of choice. The transverse plane could not be cut consistently with this setup. Hence the knife was then exposed to the radial or tangential plane, as pictured in Figure 17A. Which of the two planes was exposed depended on the veneer's

location in the tree, as clearly displayed in Figure 17B. For most veneers in this study one specimen side showed the radial plane, and the opposite side the tangential plane, as depicted in Figure 17C. For both planes stable 20μm slices could be cut with little damage, and transferred with tweezers as required for the staining procedure.

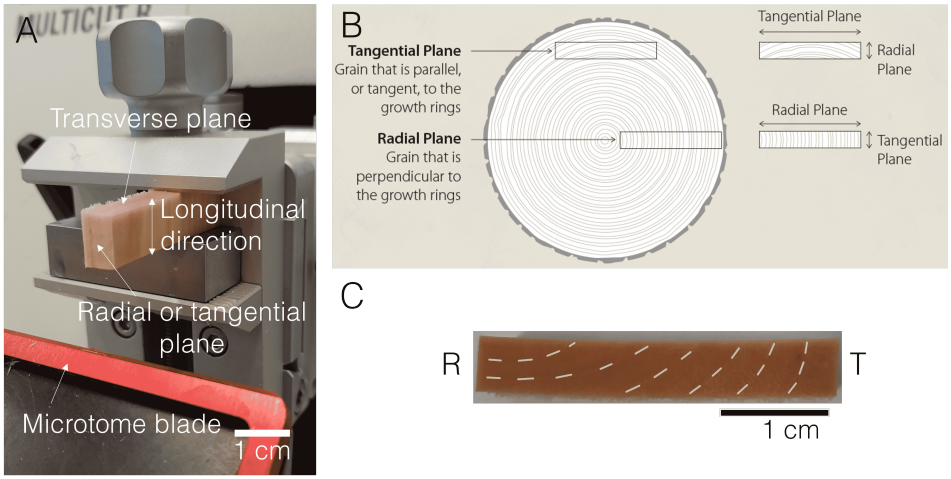

Figure 17: A: Veneer placement in the Microtome, with the radial or tangential plane exposed to the blade, and wood fibres in line with the cutting direction. B: The location of the radial section on veneer samples depends on the location of the veneer in the initial wood (Image source: http://www.jefflefkowitzchairmaker.com/). C: The veneer's orientation determines which plane of the wood is cut, where often one sample side corresponds to the radial plane (R) and one to the tangential plane (T).

Per specimen, six slices were stained with safranin red and astra blue. The wood slices were first placed on a microscope glass slide covered with distilled water, to retain their orientation and prevent dehydration. First a solution of 0.05 gr safranin O (C.I. 50240, Carl Roth) in 100 mL distilled water, following supplier's instructions, was pipetted onto the sample. After 5 minutes the slices were taken with a tweezer, and washed in distilled water. With the same steps the samples were stained with astra blue FM (C.I. 48048, Carl Roth), of which 0.1 gr was diluted in 97.5 mL of distilled water and 2.5 mL glacial acetic acid. After the final washing step the samples were fixed on the glass slide with drops of glycerol, and small weights were applied to force excesses outwards. The most representative and clean slice was analysed under the microscope.

A Keyence VHX-7000 digital microscope was used to observe the slices at different length scales with transmitted light. Full ring and non-polarised light was used for complete slice images and pictures at lower magnifications, of 30 to 200x. Polarised and full coaxial light was used at larger magnifications, up to 1500x. The primary location for feature observation was in the slices' middle, away from the sides with potential microstructure damage caused by the first saw cut.

SEM

Observing the middle veneer pieces with SEM required full dehydration of the material, to not damage the vacuum pump of the apparatus in the long-term. The frozen veneer pieces were put in a freeze-dryer (Buchi Lyovapor L-200) after cutting, where by reducing the pressure to 0.5 mPa the ice in the sample is directly converted to gas without passing the liquid stage. This retains the microstructure of the sample, now ready for SEM specific sample preparation.

The non-conductive organic specimens required a conductive coating to allow imaging with the SEM. A 15 nm thick gold layer was sputter coated on the samples, after which images could be retrieved form the secondary electrons emitted by the sample surface. Images were taken with a JEOL JSM-7500F Field Emission Scattering Electron Microscope, with an acceleration voltage of 5.0 kV and emission current of 5.0 μA. The low magnification mode, LM, using either the upper or lower secondary electron detector, SEI or LEI, provided the best images, with an incidental use of the SEM mode. Images were

taken systematically by starting at the middle of the mycelium-veneer interface plane, and taking pictures every mm downwards. Sideway deviations from this mid-line were only made if no hyphae were observed in the initial image.

4.4.2. FTIR

The DCB specimens were evaluated with FTIR without additional sample preparation. Of the ME parameter sweep group, another representative specimen at each ME concentration was taken. The bottom arm veneers were, after testing, placed on a Perkin Elmer Spectrum 100 FT-IR. The inoculated side of the veneer was placed downwards on the diamond crystal, and pushed with a clamping force in between 30 and 50. Attenuated total reflectance (ATR) measurements were taken for wavenumbers between 650 and 4000 cm^{-1} with 16 scans per sample, and a resolution of 0.5 cm^{-1}. Each sample was measured at three different locations across the sample, the same as for microscopy. Additionally, non-degraded veneer, a mycelium mat, and the printing ink were scanned to facilitate a good interpretation of the acquired spectra.

The evaluation of the spectra was based on commonly evaluated peaks in literature on MBC and white-rot decay of wood. The responsive groups in lignin and carbohydrate molecules primarily absorb in the so-called fingerprint region, corresponding to the lower IR range of 1500-400 cm^{-1}. A comparison of work performing FTIR on MBC materials [55, 78], their main sources [113, 114], and a specific study on hornbeam [115], generated an overview of the most important peaks to consider, presented in Table B.1 in Appendix B. The exact locations of peaks observed in this study can deviate from those reported with a few cm^{-1}, due to the varying structure of the molecules in different plant materials.

The final three evaluated peaks corresponded to lignin, which is appropriate for the hypothesised selective rot strategy in *G. lucidum*. Wavenumbers 1504 cm^{-1} and 1594 cm^{-1} correspond to aromatic skeletal vibrations in lignin, where 1646 cm^{-1} identifies its conjugated carbonyl groups [113, 78]. The first two are understood to decrease upon fungal degradation, the latter will increase [113]. Next to a qualitative comparison at these wavenumbers, peak intensity ratios were evaluated at both I_{1504}/I_{1646} and I_{1594}/I_{1646}, to give a more quantitative grasp on the data. Both should decrease upon fungal degradation. The ratios were taken of each spectra and averaged over the three scanning locations.

5

Results and discussions

5.1. Mycelium hydrogel development

5.1.1. Optimised rheology

The ink production procedure described in section 4.1 does not provide an ink with the same properties as those described by Gantenbein et al. (2023) when using the same ink recipe [1]. Specifically, the ink exhibits a higher measured yield stress and longer recovery time, as presented in Table 5.1 [1]. While it is still possible to print a relatively stable grid using the ink, as presented in Figure 18A, the higher yield stress causes it to fail as a stable inoculum suitable for this study. The deposition of a single line is susceptible to disturbances due to the granulate appearance of the ink, as shown in Figure 19A. This difference in ink properties could stem from the differences in the exact ingredients used, which were modified to generate an ink suitable as a stable fungal inoculum.

Ink	Yield stress (Pa)	Recovery time (s)
Gantenbein et al. (2023)	424	Few seconds
Original recipe	1455 $\pm$ 11	13.1
Altered recipe: agar content - 75%	461 $\pm$ 5	6.9

Table 5.1: Yield stress and recovery time determined by rheology experiments for the ink presented by Gantenbein et al. (2023), the replicated ink of the original recipe in this study, and the replicated ink with agar content decreased by 75% [1].

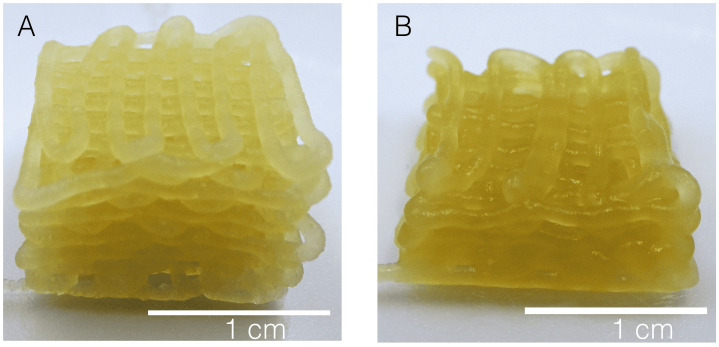

Figure 18: Printed grids of the inks produced according to the original recipe of Gantenbein et al. (2023) (A), and with lower agar content (B), showing the reduced stiffness of the latter, limiting the retainment of 3D printed structures [1].

The agar content was adjusted to reach the yield stress and recovery time of Gantenbein et al. (2023) [1]. Of the three ingredients that mainly determine the rheological properties and therefore printability of the ink, cellulose based thickener, agar, and κ-carrageenan, the agar content mainly sets

[1] Settings in the recovery time experiment for the altered recipe were changed to increase the amount of data points, and therefore decrease the time between acquisition of two data points from 3.6 s to 1 s. This improving the accuracy of the data, but limits comparisons between the different inks.

its elasticity. For the original recipe the difference in yield stress could potentially be attributed to the difference in agar gel strength. It ranged between 700-800 g/cm^2 and >1100 g/cm^2 for Gantenbein et al.'s (2023) supplier Duchefa, and was reported >300 g/cm^2 for the supplier of this study, Sigma Aldrich, a stable TU Delft supplier [1]. To lower the ink's stiffness, the rheological properties of the ink were therefore studied while decreasing the agar content to a lowest value of 25%, with 25% intervals. Decreasing the agar content with 75% from 15 g/L to 3.8 g/L gives a yield stress of 461 Pa and recovery time of 6.9 s, as shown in Table 5.1 and Figure 20A. This is hence similar to Gantenbein et al. (2023), but decreases the load-bearing capacity of the ink while improving its single print line consistency [1].

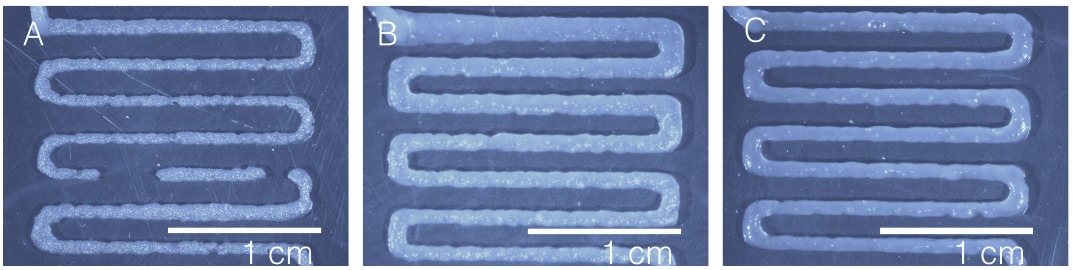

Figure 19: Single line prints of the inks produced according to the original recipe of Gantenbein et al. (2023) (A), and with lower agar content (-50% (B), -75% (C)), showing the better applicability of the latter for a continuous fungal inoculum [1].

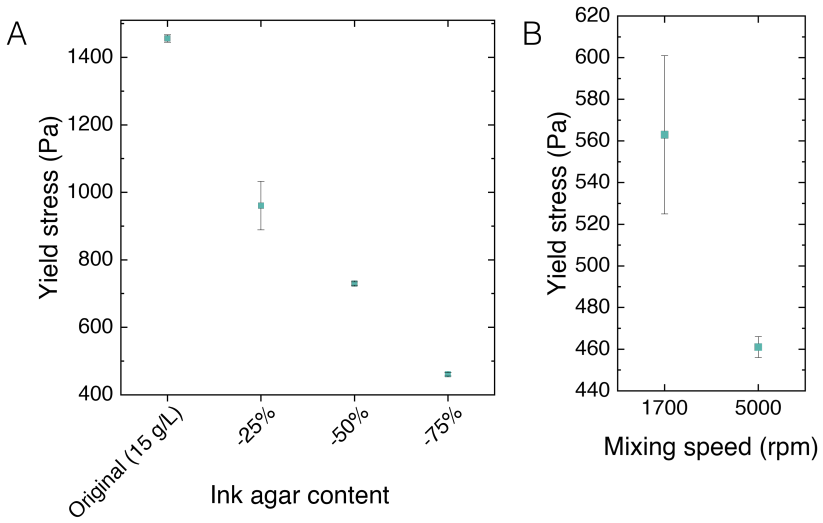

Figure 20: The yield stress of the agar-based inks decreases with a decreasing agar content (A). A lower standard deviation in its yield stress was found to be caused by an increased homogeneity when mixed at higher speeds (B).

Although the stable grids of Gantenbein et al. (2023) are not reproduced with these rheological properties, the ink serves a stable inoculum [1]. The printed grid sagging was the most severe for the lowest agar content ink in Figure 18B, in line with results of Gantenbein et al. (2023) [1]. This happens as the gravitational forces of the printed layers exceed the yield stress of the ink, of which an analytical explanation is given by Gantenbein et al. (2023) [1]. This effect will not be pronounced in the proposed setup described in section 4.2.2 with a 2-layer print height and large print area to support the upper layer. Hence observations on the zigzag print lines are more important, which show no discontinuation for the second ink in Figure 19C, as desired. This relies on the ink mixing speed during production, where 5,000 rpm facilitates a homogeneous ink as plotted in 20B. Lastly, the increase in linewidth due to build-up of pressure in the nozzle is less severe than for inks with higher agar content in Figure 19B. Hence the recovery time and yield stress of the ink with 75% lower agar content provide the most stable line as fungal inoculum, while retaining substrate surface area available for fungal growth.

5.1.2. Ink with mycelium

The 12-day growth period of the mcycelium did not always provide a full dish coverage due to biological variability as shown in Figure 21. This 2 to 5 day longer required growth period in comparison to literature could be due to a difference in the mycelium's initial morphology [1]. *G. lucidum* can display different morphologies, where its growth speed and density is related to the amount of provided nutrients. Gantenbein et al. (2023) highlighted their use of the rhizomorph, which shows a rod-like structure and is known for faster radial growth, in contrast to cotton-like fluffy mycelium [1] (Figure 22A). This behaviour should be obtained by multiple transfers of the fungus on nutrient poor plates [116]. This procedure did not result in the rhizomorph structure for the fungus used in this study, as shown in Figure 22B. Hence the influence of this morphology discrepancy on the growth time difference between the current and previous study could not be assessed. As the morphology after inoculation however optically did not differ from the mycelium of Gantenbein et al. (2023), and could anyways be reversed to the cotton-like structure when the fungus is grown on the highly nutritious ink, the rhizomorph morphology was not seeked after further [1].

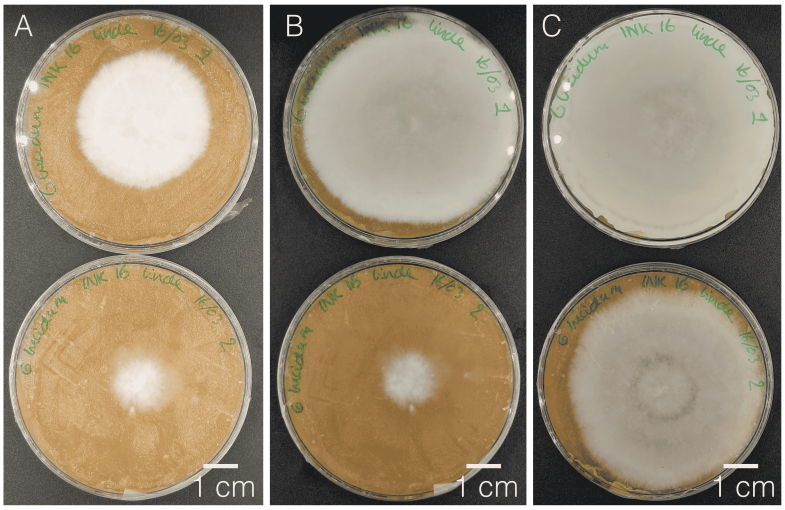

Figure 21: Growth of mycelium on 10% ME ink after 5 (A), 8 (B), and 12 (C) days. Showing no full coverage of the plate yet reached after 7 days, and biological variability between plates.

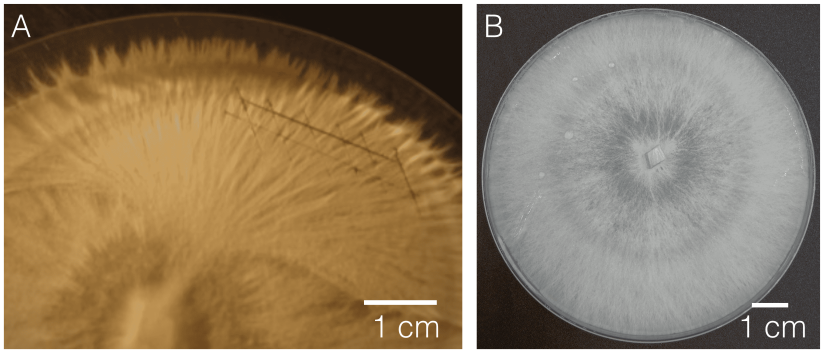

Figure 22: The rod-like rhizomorph mycelium morphology growing next to the fluffy, cotton-like morphology (A) [116]. The rhizomorph could not be obtained during experimental efforts in this study, where four transfer cycles were performed on nutrient poor MEA plates (0.2% ME, 1.6% agar, 0.05% peptone) (B).

5.1.3. Discussion

Several slight deviations of the mycelium ink production procedure from Gantenbein et al.'s (2022) could have caused differences in the material properties and fungal development [1]. First, their amount of inoculation was not reported, for which also a different strain of *G. lucidum* was used, China strain

number 112001 for [1] and M9726 in this study. Then, concentrations of ink ingredients were based on the water volume, instead of the total ink volume. This decreases the ingredients' concentration, hence reducing the ink's elastic properties. Besides, this could have caused the fungal growth to take 12 instead of 7-10 days, as it is estimated to lower the ME content with 10%. Secondly, the present mixer only allowed safe and homogeneous mixing up until a rate of 10,000 rpm, hence half of the original mixing rate. As no specifications regarding the rate of shear mixing were given in the manual of the cellulose based thickener this was taken as sufficient. Then, the growth chamber used had a temperature and humidity of 26 ℃ and 50-60%, instead of room temperature and 95%. Although 60-65% is optimal for fungal growth, it might have induced a difference in growth time [62, 61]. Furthermore, it could affect the final printability of the inoculated hydrogel due to increased dehydration during fungal growth. As additionally Gantenbein et al. (2023) show that after mycelium growth the yield stress is increased by more than half of the initial value, care was taken during continuation of this study for print line discontinuities and line width increases. [1].

The lower grid printability reached in this study with similar rheological properties as compared to Gantenbein et al. (2023) could be caused by two differences [1]. Firstly, a shortly longer recovery time could have allowed sagging of the print. Lastly, a discrepancy between the exact test method used during rheology might have resulted in a difference in the recorded yield stress.

5.1.4. Summary of the hydrogel development

The mycelium-laden hydrogel as developed by Gantenbein et al. (2023) can be reproduced in the lab environment of the Aerospace faculty, and after decreasing the agar content of the original recipe by 75% be used as a stable fungal inoculum in this study [1]. The replicated ink cannot be used for printing stable 3D structures, but generates required undisturbed print lines. It is here essential that the second mixing step after autoclaving is performed at mixing speeds of 5000 rpm, to increase the ink's homogeneity and thereby smoothness. Then, where no rhizomorph morphology could be reached, a fungal growth period of 12 days on the ink can generate a stable inoculation method for the DCB specimens. Every iteration requires the production of several plates to account for biological variability and allow the consistent use of a fully covered plate.

5.2. DCB testing

5.2.1. Arm moisture content and flexural modulus

The critical wood moisture content of 30% for fungal growth is achieved with 46 hours of soaking for hornbeam and beech veneers, and 23 hours for spruce veneers, as shown in Figure 23A. It is sufficiently maintained during the planned fungal growth period of 4 weeks. A 3 week period shows a higher moisture content for hornbeam veneers, which predicts the moisture content to decrease further towards a 5 week period, but remain above the critical limit. Scattering in the results is primarily caused by the veneers heterogeneous microstructure, which is similarly observed during veneer 3PB tests.

A large variability in E_f of the wood veneers is observed, as plotted in Figure 23B. Despite the large standard deviation, the average value of each mycelium overgrown specimen group is taken further to analyse the DCB testing results. Given the similar E_f values found for overgrown and non-overgrown hornbeam samples, no distinction is made with regards to their moduli in the DCB specimens that were not fully overgrown along their length. Finally, the measured E_f for hornbeam represents only one of the six specimen groups with this substrate, but is nevertheless used to calculate G_I of all hornbeam samples.

5.2.2. Mode I interlaminar fracture toughness

The corrections based on the parameters F and N, as per standard ASTM5528, are not required for the results of this study [102]. Firstly, the δ/a values at the onset of delamination for all tested specimens are below 0.4, and do not exceed 0.12. This ensures that F remains above 0.97, eliminating the possibility of significant errors due to a large displacement of the beam. Neither is there a large error due to stiffening of the arms by the loading blocks, where N always is above 0.95. Consequently, the data analysis can be proceeded without corrections based on the ASTM standard factors F and N.

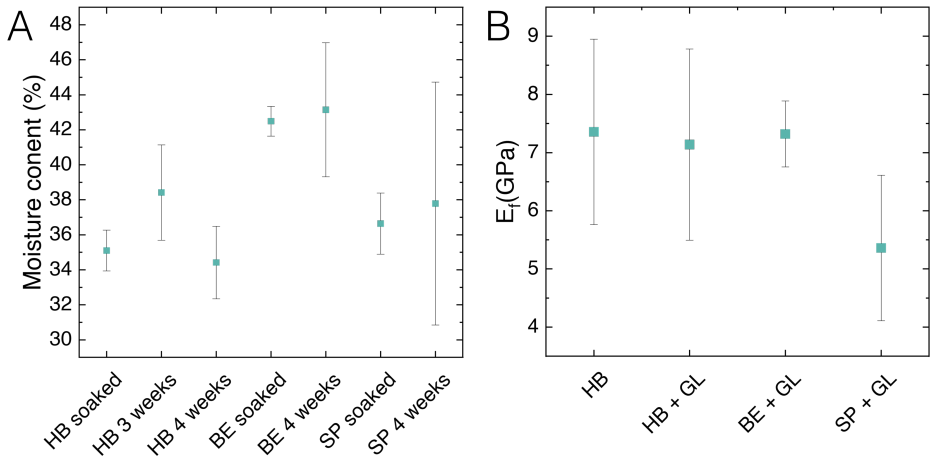

Figure 23: A: Moisture content of hornbeam (HB) and beech (BE) after 46 hours of soaking, and spruce (SP) veneers after 23 hours of soaking, left in DCB specimen growth conditions for 3 or 4 weeks. B: Flexural modulus obtained from 3PB tests on the veneers. Samples were either tested with or without printed and overgrown *G. lucidum* (GL). Squares mark the average of 10 measured specimens, and error bars reflect their standard deviation.

Very low values arise for G_I using the analytical method presented in equation 4.3, limiting the data evaluation. It causes the virtual crack length, calculated using MBT with equation 4.4, to exceed the crack lengths physically possible if evaluated for the complete DCB test. A typical and representative case is presented in Figure 24, where G_I is determined from the maximum load point in the P versus δ curve onwards. If the crack length obtained from the MBT is only evaluated in the physical reachable range, a stable value for G_I with respect to a is found. However, this MBT method leaves only one third of the tested samples for analysis, as for the other two thirds the calculated crack length already exceeded the physical reachable range at the peak load. Hence in order to well compare specimen groups it is decided to determine the G_I of all samples at the onset of delamination.

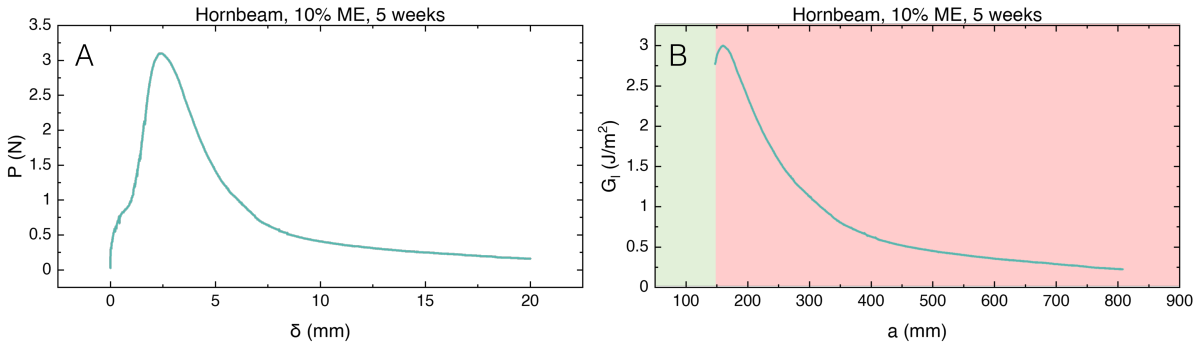

Figure 24: Force P versus deflection δ (A) and interlaminar fracture toughness G_I versus virtual crack length a (B) for one specimen. The virtual crack length overwrites the physically available crack length of 149 mm, marked by a transition from green to red.

The delamination onset G_I is evaluated for all except a few specimens. Those with insufficient mycelium growth or a non-perfect removal of the network between the growth stopper and the veneer are disregarded, as this caused either the DCB testing to not exceed 0.2 mm of crosshead displacement, or an extraordinary large peak load to occur, respectively. Subsequently, the first 100 data points from the peak load onwards are considered, to limit sensitivity to outliers and variations in the data. This corresponds to 0.17 mm of crosshead displacement. Obtained values for G_I are presented in Figure 25.

All G_I values obtained for hornbeam are higher than those for beech and spruce samples, and on the order of 1 J/m^2. The calculated values show much scattering, hence conclusions should be carefully drawn. Firstly, the G_I values measured for hornbeam at 3-5 weeks with 10% ME in Figure 25A suggest that 3 weeks are not sufficient for mycelium binding, after which its G_I becomes more stable from 4 weeks onwards, around 1.5 J/m^2 on average. Here maximally a toughness of 2.70 J/m^2 is reached, which is only increased to 2.83 J/m^2 for 5 weeks of growth. When varying the ME concentration with 4 weeks of growth in Figure 25B, the highest value is actually yielded when the mycelium grows from 5% ME ink, with an average value of 1.87 J/m^2 and maximum of 3.46 J/m^2. In contrast, growing the fungus on thinner wood veneers of beech and spruce in Figure 25C lowers the G_I to below 1 J/m^2 for beech, and even below 0.1 J/m^2 for spruce. The strongest beech sample had a toughness of 1.17 J/m^2. The last two veneer species, together with the 3 weeks growth on hornbeam specimens, show less scattering in their results.

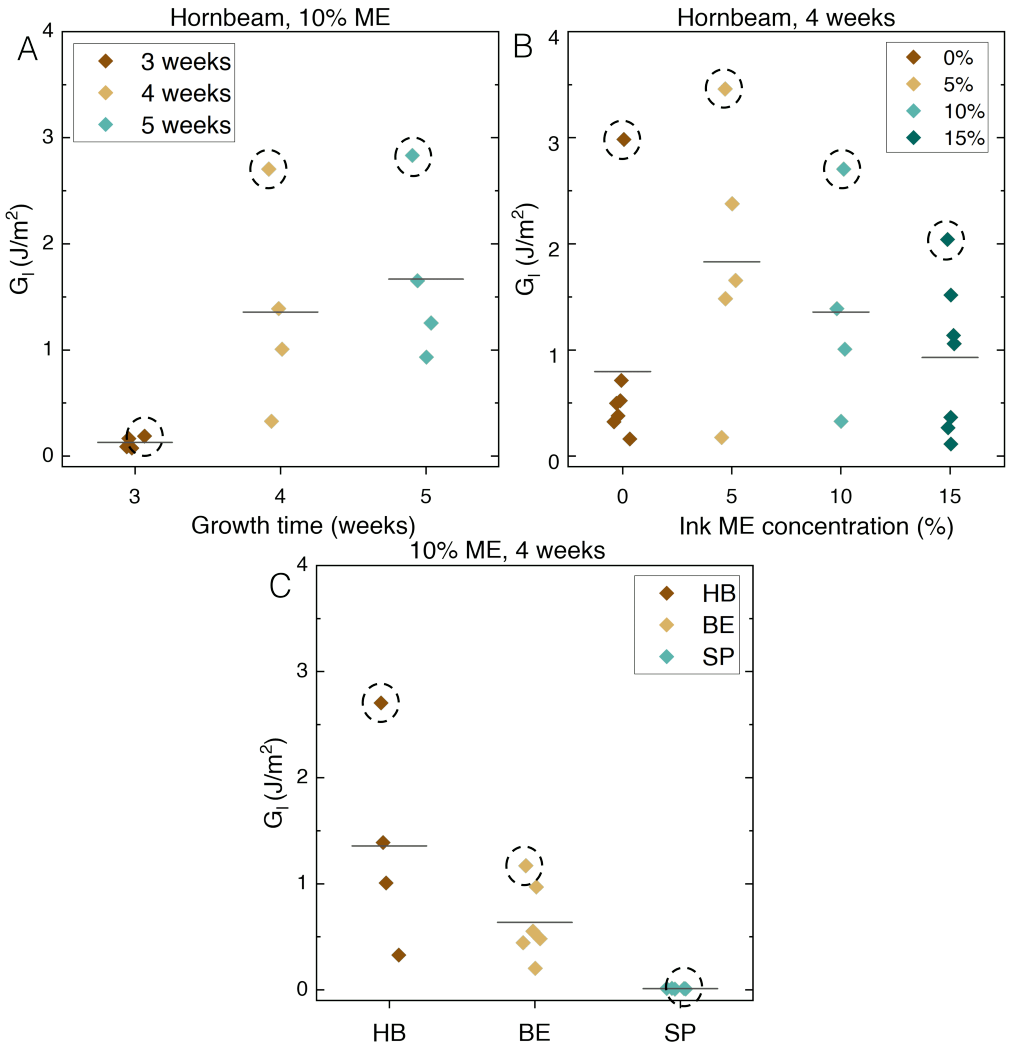

Figure 25: G_I obtained at the onset of delamination plotted as a function of hydrogel ME content (A), growth time (B), and for different substrates considered: hornbeam (HB), beech (BE), and spruce (SP) (C). The highest values per group are encircled, and a horizontal bar represents the average per group.

5.2.3. Interface and failure modes

The fracture surfaces are evaluated upon five criteria that appeared to vary across samples:

- Bridging ink: yes (BI) or no (NBI).
- Ink failure mode: cohesive (IC) or adhesive (IA)
- Mycelium growth: limited to the sample surface (G-), showing more aerial hyphae (G), or a dense aerial hyphea network (G+).
- Pigmentation: no (NB) or brown (B)
- Mycelium failure mode: cohesive (MC) or adhesive (MA)

The interfaces of the specimens that gave the the highest and lowest value for G_I per batch of samples were analysed, of which their evaluation is presented in Table 5.2. A few criteria can be recognised on the fracture surfaces of the few samples presented in Figure 26.

Specimen	G_I	Surface
HB, ME 10%, 4 weeks, P	Low	G-, BI partially, IA IC, NB, MC
	High	G, BI, IC IA at sides, B, MC
HB, ME 0%, 4 weeks	Low	G, BI front not back, IC, B, MC
	High	G+, BI, IC IA back, B-, MC
HB, ME 5%, 4 weeks	Low	G, BI partially, IC if IB, B-, MC
	High	G+, BI, IC IA, NB, MC
HB, ME 10%, 3 weeks	Low	G-, BI front not back, IC, NB, MC
	High	G, BI front not back, IC, NB, MC
HB, ME 10%, 4 weeks	Low	G-, BI-, IC, B, MC
	High	G+, BI, IC IA, B, MC
HB, ME 10%, 5 weeks	Low	G, BI only middle, IC, B, MC
	High	G+, BI, IA, B, MC
HB, ME 15%, 4 weeks	Low	G-, BI, IC, NB, MC
	High	G+, BI, IC bit IA, B, MC
BE, ME 10%, 4 weeks	Low	G-, BI, IC bit IA, B-, MC
	High	G/G-, BI, IC bit IA, B-, MC
SP, ME 10%, 4 weeks	Low	G–, BI, IC IA opposite sides, NB, MC
	High	G-, BI, IA, B, MC

Table 5.2: Optical evaluation of the fracture surfaces of all specimen groups according to the criteria described in this section. For each group the specimens with highest and lowest apparent G_I were evaluated.

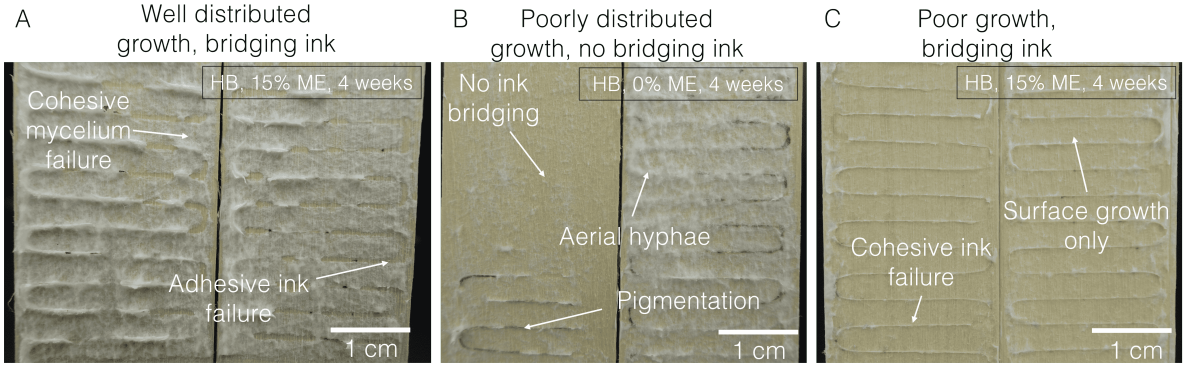

Figure 26: Fracture surfaces of different DCB specimens, displaying several of the evaluation criteria.

The mycelium growth varied significantly among specimens within the same group, which was correlated to the measured G_I. In each group, higher G_I fracture surfaces exhibited stronger growth on both the top and bottom veneers compared to the lowest measured G_I sample, which relied on successful

ink bridging. Such bridging was not achieved for all veneer duos across the complete specimen length. If the ink did not cross the 1 mm gap, the mycelium growth was either robust on only one surface, or almost absent. However, successful ink bridging did not always cause robust growth, as shown in Figure 26C. The veneer's surface was for all specimen arms, except for the spruce specimens, covered by surface mycelium and aerial mycelium. There were no observations of mycelium film development at the surface, and no cases of adhesive failure of the mycelium that crossed the gap between veneers. Networks grown closer to the inks sometimes exhibited brown pigmentation, unrelated to the measured G_I values.

The ink itself also exhibited different failure modes, which was not related to differences in G_I between specimens. Single specimens exhibited both cohesive and adhesive ink failure. Its limited contribution to G_I is clear from the specimens with little growth that show low G_I values.

5.2.4. Discussion

Flexural testing

The variability in E_{xx} is most likely a result of different amounts of earlywood and latewood regions in the veneers, as no large specimen deformations were observed. Earlywood is of lower density than latewood, hence a relative difference in their presence will have caused a different stiffness to be measured. This induces an uncertainty in the DCB testing results, as their presence was not accounted for in DCB substrate material selection. Another, though limited, uncertainty is introduced by the limited testing of hornbeam veneers.

Of the hornbeam specimens tested in DCB only one of the six groups was represented in the flexural tests, where their E_f is estimated to be sufficiently similar for two reasons. First, a prolonged growth time from 3 to 4 weeks only dropped the moisture content in the veneer with 4% in the developed growth environment, as shown in Figure 23A. This indicates that a change in growth time will not cause a large change in the hornbeam's E_f, as E_f is more dependent on the wood's structure and density. Furthermore, little effect of the printed ink and overgrowing mycelium was observed on E_f, as shown in Figure 23B, hence changing the sugar content is estimated to not largely influence E_f.

DCB setup sensitivity and specimen variability

Strong mycelium growth across the gap between veneers was reliant on ink bridging, which was not constant throughout the samples. This could have been caused by slight bending of some veneers during soaking, causing the print to fall short of its intended height or the gap size between veneers to be increased. Alternatively, the specimens with no ink bridging could have been of lower moisture content, causing the arms to absorb more of the printed ink. Regardless of the explanation, a limited ink bridging clearly showed to influence the mycelium growth distribution, as already shown in Figure 26A and B. Successful ink bridging however did not necessarily facilitate strong mycelium growth, as shown for the interface presented in Figure 26C.

This difference in growth within specimen groups could be attributed to different causes. Firstly, in instances, a group of four specimens in the same container could show below average growth. Hence even though efforts were put in the creation of perfectly similar micro-environments, this might not have been optimally achieved. Most often, however, the overall growth within single containers was similar, and could not explain the variation in G_I. This could have been caused by the varying growth along single specimens' lengths, due to either a variation in print deposition due to veneer deformation, or an inhomogeneous distribution of hyphae in the inoculating ink. The latter could especially explain the large variation in the 0% ME samples. An example of such inhomogeneous growth is shown in Figure 27A, where it should also be noted that every individual organism per specimen is always prone to biological variability. Lastly, the differences in Parafilm wrapping and wood veneer moisture content or chemical composition could have been of influence, although not likely to be accountable for the observed substantial growth variations.

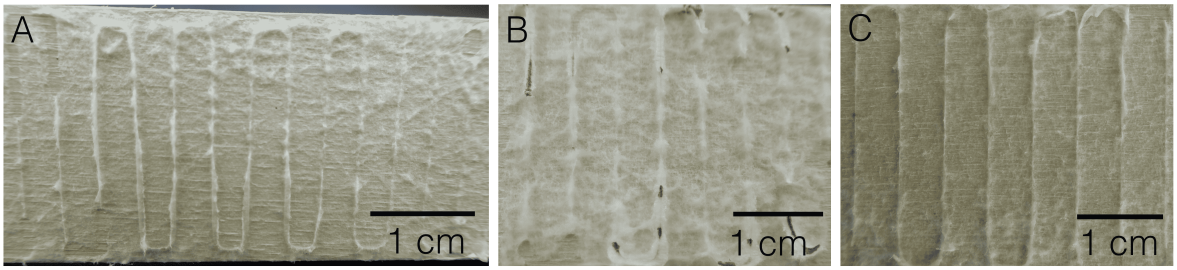

Figure 27: A: Growth variation across one of the hornbeam samples with 10% ME inks and mycelium grown for 4 weeks. B and C: both robust and less overgrown samples show surface mycelium and aerial mycelium.

The variability in growth across specimen groups over time could potentially be attributed to variations in the inoculated fungus' age. This is especially noteworthy as literature suggests beech wood to support better mycelium growth than hornbeam, which contradicts the findings in this study [103]. The fungus for beech and spruce specimens was taken from a different petri dish for hornbeam samples, that was stored in the fridge for 3 additional weeks. It overgrew the ink but formed a less coherent film, implying a potential lower metabolism and therefore limited growth activity. This observation should not be disregarded during the comparison of substrate materials. Fortunately, never was a lower degree of growth caused by contamination, which was evaluated for under a stereomicroscope.

Microscopy after testing did reveal various degrees of mycelium colouration on the fracture surfaces, which was not related to specimen's G_I. In mycology, it is generally understood that pigmentation occurs in fungi when these reach a more mature state of growth. This is in agreement with literature on *Ganoderma* species, which are reported to contain brown-tinted skeletal and binding hyphae in their basidiospores [117]. In the current work, the pigmented mycelium appeared only on the inks and looked more like compact mycelium tissues, which also appeared on the outside of wrapped samples. Even though these small areas of different mycelium structure had development, these did not induce a different crack-resistant behaviour.

Next to the clear relation between apparent growth and measured G_I, the large variation in its measurements in the DCB tests could be caused by several other sources of inconsistency that exist in the tested specimens. These should not be overlooked, and will be discussed shortly for the degree of error caused:

- **Mismatching veneer width, or veneer misalignment** - Both were minimised by choosing veneer duos that could stack with the least amount of misalignment. The maximum misalignment observed was 1 mm, which could cause an underestimation of G_I from 2 to 7.5%. It did however not show to relate to specimens with lower G_I.
- **Twisted loading block** - It never increased the beam arm length more than 1 mm. Using the formula for max deflection of a single-sided clamped beam:

$$\delta_{\text{max}} = \frac{PL^3}{3EI} \tag{5.1}$$

  with a force of 1 N and the previously determined veneers' stiffness and thickness shows that a twisting of 1 mm would maximally cause a difference of 3% in arm deflections. Hence the error introduced by load block twisting is small and not considered in this study.
- **Wood flexural modulus** - The measured E_f showed a maximum standard deviation of 23%, which could cause an over- or underestimation of the calculated G_I with 10%. Furthermore, the load arm length in the DCB tests yields a different span to thickness ratio than the 3PB tests. In contrast to a ratio of 24 in 3PB, in DCB this becomes 26 for the 3 mm veneer and 16 for the 5 mm veneer, at the smallest crack length of 39 mm. Decreasing the span to thickness ratio decreases the apparent E_f, due to a higher degree of shear deformations [118]. Hence this discrepancy between 3PB and DCB could cause an under- or overestimation of G_I in the presented calculations, depending on the propagated crack length. However, as the lowest ratio

during DCB of 16 is still higher than the 14 recommended to limit shear deformations in wood flexural testing, the variance induced is estimated to be negligible.

- **Prior adhesive shear** - The sensitive specimens were occasionally subjected to small shear loads due to specimen preparation. Despite efforts to keep this limited, it could have induced damage in the mycelium network and therefore underestimation of G_I in the DCB tests.

Given that the growth observations are related to G_I measurements, it can be argued that the encircled maximum values in Figure 25 are not outliers, but the strongest achievable mycelium in those growth conditions. These values do not alter the observed trends, except for the 0% ME group. It had one extraordinary strong specimen due to inhomogeneous mycelium distribution in the ink. Nevertheless, and despite all potential causes of inaccuracies, the overall results portray a somewhat stabilisation in toughness between 3 and 4 weeks of mycelium growth. Given 4 weeks, the optimal ink ME concentration lies between 0 and 10%. It should be noted that the 4 weeks and 5% ME concentration do not per se present the optimal combination of both parameters, which future work could experiment with. Lastly, where spruce samples were weak, beech samples could reach a G_I of 1.1 J/m^2, despite the group's overall poor growth. This sample's fracture surface shows more growth at the loading site than on the rest of the sample, which could explain these results.

Regardless of the growth variability the mycelium always showed cohesive failure, as already described in subsection 5.2.3. This was recognised by the observation of gap crossing hyphae in between all samples' veneers before testing, and mycelium covering all fracture surfaces. These hyphae types can be compared to the mycelium variations developed during solid state fermentation, where surface, biofilm, penetrative, and aerial hyphae can be recognised [119]. On DCB samples no biofilms are developed, but surface and aerial hyphae appear in different degrees, as shown in Figure 27B and C. It can therefore be hypothesised that the overall network of these hyphae types together binds well to the veneer surface, and the measured G_I reflects the failure of the crossing aerial hyphae.

DCB data analysis

The obtained values for G_I allow a re-evaluation of the ASTM criteria for thicker DCB specimens. The veneer's stiffness and final measured mycelium G_I left the specimens' thickness and initial crack length in line with the standard, confirming the specimen design's success. Hence no disturbances in the data evaluation are caused by the large displacement of specimen arms, which was already confirmed by the calculated values for correction factor F. The limited displacement due to the veneer's stiffness did increase the adhesive mycelium's bridging length, the region along which it is loaded in tension.

The large bridging length due to the veneer's stiffness explains the large virtual crack length obtained with the MBT method, limiting its applicability. Namely, the calculations assume clamped boundary conditions, and incorporate the process zone in front of the crack tip into the crack length. This zone is not measured in standard DCB measurements, where a is optically determined. The limited specimen number available for analysis with the MBT method hence shows unstable fracture behaviour, where the mycelium is so weak that the crack rapidly propagates through the complete specimen. This was slower for the thinner beams, which deflected more upon the same load and hence induced slower crack propagation. Therefore, either a longer specimen length or thinner specimen beam could allow a more stable measurement of G_I, and limit potential edge effects on the long end of the specimen, which were not accounted for in the current analysis. Growth around this edge was observed to aid the specimen in holding their own weight, to which it was vulnerable in the DCB tests.

In several specimens, a kink in the crack propagation curve reveals a sudden inability of the mycelium to carry the weight of the bottom specimen arm, marking the sample and data interpretation's vulnerability. The kink resembles a change in the bottom veneer's condition from tensile loading to leaning on the bottom clamp. The discontinuity could not clearly be tracked in all specimens, and for some the bottom arm had never been lifted at all. This limits a discussion on the influence of the sample weight on the obtained results, and suggests future work to limit the test setup's sensitivity to the specimen's weight. Furthermore, it informs that if other potential data analysis methods were to be used, such as load-curve fitting, these should be limited to a load range in which no arm dropping occurs.

DCB results and literature

The degree of mycelium growth from the inks on the veneers over time agrees with literature. Growth from the hydrogel is best compared to the work of Gantenbein et al. (2023), where the mycelium grown on grids increased in biomass up until 10 days, after which it stabilised due to nutrient depletion [1]. Contrarily, this time period could not yet facilitate fungal adherence between veneers in the current study. The continued growth and increase in veneer binding after 21 days suggests the fungus to continue its growth by digesting the veneer substrate material. This agrees with the work of Sun et al. (2020), who evaluated the mass loss of birch veneers soaked in 2% corn steep liquor after different duration of *T versicolor* incubation [98]. Their discrepancy between an increasing fungal biomass after 4 days and a veneer mass loss starting after 10 days, indicated the degradation of the veneer to only start after sugar depletion, similar to the observations in this study.

The influence of the absolute amount of provided sugars to the mycelium's mechanical behaviour is harder to various other studies, due to the large variability of nutrients studied. Again the work of Gantenbein et al. (2023) can be considered, who found an overgrown grid stiffness of 23 kPa at 5% and 26 kPa at 10% ME concentration compared to 5 kPa at 0% and 13 kPa at 15% [1]. Hence almost in agreement with the strongest mycelium found at 5% ME in this study. A stronger network at lower sugar concentrations however is in agreement with the work of Haneef et al. (2017), who show a 2-fold higher stiffness for *G. lucidum* mycelium films developed on growth media with less easy sugars [120]. This could be attributed to the fungus' increased chitin production as response to harder to penetrate nutritious media, the component responsible for the stiffness of its cell walls. Their cell walls furthermore showed a lower content of proteic and lipids, that are hypothesised to act as plasticisers. Even though their results are preliminary and based on FTIR measurements, it could be hypothesised that in the current work a stiffer mycelium network developed at 5% ME while digesting the wood. During DCB testing this would increase the measured fracture toughness.

Where no literature reports on the fracture toughness of purely living or dead mycelium grown in MBC, a comparison to tensile measurements provides a confirmation of the accuracy of the procedures employed. We assume the average peak load across all DCB samples in this study, 1.5 N, to have debonded the entire adhesive area of 110x25 mm. This is a conservative approximation, but plausible given the weak matrix and the beam's stiffness. Consequently, a peak stress of 0.55 kPa causes failure. Non-compressed composites loaded in tension for Appels et al. (2019) have peak loads of 0.015 MPa, which is approximately a factor 30 higher than our results [42]. However, for some of the stronger specimens in this study, the deviation is only a factor 10. This seems reasonable, as their stress distribution is less concentrated, their mycelium could internally experience more complex loading conditions including shear, and their fibres could also contribute to the strength of the composite. A similar comparison can be made to internal bond strength (IB) measurements.

Given that IB measurements are tensile tests parallel to a compressed composite's surface, the same reasoning as above can be applied. Elsacker et al. (2021) obtained strengths of 0.007 MPa for mycelium hemp composites hot pressed at 70°C [85]. Once dehydrated, further increasing the pressing temperature from 160 to 200 °C showed the IB to increase from 0.05 to 0.18 MPa in the work of Liu et al. (2019) [22]. This indicates that high temperature induced chemical reactions enhance the mycelium binding potential. Water immersion prior to heat pressing even further increased IB to 0.34 MPa [90]. Contrarily, hot-pressed wood mycelium panels of Sun et al. (2019) were too weak to be tested without the addition of cellulose nanofibrils as an extra binder, showing the versatility of MBC across studies [91]. However, with the inclusion of 7.5% binder their IB reached 0.06 MPa. Thus, while the results of Liu and co-authors were orders of magnitude higher, the values reported by Elsacker et al. (2021) were only a factor of 10 higher than the peak stresses of this study [22, 90, 85]. This further confirms the validity of the reported results, where the lower values could be attributed to either pure mode I loading or the hydrolysed state of the material.

The measured G_I values for the mycelium network are orders of magnitude lower than synthetic materials. Common acrylic based adhesives used in regular composites have a fracture toughness of about three orders of magnitude higher [121, 122], where even more comparable materials such as PDMS have a fracture toughness of one to two orders of magnitude higher [123, 124]. This observa-

tion should inspire future MBC designers to develop alternative approaches to improve the composite's mechanical properties, which do not strongly rely on a high mycelium G_I.

5.2.5. Summary of the DCB testing

A DCB testing setup was built that allowed the quantification of G_I of a living mycelium network grown between lignocellulosic substrate materials. The use of wood veneers inoculated with a mycelium-laden hydrogel as specimen arms created sufficiently stable specimens, but displayed much variability in the degree of mycelium growth. This caused a large variation in test results, where the robustness of growth was strongly related to G_I values. G_I was calculated based on an analytical approach that relied on the decrease in specimen arm compliance. This method could solely be applied at the onset of delamination due to the mycelium's unstable fracture behaviour, but allowed the identification of trends within the parameter sweeps of this study.

The low binding ability of the fungus showed to depend on its growth time and supplied nutrients. A growth period somewhere in between 3 and 4 weeks was sufficient to stabilise the maximum binding ability of mycelium grown from 10% ME ink, with a G_I of around 1.5 J/m^2 from 4 weeks onwards. The best overgrown sample at 4 weeks showed a G_I of 2.70 J/m^2. With this growth time, supplying the fungus a ME concentration of 5% in the ink created the strongest adhesion, with an average G_I of 1.83 J/m^2. The best overgrown specimen even reported a G_I of 3.46 J/m^2. Hence the optimal value lays somewhere between 0 and 10% ME concentration, which could be a result of the enhanced stiffness of hyphae growing on less simple sugars. Furthermore, where all specimens show cohesive failure of aerial mycelium, the hypothesis is that the measured G_I results from the cohesive aerial mycelium. The surface is bound well by surface hyphae, which was less prominent on beech and spruce samples.

The level of G_I for hornbeam veneers was not reached on beech and spruce specimens. Due to their lower thickness, this lower toughness could have resulted from either the higher beam compliance and therefore smaller adhesive loading area, or the older fungus from a different plate used for inoculation that likely resulted in limited mycelium growth. A stronger binding on beech than spruce does suggest a more important role of the substrate chemistry than its density. An absence of G_I measurements on mycelium networks in literature limits an evaluation of the success of the employed method.

In comparison to IB measurements on heat-treated and heat-pressed MBC, the loads reachable are an order of magnitude lower, which could be attributed to either the pure mode I loading condition or the hydrolysed state of the fragile living mycelium network grown. Nonetheless, the presented experiments display that the ink developed by Gantenbein et al. (2023) can be employed to inoculate lignocellulosic substrate materials, and allow an adhering mycelium network to grow [1].

5.3. Interface evaluation

5.3.1. Optical microscopy

In all evaluated veneer slices four typical features appear, that are used to identify differences between specimens. Astra blue staining appears at specific regions, as highlighted in a typical slice obtained at the front of a 0% ME veneer in Figure 28. The occurrence of surface staining, ray staining, stained regions, and vessel pit staining by astra blue was evaluated for the ME concentration parameter sweep. This evaluation is summarised in Table 5.3, where of each cut location a representative slice is pictured in Appendix C. In this appendix also a slice of non-degraded and heavily degraded veneer is presented, to proof the created contrast by fungal degradation.

Comparing the optical images to the ME parameter sweep, no obvious correlation can be determined, where all samples show heavily stained ray regions around stained vessels. All show a blue surface staining on the order of 10 μm, which reaches beyond 50μm in case ray cells are present at the surface. Most, except for one slice of the 5% ME and one slice of the 15% ME specimen show regions of darkly stained rays. Their location is not limited to the upper side of the veneer, as they occur at heights in the slices. Their position is however related to that of the heavily stained vessel pits,

with vessels crossing horizontally. Whether these stained regions result from solely the presence of digestive enzymes or really correlate with hyphae penetration should be confirmed by SEM.

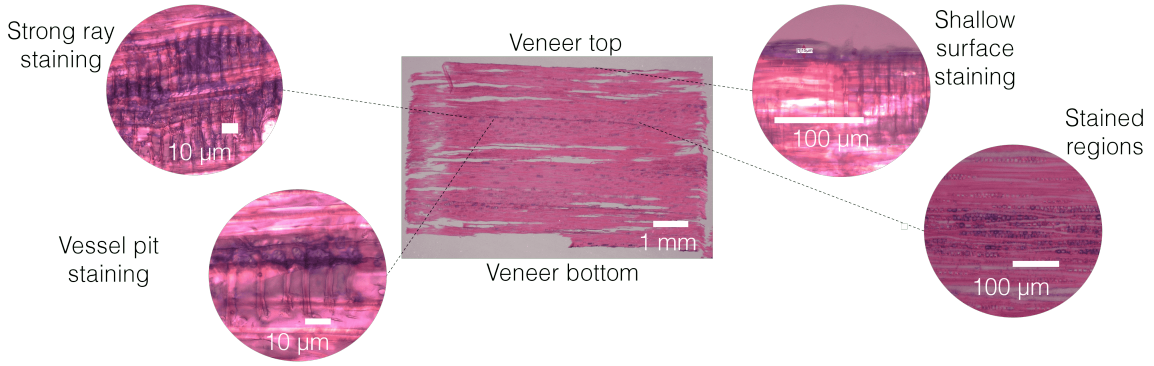

Figure 28: Optical microscopy images on a 0% ME veneer slice, displaying four typical features.

ME concentration	Feature	Observation
0	Surface	15-80 μm
	Rays	Y in A
	Regions	Y in A
	Pits	Y in A
5	Surface	12-100 μm
	Rays	Y in M and B
	Regions	Y in M and B
	Pits	Y in M and B
10	Surface	21-50 μm
	Rays	Y in A
	Regions	Y in A
	Pits	Y in A
15	Surface	12-86 μm
	Rays	Y in F and B
	Regions	Y in F and B
	Pits	Y in F and B

Table 5.3: Evaluation of optical microscopy images of Group 2 for the depth of surface staining, and the identification of ray bundle staining, stained regions, and pit staining. The latter three were either present (Y) or absent (N), in all (A) or solely the front (F), middle (M), or back (B) cut location.

5.3.2. SEM

The mycelium on top of the samples captured by SEM shows varying structures, which serve as a reference for hyphae identification through the specimen. Namely, variations in thickness could result from either the fixation method, image acquirement, or actual thickness of the hyphae. This limits the identification of hyphae based on the thicknesses reported in literature. The hyphae diameters on the veneers' surfaces range from 0.5 to 3 μm. They appear either in a branched or more isolated form, where these morphologies do not differ when growing from inks containing 0% to 15% ME, as displayed in Figure 29. Both morphologies are also observed at further depths in the overgrown veneers.

The images of all four specimens are evaluated without a categorisation according to set criteria:

- **0% ME** - The occurrence of hyphae is related to the presence of vessels. These are only visible deeper in the sample, where in and around some vessels, but not all, hyphal growth is observed. These hyphae are on the thicker end of the width range earlier described, show slight branching, but no network formation. Such hyphae can be seen in Figure 30A. Across most of the specimen no vessels are present, and no hyphae are observed.
- **5% ME** - Similar hyphal growth as the 0% ME samples. Near some but not all vessel elements hyphae grew in little branching form, visible through the complete depth of the specimen. One thin hyphae network is observed 1 mm from the bottom of the sample, inside a ray cell. In the top 1 mm of the sample growth is observed to also occur in between and onto fibres.
- **10% ME** - Again, few μm thick hyphae are visible all throughout the depth of the specimen with limited branching, in the nearby occurrence of almost all vessel elements. Vessel pit penetration can be observed.
- **15% ME** - Samples show a different mycelium morphology than observed in the other three ME concentrations. At all depths in the specimen thin hyphae branched to form mycelium networks inside almost all vessel elements, as shown in Figure 30B. 10 μm long balloon like structures appear in the networks. Vessel pit penetration is observed. Also μm thick hyphae with little branches are present all throughout the depth.

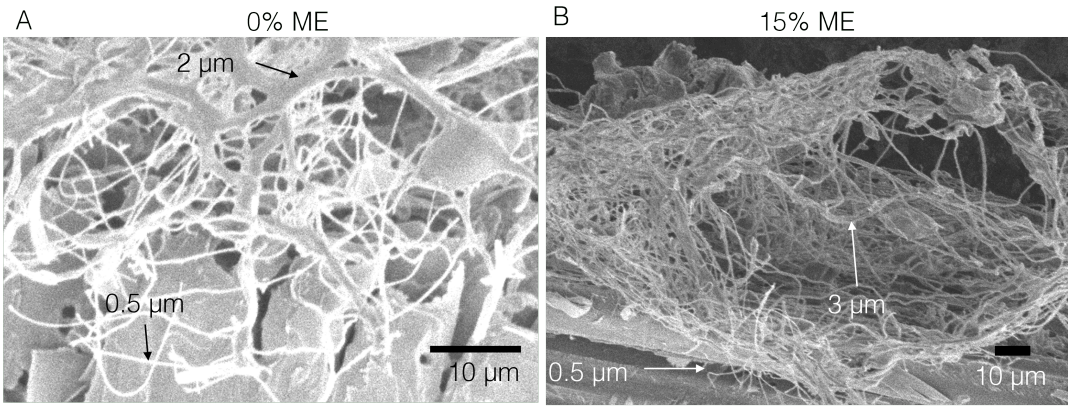

Figure 29: SEM images of mycelium grown on top of DCB samples. Mycelium morphology does not vary much when provided either 0% (A) or 15% (B) ME in the ink, with hyphae diameters varying between 0.5 and 3μm.

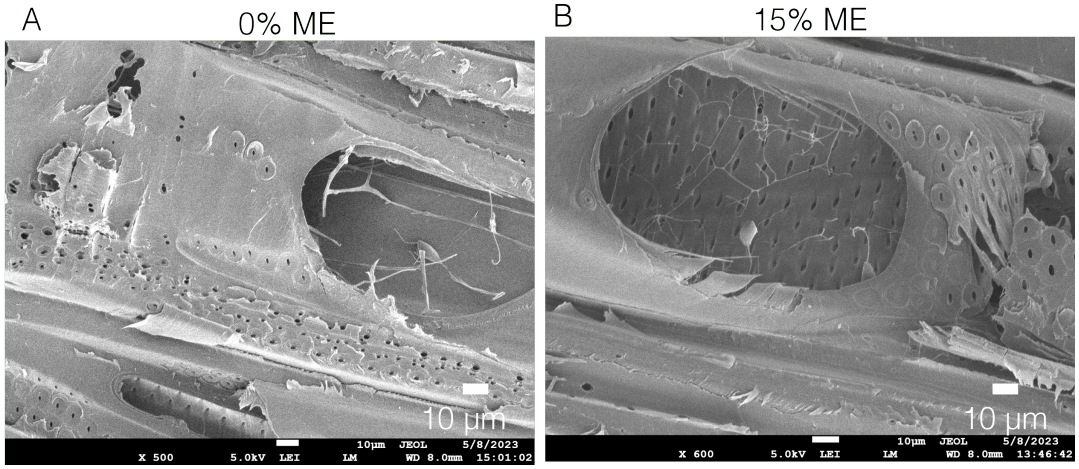

Figure 30: SEM images of the DCB samples' cross section. Mycelium grown inside showed thicker hyphae with less branching for lower nutrient concentrations (A), and thinner hyphae with more branching for higher nutrient concentrations (B).

Finally, the observations on beech and spruce samples are described below:

- **Beech** - Regularly, 10 μm balloon like structures appear on the hyphae. Few μm thick hyphae with little branching grew through vessels. Both cell wall and pit penetration were clearly identified, as shown in Figure 31. Hyphae were visible all throughout the depth of the specimen.
- **Spruce** - Little mycelium is identified in the veneer at any depth, neither at its top surface. A few exceptional cases of a few μm thick non-branching hyphae growing inside ray cells are visible, as displayed in Figure 31.

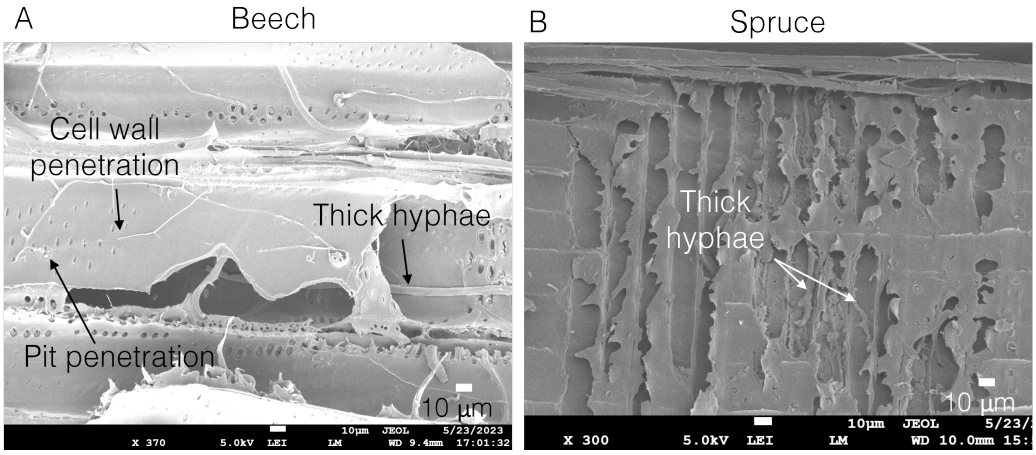

Figure 31: SEM images of mycelium grown inside beech (A) and spruce (B) veneer. Hyphae were more prominently present in beech samples, where furthermore cell wall and pit penetration was clearly visible.

5.3.3. FTIR

Where microscopy did not show a trend in veneer's lignin degradation when inoculated with varying ME concentrations, FTIR was used for a quicker and more quantitative evaluation on the substrate's top surface. A qualitative comparison of the spectra taken from the DCB samples does not show a clear trend in peak occurrences when changing the ME concentration in the inoculum. Peaks at 1504 cm^{-1} are slightly more prominent in the spectra of 0% and 15% ME concentration, as shown in Figure 32. It appears as a kink, or shoulder, which is slightly more evident in those two samples. The other lignin peak at 1594 cm^{-1} also emerges as a kink, which sticks out a bit more for the 15% ME sample. Finally, the peak at 1646 cm^{-1} is evidently present in all samples with the same shape. Its intensity cannot directly be compared as the spectra were not corrected and/or normalised. Hence a more appropriate evaluation could be done based on the relative peak intensities.

The relative peak intensities are almost the same for all DCB samples, indicating the same degree of lignin degradation at the sample surface. For all DCB samples I_{1504}/I_{1646} is around 0.45, and I_{1594}/I_{1646} around 0.64, as plotted in Figure 33A. This is substantially lower for the ratios found for non-degraded veneer, that are 1.06 and 1.21 for I_{1504}/I_{1646} and I_{1594}/I_{1646}, respectively. Hence the same trend for all DCB specimens confirms a substantial lignin degradation at the samples' surfaces. Their ratios are closer to but still lower than those of pure mycelium, which are 0.56 and 0.78. The surface mycelium is also taken into the DCB sample measurement, and hence contributes to the lower peak intensity ratios found. A small contribution to this lowering could have also been caused by the lowest ratios are found for the ink, which are 0.31 and 0.60 for I_{1504}/I_{1646} and I_{1594}/I_{1646}. The individual roles played by the wood, mycelium, and ink, become apparent from their individual spectra, as plotted in Figure 33B.

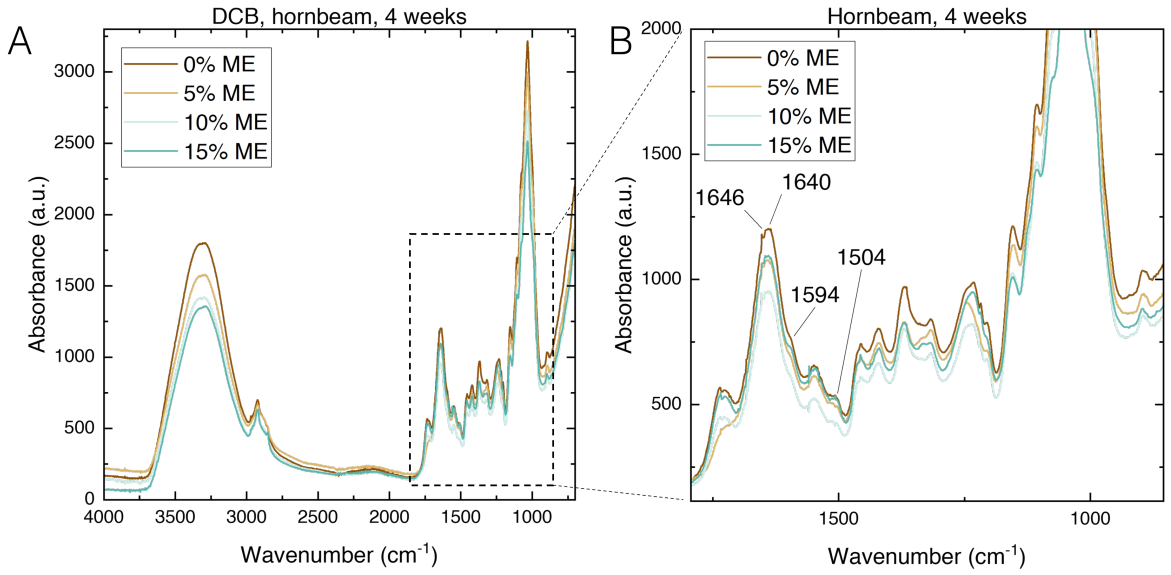

Figure 32: FTIR spectra of bottom DCB arms, that were inoculated with varying malt extract (ME) concentration. The overall spectra with numbers from 4000-700 cm^{-1} (A) and fingerprint region around 1800-800 cm^{-1} (B) are presented.

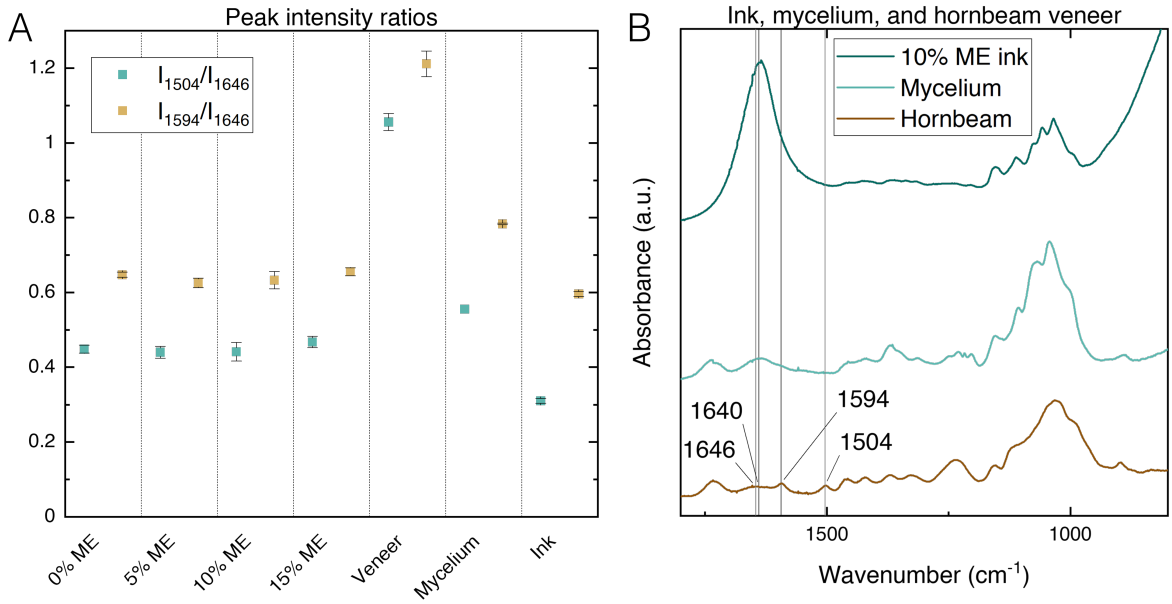

Figure 33: A: Peak intensity ratios at lignin specific wavenumbers. Ratios are plotted for DCB samples inoculated with varying malt extract (ME) concentrations, non-degraded hornbeam veneer, pure mycelium, and pure ink spectra. B: FTIR spectra for wavenumbers from 1800-800 cm^{-1} for ink, mycelium, and hornbeam veneer separately. Individual spectra for plot B were baseline corrected and normalised with respect to the highest peak intensity.

5.3.4. Discussion

Microtomy and staining

Optical microscopy on stained veneer slices did not identify fungal digestion or penetration as presented in literature. The resolution of the images did not allow identification of single hyphae or mycelium networks growing into the wood as shown by Lehringer et al. (2010) [100] in Figure 9C. Neither could microstructural changes induced by fungal digestion, such as cell wall or pit membrane degradation, be clearly identified at any depth. Lehringer et al.'s (2010) clearer images and red-blue contrast could resuls from more lab experience and longer growth times [100]. Furthermore, they evaluated the softwood Norwegian Spruce, where the generally higher lignin content in softwoods compared to hard-

woods could have resulted in higher contrast, given sufficient degradation has taken place [53]. The work of Srebotnik et al. (1994) on hardwood did also show delignification to start at the rays, in agreement with the observations in this study [99]. They were able to display an increase in the area of blue stained regions upon longer periods of fungal degradation, hence it was expected that the staining in the current study would mark more heavily stained regions from the mycelium-interface downwards.

A strongly stained region was present at the top of each specimen, while deeper staining appeared to originate from vessel cells. It is worth noting that the top region was only a few microns thick and therefore sensitive to damage induced by cutting. Furthermore, it did not show a gradual decrease in intensity throughout the sample's depth. Instead, each specimen showed regions of heavily stained ray cells around the horizontal paths marked by heavily stained vessel pits. These regions were more clearly visible in radial than tangential cuts, and could be a result of early-wood and late-wood regions. Their random locations suggest that the vessels provide a pathway for the fungus and/or its digestive enzymes to grow into and digest the hornbeam veneers all throughout its 5 mm depth. This hypothesis can be confirmed with literature on fungal wood degradation.

Similar white-rot fungal growth and degradation strategies have been observed in literature. Hyphae travel across paths of least resistance, and perform their degradation from the cell lumen outwards [54]. Where some white-rot perform heavy degradation while leaving the vessel elements almost undigested, others start proceeding their degradation from the most porous regions outwards. Hence fibres are solely degraded in the near viscinity of vessels and rays, as is apparent in this study's images. The blue could either mark the delignification of the middle lamella around these porous regions, or the degradation of the inner wall of the cell lumina. For *G. lucidum*, generally reported to be a selective fungus, this in agreement with the relatively high lignin content of the vessel cell wall.

The obtained slices do not facilitate a further quantitative image analysis for two reasons. Firstly, the degree of staining per slide depended on the cutted plane, whereas the orientation of the veneer's microstructure was not controlled throughout the specimen production. Especially the orientation of rays induced a large difference between slices as can be understood from images of non-degraded veneers as shown in Figure 34. Secondly, a transverse slice on a heavily degraded sample as displayed in Figure 35 shows the sensitivity of the cutting location to earlywood and latewood regions, where the first are more porous and heavily stained. This could make the slice location unrepresentative for the complete specimen, where three cutting locations do not suffice to account for this variability.

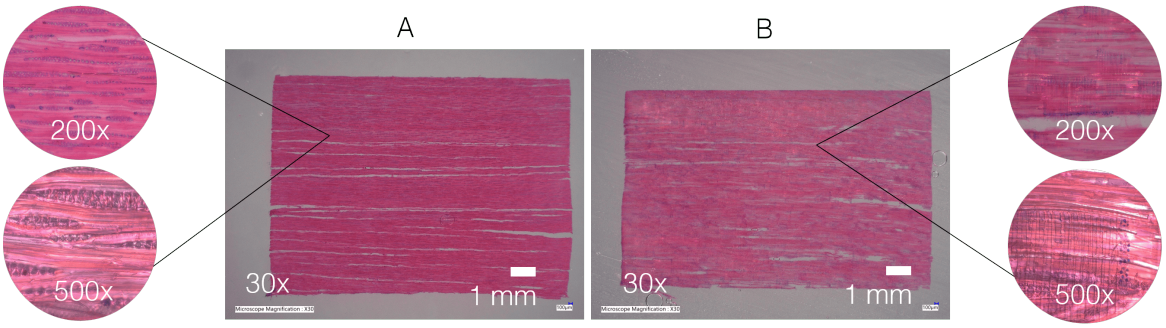

Figure 34: Tangential (A) and radial (B) slices of non-degraded hornbeam veneer. Rays appear in bundles in tangential slices, whereas in radial slices they appear in their length.

On single images, it cannot be concluded whether the astra blue staining is marking hyphae, or solely their excreted lignin degrading enzymes. Namely, literature highlights that low molecular weight (LMW) metabolites can penetrate into cell walls and catalyse depolymerisation of cell wall components [57]. Hence this could potentially induce lignin degradation that marks blue, without an actual presence of hyphae. Therefore, whether indeed the hyphae of *G. lucidum* have penetrated the veneer fully and used it as interlocking mechanism, or whether the apparent degradation is solely a result of the inner diffusion of digestive enzymes, should be confirmed with SEM in the following subsubsection.

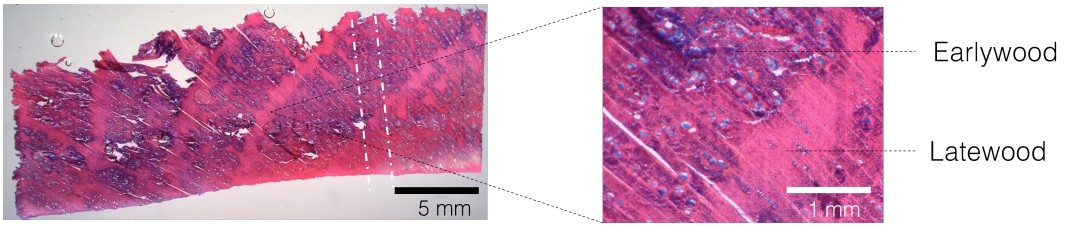

Figure 35: A transverse section of a heavily overgrown hornbeam veneer. White dashed lines indicate the typical slice location taken for microscopy imaging.

The correlations between staining observations and fungal growth and/or digestion on DCB specimens were established by comparing them with one undigested wood veneer that showed minimal staining. It is thereby assumed that there is no variation in staining caused by prior degradation by microorganisms across the batch of veneers used. Furthermore, that there are no inherent regions of relatively lower lignin content in the veneers, as for example known to appear in tension woods that develop in hardwoods growing on inclined surfaces [125]. However, given that the woods have been transferred and grown by professionals for commercial purposes, both are valid assumption.

SEM

The SEM observations are in line with the robust staining of vessel elements, vessel pits, and their surroundings. Namely, in all samples thick hyphae were observed to grow inside vessel elements across the specimen depth, and occassionaly penetrate their cell wall pits. In contrast, the strong staining of rays around these vessel elements could not be related to fungal growth in SEM observations. This could however be a consequence of the cutting methods.

The observations in SEM are limited due to the single cross section evaluated for each group of specimens and the little appearance of fibre and ray lumen. The first makes the conclusions drawn sensitive to the heterogeneous structure of the wood, where again fungal penetration might differ for early- and latewood regions. Furthermore, the cuts induced by the craft knife seemed to not open wood fibre and ray cells along their lengths. Likely, the wood deformed such that the cuts were made in between cells instead. Furthermore, this effect was enlarged by the non-parallel orientation of ray cells with the cut direction, where only the cell's cross section and parts of its sides were visible. This limits the observations of any hyphae that have grown within their lumen. It especially applies to the spruce specimen, where the limited growth observed either resulted from actual poor growth, or the absence of vessels in the softwood. The morphology of the other hyphae could however be compared with literature observations.

The SEM observations are in agreement with the growth strategies described in the work of Gantenbein et al. (2023) [1]. In their work, when an excess of nutrient is present, the mycelium displays an exploitation growth strategy in which it progresses slowly and forms highly branched hyphae. In the opposite case, with little nutrients present, the hyphae advance faster and show little branching. Even though this case is more typically applied to the fungi's growth strategy in surfaces without obstacles, the observations in SEM are in agreement with this description. Namely, branched hyphae networks seemed to occur solely inside the wood vessels in veneers overgrown in highly nutritious environments or inoculated with 15% ME ink. Their growth speed was on the other hand harder to compare.

The origin of individual hyphae could not be retrieved, limiting an assessment of their depth and speed of penetration, and a comparison thereof to literature. The heterogeneous wood structure and 2D imaging did not allow tracing of the fungus along the wood cells. However, the occurrence of hyphae across the full depths of all specimens suggests their penetration depth to be at least 2.5 mm for hornbeam and 1.5 mm for beech. This is half the specimen thickness, as the non-tight coverage of Parafilm allowed the fungus to also overgrow the specimen's bottom. Here it is assumed that penetration from the top and bottom surface is faster than penetration from the sides, of which the validity might vary with respect to the wood rings' orientation in the veneer. Nevertheless, this penetration depth would

correspond to a hyphal penetration speed of at least 0.09 mm in depth per day. Hyphal growth rates in literature range from 40 μm per day in wood cell lumen [126] to 0.7 mm per day across air [1], and even 7 mm per day on MEA plates [32]. Hence it is unlikely that speeds of 0.09 mm per day could be reached from the interface downwards across many cell walls. A more acceptable hypothesis would be that the hyphae entered a vessel at the mycelium-wood interface, and used that as a fast pathway to move downwards into the hardwood veneers.

The limited hyphae penetration in spruce could both originate from more difficult penetration pathways or an incompatibility between the spruce and *G. lucidum*. Namely, in contrast to the $\pm$90 μm diameter vessels, the tracheids have a smaller diameter of $\pm$30 μm. Even though their lumen provide sufficient space for the hyphae to pass, their cell walls and pits could have been more resilient to fungal penetration. Furthermore, where literature reports *G. lucidum* to grow mycelium with similar growth rates on all species of wood evaluated, it could be that the current environment, substrate, and fungi combination did not allow the fungus to well degrade and thereby grow on spruce [103, 127]. This could have also resulted form a different lignin chemical structure, as already highlighted in subsection 2.1.2.

FTIR

A general understanding of lignin's chemical structure explains what was captured by the chosen peaks in FTIR. Lignin's highly complex structure is build up of three coniferyl alcohol units, bound by ether bonds, as presented in Figure 36. [2] Fungi perform an oxidative attack on lignin's side-chains, which increases the amount of conjugated carbonyl groups [129]. The cleavage of primarily the α-β carbon bonds creates more aldehydes and carboxylic acids [130]. Furthermore, as fungal decay progresses, the oxidative extracellular enzymes oxidise lignin's phenyl rings by one-electron abstraction, which further elevate the amount of conjugated carbonyl groups [47]. Their C=O vibrations, in the near proximity of another double bound, generate the increasing peak intensity at 1646 cm^{-1}. Clearly, the phenolic ring breakage decreases the peak intensity of the aromatic skeleton vibrations, at both 1504 and 1594 cm^{-1}.

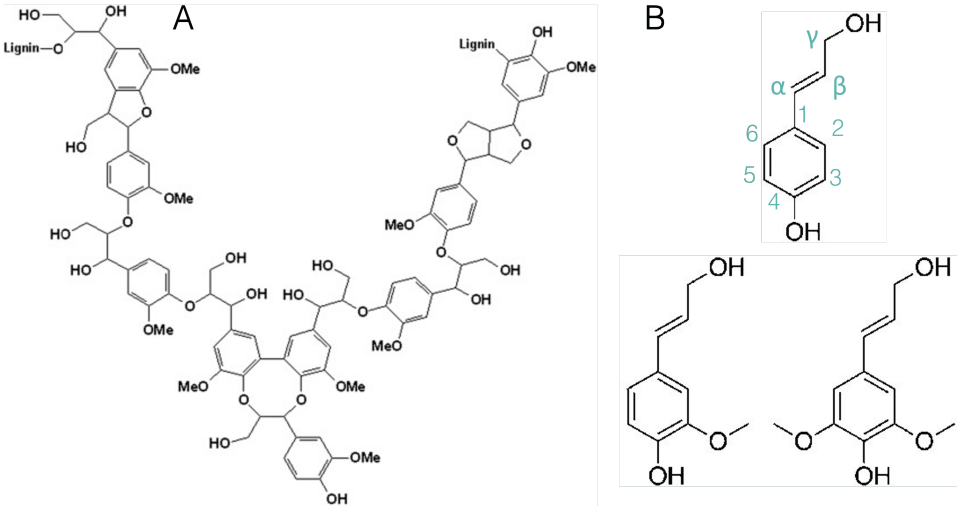

Figure 36: One model of the lignin stucture (A) [131], and its coniferyl subunits (B) [132]. The numbers and letters used to identify C atoms in their structure are given in green.

The decrease in peak intensity ratio could be concluded to at least result partially from fungal degradation, despite overlap of the different materials' spectra. FTIR measured wood, mycelium, and potential traces of ink together, complicating the spectra's interpretation. Especially the absorbance at 1646 cm^{-1} that overlaps with an intense ink peak at 1640 cm^{-1}, and also shows a slight peak in mycelium.

[2] Many models exist for lignin's molecular structure, where other models can be found in books such as presented by Huang et al. (2019) [128].

The mycelium network on the samples in condensed and hence measured, but the several μm penetration depth still reaches the veneer. This is confirmed by the lower relative ratios for DCB samples than pure mycelium. Furthermore, the ink is not prominent in the DCB spectra, as the gap between printed ink lines of 2.5 mm is sufficiently larger than the measurement area size of 1.5 mm for it to not be detected substantially. This is confirmed by the fact that only a small standard deviation in the DCB sample's peak intensity ratios was observed. This was larger if the ink was included in the measurement, appearing in different degrees due to the porous heterogeneous structure of the veneer.

The FTIR analyses in MBC literature show comparable results for lignin degradation by white-rot fungi, which is a good indicator of its mycelium growth. Both Elsacker et al. (2019) and Rigobello et al. (2022) report a decrease in the lignin-associated bands in their lignocellulosic fibres, which in the latter study on *G. lucidum* was more pronounced than the decrease in cellulose and hemicellulose related bands [78, 55]. This is in agreement with genomic, transcriptomic, and secretomic analyses on the digestive enzymes of *G. lucidum* throughout its growth stages by Zhou et al. (2018) [56]. Their results indicated that genes of lignin-modifying enzymes were most expressed during its mycelium growth phase, which went hand-in-hand with their high enzyme activity. In contrast, cellulose and hemicellulose degrading enzymes became more active once the growth of a fruiting body was induced. Hence literature shows that lignin-degradation analysis as performed in this study serves a good indication for the interaction of the fungus with the lignocellulosic substrate material. Furthermore, the obtained results therefore show the ink to serve an inoculation method that generates mycelium growth robust enough to digest lignin in wooden substrate materials.

5.3.5. Summary of the interface evaluation

Optical microscopy, SEM, and FTIR evaluations of the DCB sample arms were able to capture the growth behaviour and lignin degradation of/by *G. lucidum* on the DCB samples. The 3D printing of mycelium-laden ink as inoculation method shows to be robust enough to grow a mycelium that penetrates and digests the veneer substrate material in both hardwood substrates studied.

Regardless of the ME concentration provided, the digestion of lignin on hornbeam veneer's inoculated surfaces was marked by astra blue staining and confirmed with FTIR measurements to the same degree. The staining and microscopy method on veneer cross sections marked vessel elements to be the pathways along which the mycelium digests the wood. Individual hyphae were not be observed, and the images could not be used for a quantitative analysis due to the difference in staining intensities for transverse and radial cuts. The hyphal growth through vessels was however confirmed by SEM, which is in line with the growth strategies observed in white-rot fungal wood decay literature.

SEM showed the mycelium on all specimens grown for 4 weeks, except for spruce, to penetrate the full depth of veneers with the same morphology. Hence, not only the degree of degradation but also the depth of fungal penetration was insensitive to the ME concentration provided. Contrarily, the substrate material type, density, and microstructure is crucial, where spruce did not facilitate fungal penetration. This wood type either has a higher resistance to degradation by *G. lucidum*, or provides less penetration pathways for the fungus regardless of its lower density, for example by the absence of large diameter vessels. These cell types primarily hosted the hyphae in hardwood substrates, with a hardly branching morphology and few μm diameter. Hyphae entered the vessels via both pit and cell wall penetration, where their origin could not be traced. Hence the path and therefore penetration distance of individual hyphae remains undetermined. Nonetheless, in contrast to literature on MBC, this study is to the best of our knowledge the first to report on a mycelium's penetration depth inside the substrate material.

6

Combined discussion

The combined results of DCB testing and interface analysis imply that hyphae penetration and/or lignin digestion facilitate a mycelium's binding ability, but that it is the network grown in between veneers which determines the mycelium's fracture resistance. The first is confirmed by the inability of hyphae to penetrate and overgrow spruce in comparison to beech, where also no adhering mycelium network was formed. Contrarily, the strongest binding sample at 5% ME showed similar degrees of mycelium digestion and/or penetration during analysis by optical microscopy, SEM, and FTIR, when compared to the other ME concentration samples. Hence it is plausible that trends in the fracture resistance more so result from the aerial mycelium network in between veneers, in line with the cohesive mycelium failure found in fracture surface observations.

It should be disclaimed that this hypothesis partially results from the small-scale interface analysis performed in the current study. The summary thereof in section 5.3.5 is based on observations obtained from single samples of each specimen group, where SEM analysis was conducted on only one cross section. Therefore, their results should be considered as a basis for generating hypotheses rather than conclusive evidence of hyphae penetration pathways. Furthermore, these methods did not provide a method to quantitatively evaluate the development of the aerial hyphae network.

The presented results could not distinguish between the individual contributions of the aerial hyphae density, and/or cell wall mechanical properties on its fracture resistance. As already described in section 5.2.4, preliminary results in literature suggest the lower ME content to boost the initial mycelium growth, but not limit the formation of cell wall chitin to provide the hyphae their stiffness [120]. Simultaneously, mycelium biomass measurements of Gantenbein et al. (2023) suggest that the intermediate ME concentrations evaluated give rise to the densest mycelium, which will contribute to its crack resistance [1]. Both factors have likely increased the 5% ME samples mycelium's fracture toughness.

The highest G_I found for 5% ME and the binding ability of mycelium grown from 0% ME ink suggest that future MBC work can limit the supplement sugar content while reaching optimal mycelium binding. This is in contrast to the results of Gantenbein et al. (2023), who found less than 0.5% dry mycelium biomass for 0% ME ink in contrast to 4.5% when grown from 10% ME ink [1]. Similarly, the mycelium in the current study was only able to overgrow 10% of the 0% ME ink petri dish surface after 12 days. Hence it appears that the other ingredients in the ink, vivapur, agar, κ-carrageenan, and peptone, do not facilitate the fungus' growth, but do allow the transfer of a mycelium that can digest the complex carbohydrates in lignocellulosic substrate materials and bind them together. This is an important result for the future development of this bio-based material, limiting its use of nutritious resources.

This work is the first to capture the mycelium's penetration inside lignocellulosic materials aimed to use as MBC substrate materials, and furthermore combine it with mechanical testing results. Other work has solely reported on the appearance of hyphae penetration. It is therefore not possible to compare and contrast the penetration behaviour and binding mechanics to other work.

7

Conclusion

The work presented in this thesis comprised the development of a DCB setup based on the ASTM D5528 standard, to evaluate the interlaminar fracture toughness G_I of *G. lucidum* grown in between two wooden substrates. An analytical data procedure was used to quantify its binding behaviour on beech, spruce, and hornbeam veneers. Inoculation of the lignocellulose by DIW of an optimised mycelium-laden hydrogel allowed the automation and control of fungal placement, and to vary the additional nutrients provided from 0% to 15% ME in the ink. After an optical evaluation of the fracture surface, microscopy on stained cross section slices of the veneers and additional SEM imaging were used to track the growth and digestive behaviour of the fungus throughout the substrate's depth. The fungus' ability to degrade the veneer's lignin was furthermore confirmed by FTIR measurements. Using these methods, the research questions presented in section 3.3 can be reflected on.

Testing setup and sample configuration

Research question 1: *What are the essential steps in the mycelium-laden ink production procedure of Gantenbein et al. (2023), to facilitate its use as a 3D printed inoculum in DCB samples [1]?*

The mycelium-laden ink developed by Gantenbein et al. (2023) can be replicated in the lab environment of the Aerospace faculty [1]. The granulating mixing speed of 5,000 rpm is essential for obtaining a homogeneous ink next to decreasing the agar content from 15% to 3.8%, which facilitate continuous print lines usable as an inoculum in DCB specimens.

Research question 2: *Can a DCB setup be developed and allow the quantification of G_I of an adhesive mycelium network between lignocellulosic substrate materials?*

Wood veneers can be systematically inoculated with fungal ink, and are robust enough for DCB measurements in the Zwick apparatus at the Aerospace faculty. Loading fixtures cannot be glued but should be screwed to the beams. The weak adhesion of the porous mycelium matrix only allows an analytical data evaluation approach which relies on the decrease in beam compliance, to determine G_I at the onset of delamination. It requires additional flexural testing to obtain the elastic modulus of DCB arms, required in the data analysis.

G_I measurements

Research question 3: *Can we measure an effect on the mycelium's G_I of: (a) a prolonged growth time, (b) an increased supply of easy digestible sugars in the inoculating ink, (c) a change in substrate material, providing a different substrate chemistry and porosity?*

Changing the growth time of *G. lucidum* on hornbeam from 3 to 5 weeks is found to increase its G_I with an order of magnitude from 0.129 J/m^2 to an appearing stabilised value of around 1.5 J/m^2 after 4 weeks. This stabilisation would occur somewhere in between 3 and 4 weeks of growth. The best overgrown sample here reached 2.70 J/m^2. When given 4 weeks growth, varying the ME concentration in the ink between 0%, 5%, 10% and 15% yields the highest G_I of 1.83 J/m^2 with 5% ME. Of this specimen group, the highest measured value was 3.46 J/m^2. The optimal ME concentration hence lies in between 0 and 10%. Large variations in all specimen groups appear to result from varying degrees of mycelium growth, despite being provided the same conditions. This reflects the sensitivity of the fungal inoculation method, the limited control of the micro-environments, and the variability inherent to

biological materials. It limits a good comparison between the mycelium's binding ability on hornbeam, beech, and spruce as varying substrate material. The latter two were inoculated with an older fungus from a different plate, which likely lowered its metabolism and thereby binding potential. Nevertheless, a stronger binding on beech than spruce suggests a more important role of the substrate chemistry than its density. Overall, observations of robuster mycelium growth on samples' fracture surfaces show to relate to higher G_I values. More specifically, the overarching observation of cohesive mycelium failure marks the higher importance of its generated gap-crossing aerial hyphae network than the interface on its load carrying capability.

Interface evaluation

Research question 4: Does the mycelium's substrate penetration and digestion change as a function of the supplied amount of easy digestible nutrients, or with different substrate materials used?

Varying the supplied nutrient amount is not captured to vary the mycelium's ability to penetrate and digest the substrate. Optical microscopy shows that the mycelium fully grows within the 5 mm depth of the hornbeam samples, as observed more prominently in SEM for 10% and 15% ME inoculations compared to 0% and 5%. The hyphae travel primarily through vessel elements, which serve as a central pathway for lignin degradation. Its degradation at the surface is confirmed by FTIR measurements, which again does not show a strong correlation with the varied ME concentration provided. Finally, SEM analysis indicates that the degree of substrate penetration is similar between hornbeam and beech samples, whereas spruce exhibits limited colonisation throughout its depth. This difference may be attributed to the absence of wide diameter vessel elements in spruce, the lower preference of *G. lucidum* for digesting this wood type, and again the utilisation of an older fungal inoculum from a different plate.

The presented novel approach towards studying the mechanics of MBC materials, and the microscopy observations throughout the substrate material's depth, increase our understanding of the material's microstructure and micromechanics in the living state. This work serves a basis for future work using the printing mycelium ink inoculation method for research on MBC at the Aerospace faculty, aiming for its use in the automated manufacturing of these materials. It shows a promising pathway towards the optimisation of its living mechanical properties, by controlled fungal and substrate placement and the potentially orientation of the latter. Such continuation of this work would make a significant contribution to the development of MBC materials, and thereby the transition towards an increased applicability and use of these bio-based and sustainable materials.

8

Future work

8.1. Improvements to own work

DCB specimen preparation

The print design and inoculation method can be modified to enhance mycelium growth and reduce variation in DCB test results. Preliminary experiments with a parallel print design crossing the full veneer width with a lower inner-line distance of 2.2 mm showed a 28% higher G_I. The increased ink amount likely caused a stronger aerial mycelium network. Future work should experiment with the ink supply and available veneer surface for binding, to establish an optimised fungal inoculum for automated MBC production. However, the results still showed much variation, suggesting that a more robust alternative inoculum could be spawn insertion, which is the current standard inoculation method in MBC manufacturing [16, 11]. This approach provides a more mature mycelium with higher metabolic activity. Although controlling the amount of inoculum and nutrients will be challenging, comparing the developed mycelium's strength and assessing the consistency in its fracture resistance would be valuable.

DCB testing and data analysis

Larger DCB specimens or a more sensitive testing setup would improve testing accuracy and data processing. Increasing the specimen's width would enhance adhesion and prevent rapid crack propagation through the network, which limited the analytical data analysis as presented in section 4.2.3. Lengthening the specimen would allow a longer G_I evaluation and reduce edge effects. Such samples would likely need support during testing, to prevent mycelium breakage caused by the sample's weight. Furthermore, using a more sensitive setup would allow for separate measurements of the veneer's E_{xx} in each specimen, decreasing the errors stemming from veneer variability in 3PB tests as explained in section 5.2.4. Lastly, rotating the setup with 90°would limit the specimen's weight to induce mycelium failure, and therefore also reduce inaccuracies and limitations of the analytical data analysis.

Where the current analytical data analysis relies on the beam's clamped boundary conditions with no influence on the elastic properties of the adhesive, an alternative method based on the elastic foundation theory could be considered. Here one incorporates the elastic properties of the adhesive ahead of the crack tip in the data analysis, which could even include the heterogeneities in the adhesive, as presented by Heide-Jorgensen and Budzik (2017) [133]. The procedure models the arm as an unsupported beam with a point load behind the crack tip, and a beam supported by an elastic foundation in front of the crack tip. Due to the extremely low adhesion of the mycelium network, the tensile loading affect would be significant. Therefore, this elastic foundation model could estimate the debonding more accurately, when performed in combination with accurate tensile tests on the mycelium network.

Microscopy methods

The variable occurence of tangential and radial cuts in the optical microscopy method limited a systematic evaluation of the degradation capacity of the mycelium in different DCB specimens. Making a pre-selection of the veneers to be tested based on their initial position in the tree could limit this variability, and in combination with a stable staining method and microscopy setup facilitate a more systematic analysis of the staining intensity by programs such as ImageJ.

Other stains that are reported stain hyphal cell walls could be experimented with, for their ability to track hyphae penetration in the substrate material. Examples are calcofluor white, lactophenol blue, and analin blue [1, 134]. All are however also reported to stain lignocellulose materials, which could complicate interpretation of the staining intensity.

8.2. Alternative testing methods

Mechanical testing

Given the vulnerability of the DCB specimens, it would be of interest to study more micromechanical testing methods. Interfacial shear tests such as the single fibre fragmentation test (SFFT) and single fibre pull-out test (SFPT) could be utilised to examine the interface between natural fibres and composite matrices with smaller specimens [135]. These methods necessitate the embedding of a fibre into a block of matrix and securing it with a testing apparatus. To assess the feasibility of using a printed mycelium grid as the matrix, experiments must verify whether the material can be gripped without causing significant deformation. If successful, these tests are in comparison to DCB likely to be more easily transferrable to other fibres typically used in MBC, such as hemp and flax.

Interface evaluation

More laborious methods could be used to more accurately assess fungal degradation and/or penetration. Prominently appearing in literature are the Klason method and the glucosamine assay, both destructive testing methods. The first allows accurate quantification of the lignin content in lignocellulosic materials, and thereby the degree of digestion by the fungus [136]. The latter quantifies the glucosamine content in materials, a key components of chitin in the fungal cell wall [137]. Both approaches involve several dissolution steps with acids and alcohols, and require final evaluation of sample absorbance by either UV-VIS or FTIR. To assess the feasibility of employing these techniques at specific depths within the wood veneer, such as by slicing the veneer with microtomy, experiments should be conducted.

8.3. Expansion of current work

The binding behaviour of a broader fungal species selection could be evaluated by means of the methods presented in the current study. As the growth and digestive behaviour of different white-rot species causing different MBC mechanical properties, it would be interesting to study whether this could be caused by a difference in the mycelium's G_I due to changes in its density or cell wall thickness and/or composition [11, 16]. Furthermore, the adhesive properties of genetically modified mycelia could be studied, where literature has already experimented with ycelium missing an essential gene encoding for hydrophobins [138]. Working with this fungus could highlight the exact binding role played by the interlocking penetration of the hyphae, regardless of the presence of these hydrophobic surface binding proteins. Lastly, working with non-lignin degrading fungi could provide an understanding in their ability to play a binding role in MBC. These will have less penetrative capacities, but will harness the lignocellulosic substrate material over a longer time period in MBC materials.

Also other substrates could be tested using the DCB method, to optimise mycelium binding. DCB experiments on veneers of different densities and species in combinations with growth experiments on grinded woods could mark the roles played by their ability to feed the fungus and provided penetrative pathways facilitating its binding. Furthermore, tests on veneers with defects such as knots could predict the changes in binding on more waste-based sources. Also the potential of surface treatments such as delignification procedures could be evaluated. Work by Frey et al. (2018) showed an 25% decrease in spruce density after a full acetic bleaching procedure [139]. Shortening treatment times, lowering treatment temperatures, or lowering acetic acid concentrations could make it a controllable porosity increasing surface treatment. In combination with the more simplified resulting surface chemistry this could alter the mycelium binding, the benefits of which should be confirmed with experiments.

References

[1] Silvan Gantenbein et al. “Three-dimensional printing of mycelium hydrogels into living complex materials”. In: *Nature Materials* 22.1 (2023), pp. 128–134.

[2] Michael F. Ashby. “Chapter 1 - Background: Materials, Energy and Sustainability”. In: *Materials and Sustainable Development*. Ed. by Michael F. Ashby. Boston: Butterworth-Heinemann, 2016, pp. 1–25. ISBN: 978-0-08-100176-9. DOI: https://doi.org/10.1016/B978-0-08-100176-9.00001-3. URL: https://www.sciencedirect.com/science/article/pii/B9780081001769000013.

[3] John M Christensen and A Olhoff. “Emissions gap report 2019”. In: *United Nations Environment Programme (UNEP): Gigiri Nairobi, Kenya* (2019).

[4] European Commission. *Going climate-neutral by 2050*. 2019. URL: https://op.europa.eu/en/publication-detail/-/publication/92f6d5bc-76bc-11e9-9f05-01aa75ed71a1 (visited on 06/07/2023).

[5] Sara Corrado and Serenella Sala. “Bio-economy contribution to circular economy”. In: *Designing sustainable technologies, products and policies: from science to innovation* (2018), pp. 49–59.

[6] Ulrike GK Wegst et al. “Bioinspired structural materials”. In: *Nature materials* 14.1 (2015), pp. 23–36.

[7] Audrey Velasco-Hogan, Jun Xu, and Marc A Meyers. “Additive manufacturing as a method to design and optimize bioinspired structures”. In: *Advanced Materials* 30.52 (2018), p. 1800940.

[8] Joseph C Cremaldi and Bharat Bhushan. “Bioinspired self-healing materials: lessons from nature”. In: *Beilstein Journal of Nanotechnology* 9.1 (2018), pp. 907–935.

[9] Elise Elsacker et al. “Growing living and multifunctional mycelium composites for large-scale formwork applications using robotic abrasive wire-cutting”. In: *Construction and Building Materials* 283 (2021), p. 122732.

[10] Sehrish Manan et al. “Synthesis and applications of fungal mycelium-based advanced functional materials”. In: *Journal of Bioresources and Bioproducts* 6.1 (2021), pp. 1–10.

[11] Elise Elsacker et al. “A comprehensive framework for the production of mycelium-based lignocellulosic composites”. In: *Science of The Total Environment* 725 (2020), p. 138431.

[12] *Mogu - radical by nature*. Accessed June 07, 2023. URL: https://mogu.bio/.

[13] *Ecovative - Mycelium Technology*. Accessed June 07, 2023. URL: https://www.ecovative.com/.

[14] *Funding Mushrooms For Ecovative Design*. Accessed May 30, 2023. URL: https://cen.acs.org/articles/91/i42/Funding-Mushrooms-Ecovative-Design.html.

[15] *Hy-Fi reinvents the brick*. Accessed May 30, 2023. URL: https://www.arup.com/news-and-events/hyfi-reinvents-the-brick.

[16] Carolina Girometta et al. “Physico-mechanical and thermodynamic properties of mycelium-based biocomposites: A review”. In: *Sustainability* 11.1 (2019), p. 281.

[17] Ross M McBee et al. “Engineering living and regenerative fungal–bacterial biocomposite structures”. In: *Nature Materials* 21.4 (2022), pp. 471–478.

[18] Andrew Adamatzky and Antoni Gandia. “Living mycelium composites discern weights via patterns of electrical activity”. In: *Journal of Bioresources and Bioproducts* 7.1 (2022), pp. 26–32.

[19] Wenjing Sun et al. “Fungal and enzymatic pretreatments in hot-pressed lignocellulosic biocomposites: A critical review”. In: *Journal of Cleaner Production* 353 (2022), p. 131659.

[20] Noor Idayu Nashiruddin et al. “Effect of growth factors on the production of mycelium-based biofoam”. In: *Clean Technologies and Environmental Policy* 24.1 (2022), pp. 351–361.

[21] Isaac M Daniel et al. *Engineering mechanics of composite materials*. Vol. 1994. Oxford university press New York, 2006.

[22] Ru Liu et al. “Preparation of a kind of novel sustainable mycelium/cotton stalk composites and effects of pressing temperature on the properties”. In: *Industrial Crops and Products* 141 (2019), p. 111732.

[23] Filippo Zampieri, Han AB Wösten, and Karin Scholtmeijer. “Creating surface properties using a palette of hydrophobins”. In: *Materials* 3.9 (2010), pp. 4607–4625.

[24] HA Wösten, FH Schuren, and JG Wessels. “Interfacial self-assembly of a hydrophobin into an amphipathic protein membrane mediates fungal attachment to hydrophobic surfaces.” In: *The EMBO Journal* 13.24 (1994), pp. 5848–5854.

[25] Han AB Wösten. “Hydrophobins: multipurpose proteins”. In: *Annual Reviews in Microbiology* 55.1 (2001), pp. 625–646.

[26] Meredith Blackwell. “The Fungi: 1, 2, 3… 5.1 million species?” In: *American journal of botany* 98.3 (2011), pp. 426–438.

[27] Jeroen G van den Brandhof and Han AB Wösten. “Risk assessment of fungal materials”. In: *Fungal Biology and Biotechnology* 9.1 (2022), p. 3.

[28] *Fungal life cycles – spores and more*. Accessed June 1, 2023. URL: https://www.sciencelearn.org.nz/resources/2664-fungal-life-cycles-spores-and-more.

[29] Mitchell Jones, Tien Huynh, and Sabu John. “Inherent species characteristic influence and growth performance assessment for mycelium composite applications”. In: *Advanced Materials Letters* 9.1 (2018), pp. 71–80.

[30] John Webster and Roland Weber. *Introduction to fungi*. Cambridge university press, 2007.

[31] Corner EJH. “The construction of polypores”. In: *Phytomorphology* 1.6 (1953), pp. 152–69.

[32] Tomoko Kuribayashi et al. “Dense and continuous networks of aerial hyphae improve flexibility and shape retention of mycelium composite in the wet state”. In: *Composites Part A: Applied Science and Manufacturing* 152 (2022), p. 106688.

[33] Jean-Paul Latgé. *The Fungal Cell Wall: An Armour and a Weapon for Human Fungal Pathogens*. Vol. 425. Springer Nature, 2020.

[34] Gero Steinberg. “Hyphal growth: a tale of motors, lipids, and the Spitzenkorper”. In: *Eukaryotic cell* 6.3 (2007), pp. 351–360.

[35] Alexandra Brand and Neil AR Gow. “Tropic orientation responses of pathogenic fungi”. In: *Morphogenesis and pathogenicity in fungi* (2012), pp. 21–41.

[36] Meritxell Riquelme and Eddy Sánchez-León. “The Spitzenkörper: a choreographer of fungal growth and morphogenesis”. In: *Current opinion in microbiology* 20 (2014), pp. 27–33.

[37] Ivey Geoghegan, Gero Steinberg, and Sarah Gurr. “The role of the fungal cell wall in the infection of plants”. In: *Trends in microbiology* 25.12 (2017), pp. 957–967.

[38] Mohammad Retaful Islam et al. “Morphology and mechanics of fungal mycelium”. In: *Scientific reports* 7.1 (2017), p. 13070.

[39] Mitchell P Jones et al. “Agricultural by-product suitability for the production of chitinous composites and nanofibers utilising Trametes versicolor and Polyporus brumalis mycelial growth”. In: *Process Biochemistry* 80 (2019), pp. 95–102.

[40] Lina F Ballesteros et al. *Lignocellulosic materials and their use in bio-based packaging*. Springer, 2018.

[41] Pankaj Bhatt et al. *Microbial technology for sustainable environment*. Springer, 2021.

[42] Freek VW Appels et al. “Fabrication factors influencing mechanical, moisture-and water-related properties of mycelium-based composites”. In: *Materials & Design* 161 (2019), pp. 64–71.

[43] Hana Vašatko et al. “Basic research of material properties of mycelium-based composites”. In: *Biomimetics* 7.2 (2022), p. 51.

[44] Greg A Holt et al. “Fungal mycelium and cotton plant materials in the manufacture of biodegradable molded packaging material: Evaluation study of select blends of cotton byproducts”. In: *Journal of Biobased Materials and Bioenergy* 6.4 (2012), pp. 431–439.

[45] Iris S Santos et al. “Influence of drying heat treatments on the mechanical behavior and physicochemical properties of mycelial biocomposite”. In: *Composites Part B: Engineering* 217 (2021), p. 108870.

[46] Alexander R Ziegler et al. “Evaluation of physico-mechanical properties of mycelium reinforced green biocomposites made from cellulosic fibers”. In: *Applied engineering in agriculture* 32.6 (2016), pp. 931–938.

[47] Martina Andlar et al. “Lignocellulose degradation: An overview of fungi and fungal enzymes involved in lignocellulose degradation”. In: *Engineering in Life Sciences* 18.11 (2018), pp. 768–778.

[48] Potters, Geert and Van Goethem, Davina and Schutte, Frances. *Promising Biofuel Resources: Lignocellulose and Algae*. 2010. URL: https://www.nature.com/scitable/topicpage/promising-biofuel-resources-lignocellulose-and-algae-14255919/ (visited on 06/21/2022).

[49] Johanna Rytioja et al. “Plant-polysaccharide-degrading enzymes from basidiomycetes”. In: *Microbiology and Molecular Biology Reviews* 78.4 (2014), pp. 614–649.

[50] Joseph E Jakes et al. “Effects of moisture on diffusion in unmodified wood cell walls: a phenomenological polymer science approach”. In: *Forests* 10.12 (2019), p. 1084.

[51] George Thomas Tsoumis. *Microstructure*. Accessed May 19, 2023. URL: https://www.britannica.com/science/wood-plant-tissue/Microstructure.

[52] Oliver F Kläusler. “Improvement of one-component polyurethane bonded wooden joints under wet conditions”. PhD thesis. ETH Zurich, 2014.

[53] Dietrich Fengel and Gerd Wegener. *Wood: chemistry, ultrastructure, reactions*. Walter de Gruyter, 2011.

[54] Francis WMR Schwarze. “Wood decay under the microscope”. In: *Fungal biology reviews* 21.4 (2007), pp. 133–170.

[55] Adrien Rigobello and Phil Ayres. “Compressive behaviour of anisotropic mycelium-based composites”. In: *Scientific Reports* 12.1 (2022), pp. 1–13.

[56] Shuai Zhou et al. “Investigation of lignocellulolytic enzymes during different growth phases of Ganoderma lucidum strain G0119 using genomic, transcriptomic and secretomic analyses”. In: *PloS one* 13.5 (2018), e0198404.

[57] Barry Goodell. “Fungi involved in the biodeterioration and bioconversion of lignocellulose substrates”. In: *Genetics and Biotechnology* (2020), pp. 369–397.

[58] FWMR Schwarze and S Baum. “Mechanisms of reaction zone penetration by decay fungi in wood of beech (Fagus sylvatica)”. In: *The New Phytologist* 146.1 (2000), pp. 129–140.

[59] Francis WMR Schwarze, Julia Engels, and Claus Mattheck. *Fungal strategies of wood decay in trees*. Springer Science & Business Media, 2000.

[60] Aino A Kéérik. “Decomposition of wood”. In: *Biology of Plant Litter Decomposition V1* 1 (2012), p. 129.

[61] Galena V Angelova, Mariya S Brazkova, and Albert I Krastanov. “Renewable mycelium based composite–sustainable approach for lignocellulose waste recovery and alternative to synthetic materials–a review”. In: *Zeitschrift für Naturforschung C* 76.11-12 (2021), pp. 431–442.

[62] Mitchell Jones et al. “Mycelium composites: a review of engineering characteristics and growth kinetics”. In: *Journal of Bionanoscience* 11.4 (2017), pp. 241–257.

[63] Xin Ying Chan et al. “Mechanical properties of dense mycelium-bound composites under accelerated tropical weathering conditions”. In: *Scientific Reports* 11.1 (2021), pp. 1–10.

[64] Mariano Aquino et al. “Evaluation of mycelium composite materials produced by five Patagonian fungal species”. In: *Maderas. Ciencia y tecnología* 24 (2022).

[65] Eugene Soh et al. “Effect of common foods as supplements for the mycelium growth of Ganoderma lucidum and Pleurotus ostreatus on solid substrates”. In: *Plos one* 16.11 (2021), e0260170.

[66] Funda Atila. “Compositional changes in lignocellulosic content of some agro-wastes during the production cycle of shiitake mushroom”. In: *Scientia Horticulturae* 245 (2019), pp. 263–268.

[67] Yoshifumi AMANO et al. “Influence of Light Illumination on Mycelial Growth of Ganoderma lucidum Karst”. In: *Mushroom Science and Biotechnology* 15.1 (2007), pp. 17–24.

[68] Simon Vandelook et al. “Current state and future prospects of pure mycelium materials”. In: *Fungal biology and biotechnology* 8.1 (2021), pp. 1–10.

[69] Antoni Gandia et al. “Flexible fungal materials: shaping the future”. In: *Trends in Biotechnology* 39.12 (2021), pp. 1321–1331.

[70] Ali Ghazvinian and Benay Gursoy. “Basics of building with mycelium-based bio-composites: a review of Built Projects and Related material research”. In: *Journal of Green Building* 17.1 (2022), pp. 37–69.

[71] Zeynep Tacer-Caba et al. “Comparison of novel fungal mycelia strains and sustainable growth substrates to produce humidity-resistant biocomposites”. In: *Materials & Design* 192 (2020), p. 108728.

[72] Eda Özdemir et al. “Wood-veneer-reinforced mycelium composites for sustainable building components”. In: *Biomimetics* 7.2 (2022), p. 39.

[73] Selina Bitting et al. “Challenges and Opportunities in Scaling up Architectural Applications of Mycelium-Based Materials with Digital Fabrication”. In: *Biomimetics* 7.2 (Apr. 2022), p. 44. ISSN: 2313-7673. DOI: 10.3390/biomimetics7020044. URL: https://www.mdpi.com/2313-7673/7/2/44.

[74] Huaiyou Chen et al. “Extrusion-based additive manufacturing of fungal-based composite materials using the tinder fungus Fomes fomentarius”. In: *Fungal Biology and Biotechnology* 8 (2021), pp. 1–11.

[75] Behzad Modanloo et al. “Tilted Arch; Implementation of additive manufacturing and bio-welding of mycelium-based composites”. In: *Biomimetics* 6.4 (2021), p. 68.

[76] Elise Elsacker, Eveline Peeters, and Lars De Laet. “Large-scale robotic extrusion-based additive manufacturing with living mycelium materials”. In: *Sustainable Futures* 4 (2022), p. 100085.

[77] Aileen Hoenerloh, Dilan Ozkan, and Jane Scott. “Multi-Organism Composites: Combined Growth Potential of Mycelium and Bacterial Cellulose”. In: *Biomimetics* 7.2 (2022), p. 55.

[78] Elise Elsacker et al. “Mechanical, physical and chemical characterisation of mycelium-based composites with different types of lignocellulosic substrates”. In: *PLoS One* 14.7 (2019), e0213954.

[79] Zhaohui Yang et al. “Physical and mechanical properties of fungal mycelium-based biofoam”. In: *Journal of Materials in Civil Engineering* 29.7 (2017), p. 04017030.

[80] Maxwell Paca Matos et al. “Production of biocomposites from the reuse of coconut powder colonized by Shiitake mushroom”. In: *Ciência e Agrotecnologia* 43 (2019).

[81] JA López Nava et al. “Assessment of edible fungi and films bio-based material simulating expanded polystyrene”. In: *Materials and Manufacturing Processes* 31.8 (2016), pp. 1085–1090.

[82] Libin Yang and Zhao Qin. “Mycelium-based wood composites for light weight and high strength by experiment and machine learning”. In: *Cell Reports Physical Science* (2023).

[83] Adrien Rigobello, Claudia Colmo, and Phil Ayres. “Effect of composition strategies on mycelium-based composites flexural behaviour”. In: *Biomimetics* 7.2 (2022), p. 53.

[84] S Travaglini et al. “Mycology matrix composites”. In: *Annual technical conference; 28th, American Society for Composites*. 2013, pp. 9–11.

[85] Elise Elsacker et al. “Mechanical characteristics of bacterial cellulose-reinforced mycelium composite materials”. In: *Fungal biology and biotechnology* 8.1 (2021), pp. 1–14.

[86] Mitchell Jones et al. “Engineered mycelium composite construction materials from fungal biorefineries: A critical review”. In: *Materials & Design* 187 (2020), p. 108397.

[87] Ernest T Selig and Carl J Roner. “Effects of particle characteristics on behavior of granular material”. In: *Transportation Research Record* 1131 (1987).

[88] Mohammad Retaful Islam et al. “Mechanical behavior of mycelium-based particulate composites”. In: *Journal of Materials Science* 53 (2018), pp. 16371–16382.

[89] Lai Jiang et al. “Cost modeling and optimization of a manufacturing system for mycelium-based biocomposite parts”. In: *Journal of Manufacturing Systems* 41 (2016), pp. 8–20.

[90] Ru Liu et al. “Improvement of mechanical properties of mycelium/cotton stalk composites by water immersion”. In: *Composite Interfaces* 27.10 (2020), pp. 953–966.

[91] Wenjing Sun et al. “Fully bio-based hybrid composites made of wood, fungal mycelium and cellulose nanofibrils”. In: *Scientific reports* 9.1 (2019), p. 3766.

[92] Leyu Gou et al. “Morphological and physico-mechanical properties of mycelium biocomposites with natural reinforcement particles”. In: *Construction and Building Materials* 304 (2021), p. 124656.

[93] Elise Elsacker, Meng Zhang, and Martyn Dade-Robertson. “Fungal Engineered Living Materials: The Viability of Pure Mycelium Materials with Self-Healing Functionalities”. In: *Advanced Functional Materials* (2023), p. 2301875.

[94] Andrew Adamatzky. “On spiking behaviour of oyster fungi Pleurotus djamor”. In: *Scientific reports* 8.1 (2018), p. 7873.

[95] Michael J Berridge, Martin D Bootman, and H Llewelyn Roderick. “Calcium signalling: dynamics, homeostasis and remodelling”. In: *Nature reviews Molecular cell biology* 4.7 (2003), pp. 517–529.

[96] Andrew Adamatzky, Antoni Gandia, and Alessandro Chiolerio. “Towards fungal sensing skin”. In: *Fungal biology and biotechnology* 8.1 (2021), pp. 1–7.

[97] Andrew Adamatzky et al. “Fungal electronics”. In: *Biosystems* 212 (2022), p. 104588.

[98] Wenjing Sun et al. “Functionality of surface mycelium interfaces in wood bonding”. In: *ACS applied materials & interfaces* 12.51 (2020), pp. 57431–57440.

[99] Ewald Srebotnik and Kurt Messner. “A simple method that uses differential staining and light microscopy to assess the selectivity of wood delignification by white rot fungi”. In: *Applied and environmental microbiology* 60.4 (1994), pp. 1383–1386.

[100] Christian Lehringer et al. “Anatomy of bioincised Norway spruce wood”. In: *International Biodeterioration & Biodegradation* 64.5 (2010), pp. 346–355.

[101] J Bond et al. “Safranine fluorescent staining of wood cell walls”. In: *Biotechnic & Histochemistry* 83.3-4 (2008), pp. 161–171.

[102] ASTM-International. “ASTM D5528/D5528M-21: Standard Test Method for Mode I Interlaminar Fracture Toughness of Unidirectional Fiber-Reinforced Polymer Matrix Composites”. In: (2022). URL: https://www.astm.org/d5528_d5528m-21.html.

[103] Majid Azizi et al. “Yield performance of Lingzhi or Reishi medicinal mushroom, Ganoderma lucidum (W. Curt.: Fr.) P. Karst.(higher Basidiomycetes), using different waste materials as substrates”. In: *International Journal of Medicinal Mushrooms* 14.5 (2012).

[104] Jong Sik Kim, Jie Gao, and Geoffrey Daniel. “Cytochemical and immunocytochemical characterization of wood decayed by the white rot fungus Pycnoporus sanguineus I. preferential lignin degradation prior to hemicelluloses in Norway spruce wood”. In: *International Biodeterioration & Biodegradation* 105 (2015), pp. 30–40.

[105] *Informatie over hout, plaatmaterialen en houttoepassingen.* Accessed May 19, 2023. URL: https://houtinfo.nl/.

[106] Ran Tao. “Enhancing the bonding of CFRP adhesive joints through laser-based surface preparation strategies”. PhD thesis. 2020.

[107] ASTM-International. “ASTM D1037: Evaluating properties of wood-base fiber and particle panel materials”. In: (2020). URL: https://www.astm.org/d1037-12r20.html.

[108] ASTM-International. “ASTM D143: Standard test methods for small clear specimens of timber”. In: (2022). URL: https://www.astm.org/d0143-22.html.

[109] ASTM-International. “ASTM D3043: Standard methods for structural panels in flexure”. In: (2018). URL: https://www.astm.org/d3043-17.html.

[110] ASTM-International. “ASTM D198: Standard methods for structural panels in flexure”. In: (2022). URL: https://www.astm.org/d0198-22a.html.

[111] ASTM-International. “ASTM D4761: Mechanical properties of lumber and wood-based structural materials”. In: (2019). URL: https://www.astm.org/d4761-19.html.

[112] Nederlands Normalisatie-instituut. “NEN-EN 310 - Houtachtige plaatmaterialen. Bepaling van de elasticiteitsmodulus bij buiging en van de buigsterkte”. In: (1993). URL: https://www.nen.nl/nen-en-310-1993-en-10293.

[113] KK Pandey and AJ Pitman. “FTIR studies of the changes in wood chemistry following decay by brown-rot and white-rot fungi”. In: *International biodeterioration & biodegradation* 52.3 (2003), pp. 151–160.

[114] Qian Cai et al. “Dissolving process of bamboo powder analyzed by FT-IR spectroscopy”. In: *Journal of Molecular Structure* 1171 (2018), pp. 639–643.

[115] R Solár et al. “Study of the overall alterations of hornbeam wood chips (Carpinus betulus L.) with the emphasis on lignin in the pretreatment by white rot fungus.” In: *Drevársky vỳskum* 45.4 (2000), pp. 19–32.

[116] *Selection of mycelium strains*. Accessed May 7, 2023. URL: https://gluckspilze.com/6selektionierung-1.

[117] Jia-Hui Xing et al. “Morphological characters and phylogenetic analysis reveal a new species within the Ganoderma lucidum complex from South Africa”. In: *Phytotaxa* 266.2 (2016), pp. 115–124.

[118] Carolin Siegel, Beate Buchelt, and André Wagenführ. “Application of the three-point bending test for small-sized wood and veneer samples”. In: *Wood Material Science & Engineering* 17.3 (2022), pp. 157–162.

[119] Maura Harumi Sugai-Guérios et al. “Modeling the growth of filamentous fungi at the particle scale in solid-state fermentation systems”. In: *Filaments in Bioprocesses* (2015), pp. 171–221.

[120] Muhammad Haneef et al. “Advanced materials from fungal mycelium: fabrication and tuning of physical properties”. In: *Scientific reports* 7.1 (2017), pp. 1–11.

[121] Hyun-Bum Kim, Kimiyoshi Naito, and Hiroyuki Oguma. “Fatigue crack growth properties of a two-part acrylic-based adhesive in an adhesive bonded joint: Double cantilever-beam tests under Mode I loading”. In: *International Journal of Fatigue* 98 (2017), pp. 286–295.

[122] Hyun-Bum Kim, Kimiyoshi Naito, and Hiroyuki Oguma. “Double cantilever-beam test comparisons of Mode I fracture toughness of adherends bonded using DP8010 and DP8005 acrylic-based adhesives”. In: *International Journal of Adhesion and Adhesives* 82 (2018), pp. 173–183.

[123] Randy A Mrozek et al. “Influence of solvent size on the mechanical properties and rheology of polydimethylsiloxane-based polymeric gels”. In: *Polymer* 52.15 (2011), pp. 3422–3430.

[124] Ruofei Chang et al. “An experimental study on stretchy and tough PDMS/fabric composites”. In: *Journal of Applied Mechanics* 86.1 (2019), p. 011012.

[125] Widyanto Dwi Nugroho et al. “Gibberellin mediates the development of gelatinous fibres in the tension wood of inclined Acacia mangium seedlings”. In: *Annals of botany* 112.7 (2013), pp. 1321–1329.

[126] Michael D Hale and Rodney A Eaton. “Oscillatory growth of fungal hyphae in wood cell walls”. In: *Transactions of the British Mycological society* 84.2 (1985), pp. 277–288.

[127] Adam Brezáni et al. “Cultivation of medicinal mushrooms on spruce sawdust fermented with a liquid digestate from biogas stations”. In: *International Journal of Medicinal Mushrooms* 21.3 (2019).

[128] “Chapter 2 - Structure and Characteristics of Lignin”. In: *Lignin Chemistry and Applications*. Ed. by Jin Huang, Shiyu Fu, and Lin Gan. Elsevier, 2019, pp. 25–50. ISBN: 978-0-12-813941-7. DOI: https://doi.org/10.1016/B978-0-12-813941-7.00002-3. URL: https://www.sciencedirect.com/science/article/pii/B9780128139417000023.

[129] Don L Crawford et al. “Chemistry of softwood lignin degradation by Streptomyces viridosporus”. In: *Archives of microbiology* 131 (1982), pp. 140–145.

[130] Oskar Faix et al. “Monitoring of chemical changes in white-rot degraded beech wood by pyrolysis—Gas chromatography and Fourier-transform infrared spectroscopy”. In: *Journal of Analytical and Applied Pyrolysis* 21.1-2 (1991), pp. 147–162.

[131] S Sebbahi et al. “Characterization of lignin and derivative chars by infrared spectroscopy”. In: *Journal of Material and Environmental Science* 6.9 (2015), pp. 2461–2468.

[132] Jessica NG Stanley et al. “Reactions of p-coumaryl alcohol model compounds with dimethyl carbonate. Towards the upgrading of lignin building blocks”. In: *Green chemistry* 15.11 (2013), pp. 3195–3204.

[133] Simon Heide-Jørgensen and Michal K Budzik. “Crack growth along heterogeneous interface during the DCB experiment”. In: *International Journal of Solids and Structures* 120 (2017), pp. 278–291.

[134] Matthias Jörg Fuhr et al. “Penetration capacity of the wood-decay fungus Physisporinus vitreus”. In: *Complex Adaptive Systems Modeling* 1.1 (2013), pp. 1–15.

[135] Yonghui Zhou, Mizi Fan, and Lihui Chen. “Interface and bonding mechanisms of plant fibre composites: An overview”. In: *Composites Part B: Engineering* 101 (2016), pp. 31–45.

[136] Flavia Carolina Moreira-Vilar et al. “The acetyl bromide method is faster, simpler and presents best recovery of lignin in different herbaceous tissues than Klason and thioglycolic acid methods”. In: *PloS one* 9.10 (2014), e110000.

[137] I Cornet et al. “FTIR as an easy and fast analytical approach to follow up microbial growth during fungal pretreatment of poplar wood with Phanerochaete chrysosporium”. In: *Journal of microbiological methods* 145 (2018), pp. 82–86.

[138] Freek VW Appels et al. “Hydrophobin gene deletion and environmental growth conditions impact mechanical properties of mycelium by affecting the density of the material”. In: *Scientific reports* 8.1 (2018), p. 4703.

[139] Marion Frey et al. “Delignified and densified cellulose bulk materials with excellent tensile properties for sustainable engineering”. In: *ACS Applied Materials & Interfaces* 10.5 (2018), pp. 5030–5037.

Appendices

A

Ink production procedure

The mycelium-laden ink production employed in this study, inspired by the work of Gantenbein et al. (2023), followed the next procedure [1]:

1. Mix the cellulose based thickener in half of the total water amount with a spatula. Use a high shear mixer (IKA T25 digital Ultra Turrax, equiped with a S 25 N dispersing element) to mix the solution for 10 min at 10,000 rpm and let it rest for at least 15 minutes.
2. Mix the agar, κ-carrageenan, peptone, and ME for their concentration in the final mixture in half of the total water amount, and manually stir until fully dissolved.
3. Manually mix the two mixtures.
4. Bottle the ink, shake it for homogenisation, and autoclave for 20 minutes at 121 $^{\circ}\mathrm{C}$ (Hirayama HG-50).
5. Before the mixture cools down, shake it for homogenisation of the mixture and poor 40 mL of medium into 50 mL tubes. Let the mixture cool down, solidify, and store in the fridge.
6. Place a milk frother driven by a high speed mixer (Proxxon 28512) through a small hole in the lit of the tube, and mix two minutes at 5,000 rpm to granulate the solidified mixture into the final ink.
7. Spread the amount of ink obtained from 3 tubes over 2 petri dishes, and inoculate with the fungus obtained from an overgrown malt extract agar (MEA) plate.
8. Cover the petri dishes with parafilm, place in the incubator, and allow the fungus to overgrow the plate at a temperature of 26°C and moisture content between 50 and 60% for 12 days.
9. Remove the fungal film developed with use of tweezers, and manually mix the remaining ink with a spatula to redistribute the hyphae.
10. Load the mycelium-laden ink into a a 20 mL syringe, and centrifuge for 4 minutes at 2,000 rpm to remove any entrapped air.
11. Cut the syringe side taps to fit the printer, attach the nozzle tip and load the ink through, to be ready for printing.

All procedures described after the autoclaving in step 4 require working in a sterile environment, to prevent contamination of the ink with other micro-organisms. Hence all materials should either be ordered sterile, autoclaved, or thoroughly cleaned with 70% ethanol and sterilised in a flame. All work was performed on a bench thoroughly cleaned with 70% ethanol, and in close proximity of a gas burner.

B

FTIR peaks for lignocellulose

Peak (cm^{-1})	Molecular category	Assignment	Source
2921	-	alkyl C-H	Beech [55]
1740	Hemicellulose	non conjugated carbonyl, mainly xylan's uronic acids	Beech [130]
1738	Hemicellulose	unconjucated C=O xylan	Beech [113]
1646	Lignin	conjugated carbonyl groups	Beech [130]
1596	Lignin	aromatic skeletal vibration	Beech [113, 130]
1505,1506	Lignin	aromatic skeletal vibration	Beech [113, 130, 55]
1462	Lignin	C-H deformation	Beech [113]
1425	Lignin, cellulose, hemicellulose	C-H deformation in lignin and carbohydrates, CH2 scissor vibrations	Beech [113, 55]
1375	Cellulose, hemicellulose	C-H deformation	Beech [113]
1329	Lignin	syringyl ring breathing with C-O stretching	Hornbeam [115]
1267, 1268 (shoulder)	Lignin	guaiacyl ring breathing	Beech, hornbeam [115, 113]
1244	Lignin, hemicellulose	syringyl ring and C-O stretch in lignin and xylan	Beech [113]
1230, 1231	Lignin, hemicellulose	guaiacyl and syringyl, C-O in xylan	Beech [113, 55]
1223	Lignin	guaiacyl ring breathing and C-O stretching	Hornbeam [115]
1158	Cellulose, hemicellulose	C-O-C vibrations	Beech [113]
1143	Cellulose, hemicellulose	C-O-C vibration	Flax [78]
1124	Lignin	aromatic in plane C-H deformation syringyl	Hornbeam [115]
1122	Lignin	aromatic skeletal and C-O stretch	Beech [113]
986	Cellulose	C-H deformation	Flax [78]
898, 896	Cellulose	C-H deformation	Beech [113], flax [78]

Table B.1: FTIR peaks and their assignment for lignocellulosic materials.

C

Optical microscopy images

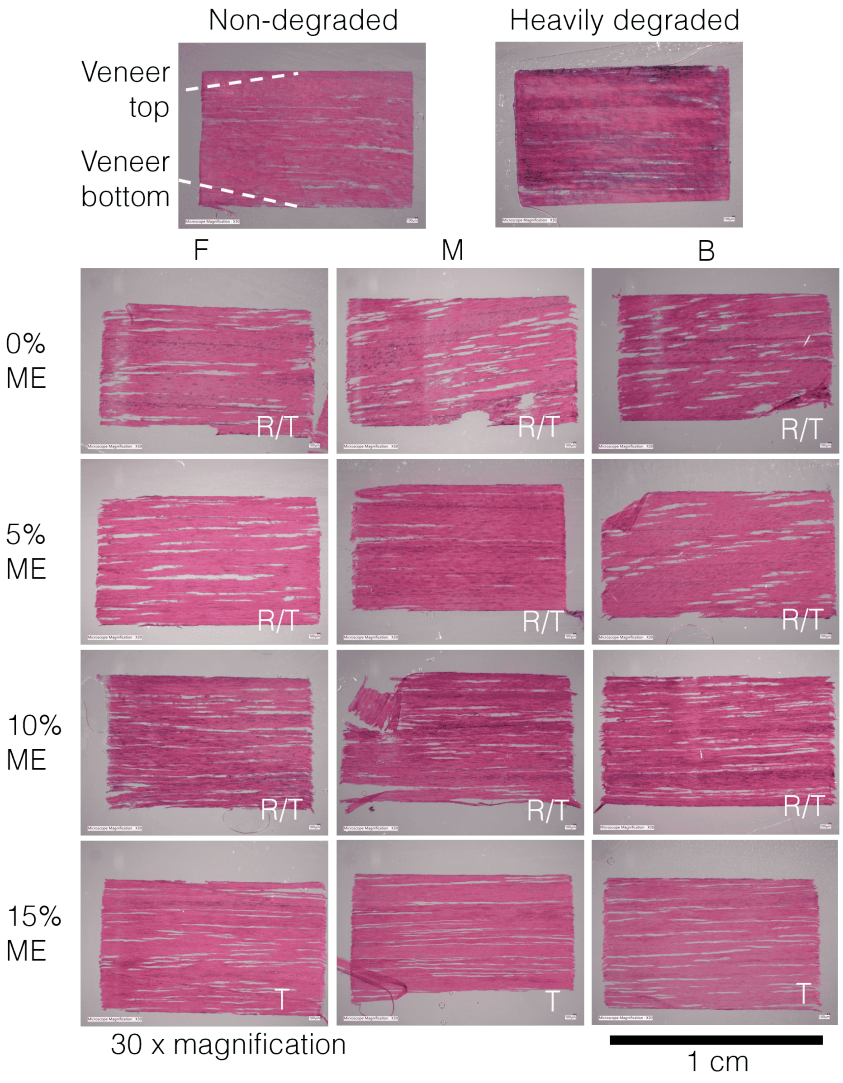

Figure 37: Microscopy images of 20μm thick hornbeam veneer slices. Veneers were either non-degraded, heavily degraded by *G. lucidum*, or inoculated with mycelium-laden ink of different ME concentrations. The latter samples were cut at three different locations: their front, F, middle, M, and back, B, as highlighted in Figure 16. Cuts were either tangential, T, or in between radial and tangential, R/T.